Physics of Solar Atmosphere, Corona and Heliosphere and Space Weather

Allan Sacha Brun
Service d'Astrophysique/AIM, CEA Saclay

- Observations of flares, CME's and surface magnetic activity
- Behaviour of rising flux tubes in the convective zone
- Parker's solar wind model

Solar eruptions

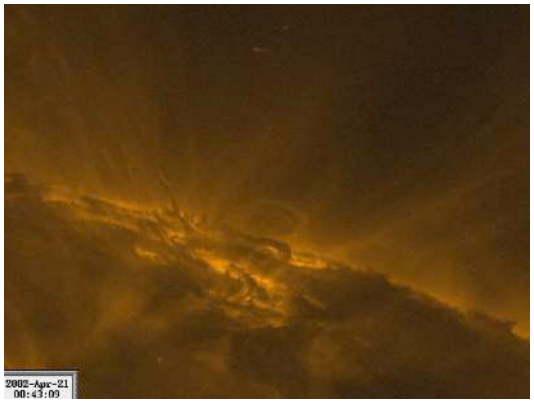

flare

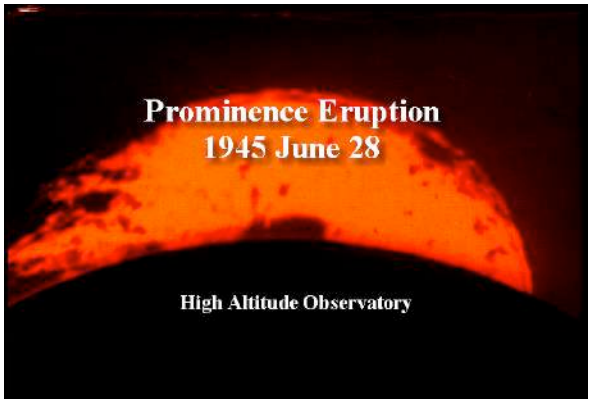

prominence eruption

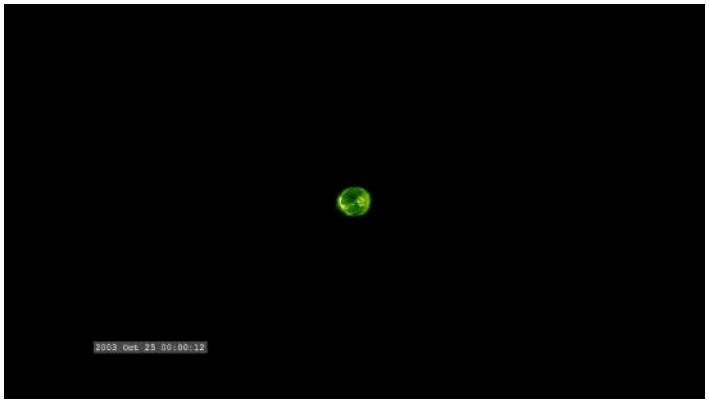

CME

- three main observational manifestations of large-scale solar eruptions
- main driver of space weather disturbances at Earth → forecast onset & impact
- basic eruption-scenario (magnetic explosion) well understood, but:

(1) what are the specific initiation mechanisms and thresholds?

(2) to what extent and how are individual eruptions coupled?

(3) how can we predict their onset and their impact at Earth?

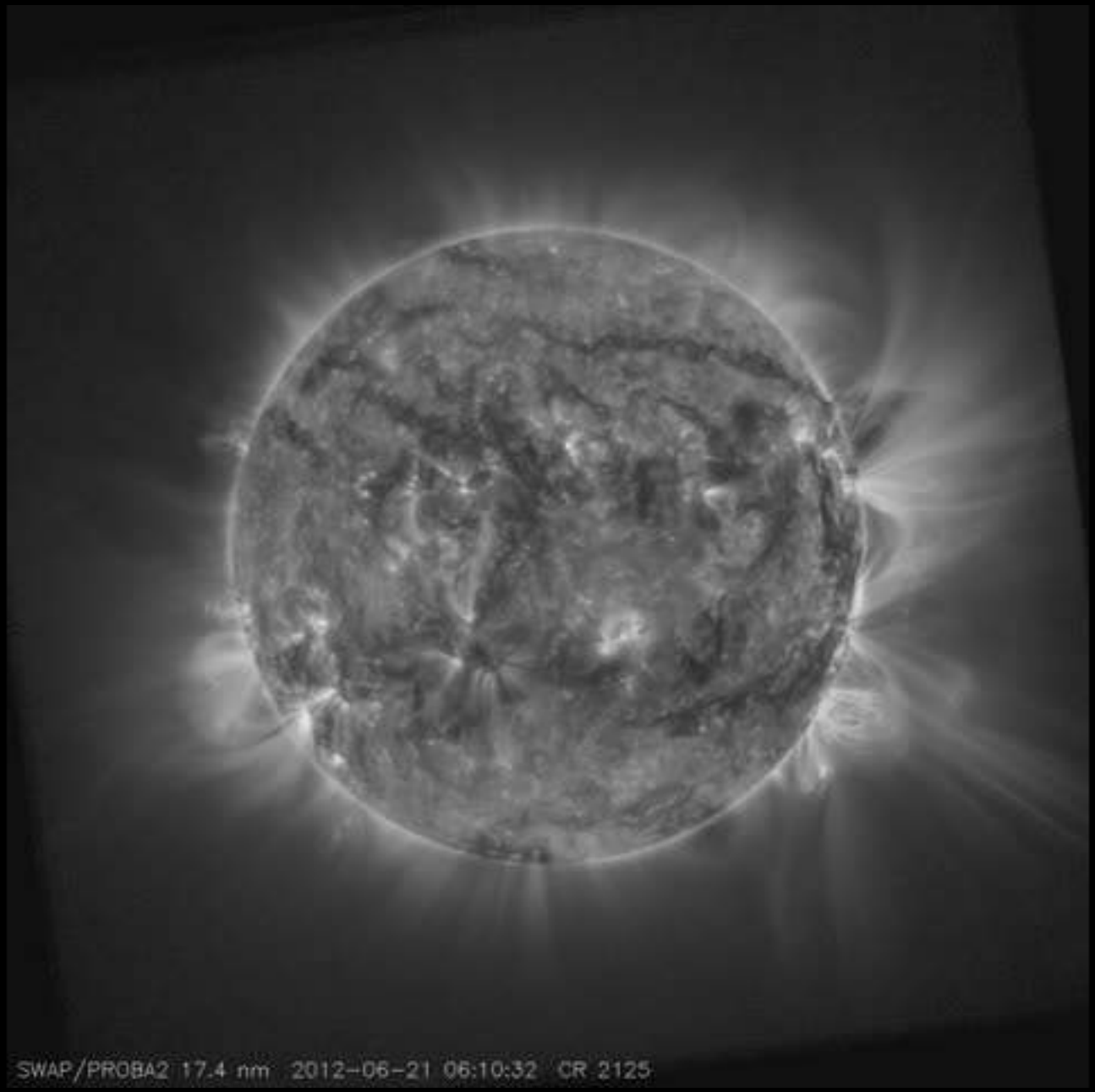
SWAP/PROBA2 17.4 nm 2012-06-21 06:10:32 CR 2125

Structure of Solar Upper Atmosphere

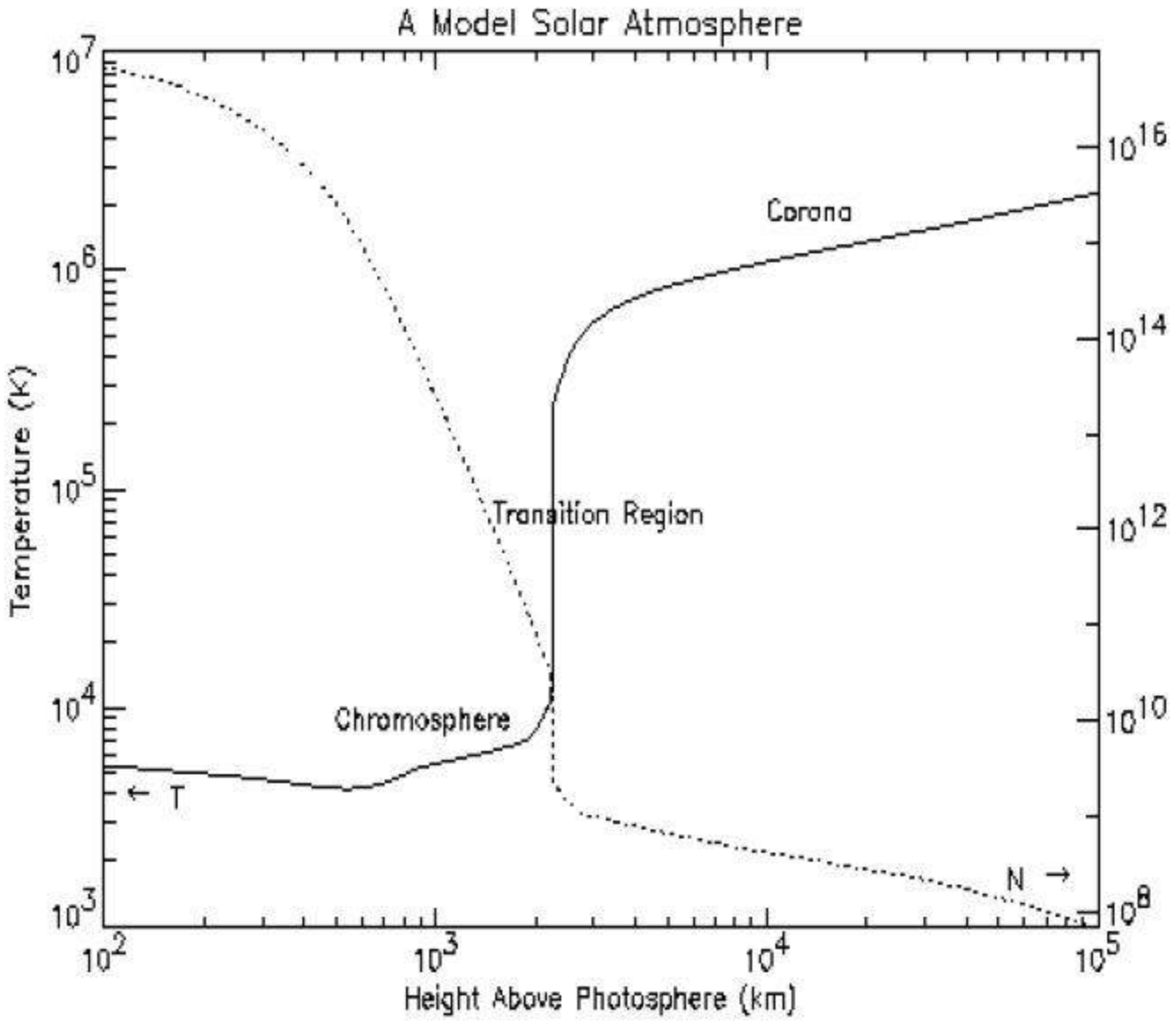

Plasma β

β=Pgaz/Pmag

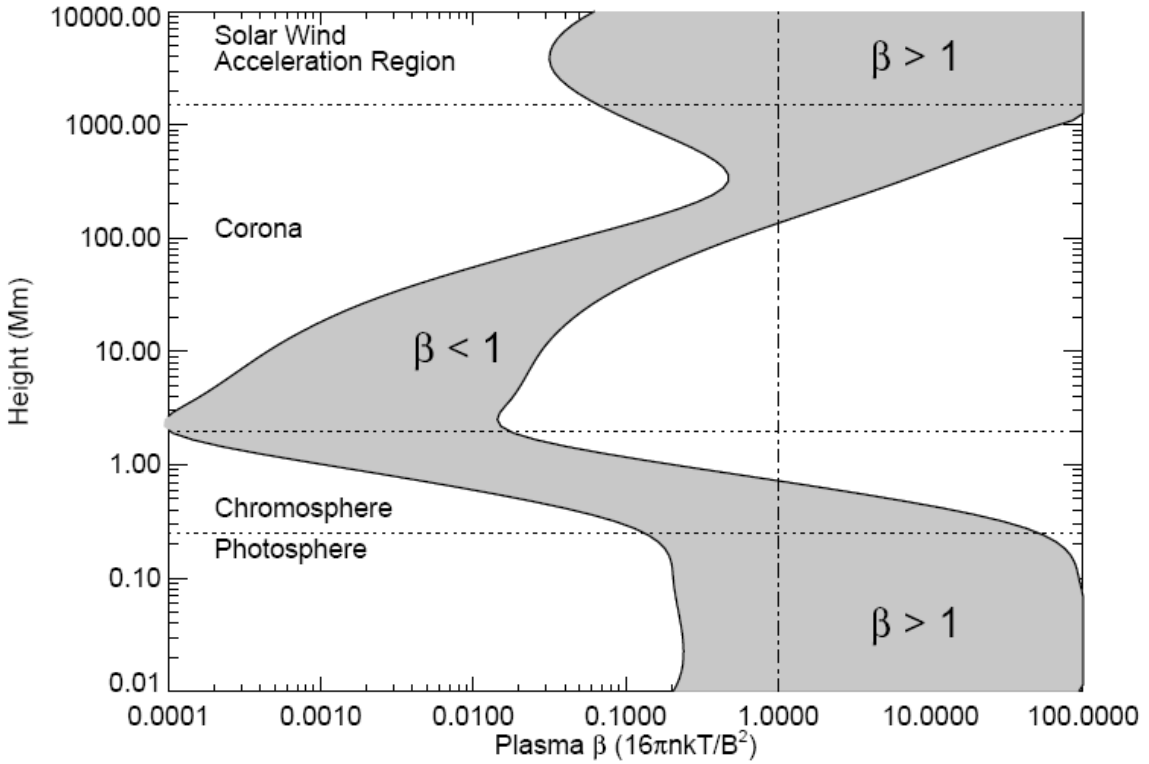

Figure 1.22: Plasma β in the solar atmosphere for two assumed field strengths, 100 G and 2500 G. In the inner corona ($R \lesssim 0.2 R_\odot$), magnetic pressure generally dominates static gas pressure. As with all plots of physical quantities against height, a broad spatial and temporal average is implied (Gary, 2001).

Table 1.1: The plasma-β parameter in the solar atmosphere.

Parameter	Photosphere	Cool corona	Hot corona	Outer corona
Electron density n_e (cm^{-3})	2×10^{17}	1×10^9	1×10^9	1×10^7
Temperature T (K)	5×10^3	1×10^6	3×10^6	1×10^6
Pressure p (dyne cm^{-2})	1.4×10^5	0.3	0.9	0.02
Magnetic field B (G)	500	10	10	0.1
Plasma-β parameter	14	0.07	0.2	7

10 dyne/cm^2 = 1 Pascal

10^3 dyne/cm^2 = 1 mbar

1 atm = 1013 mbar

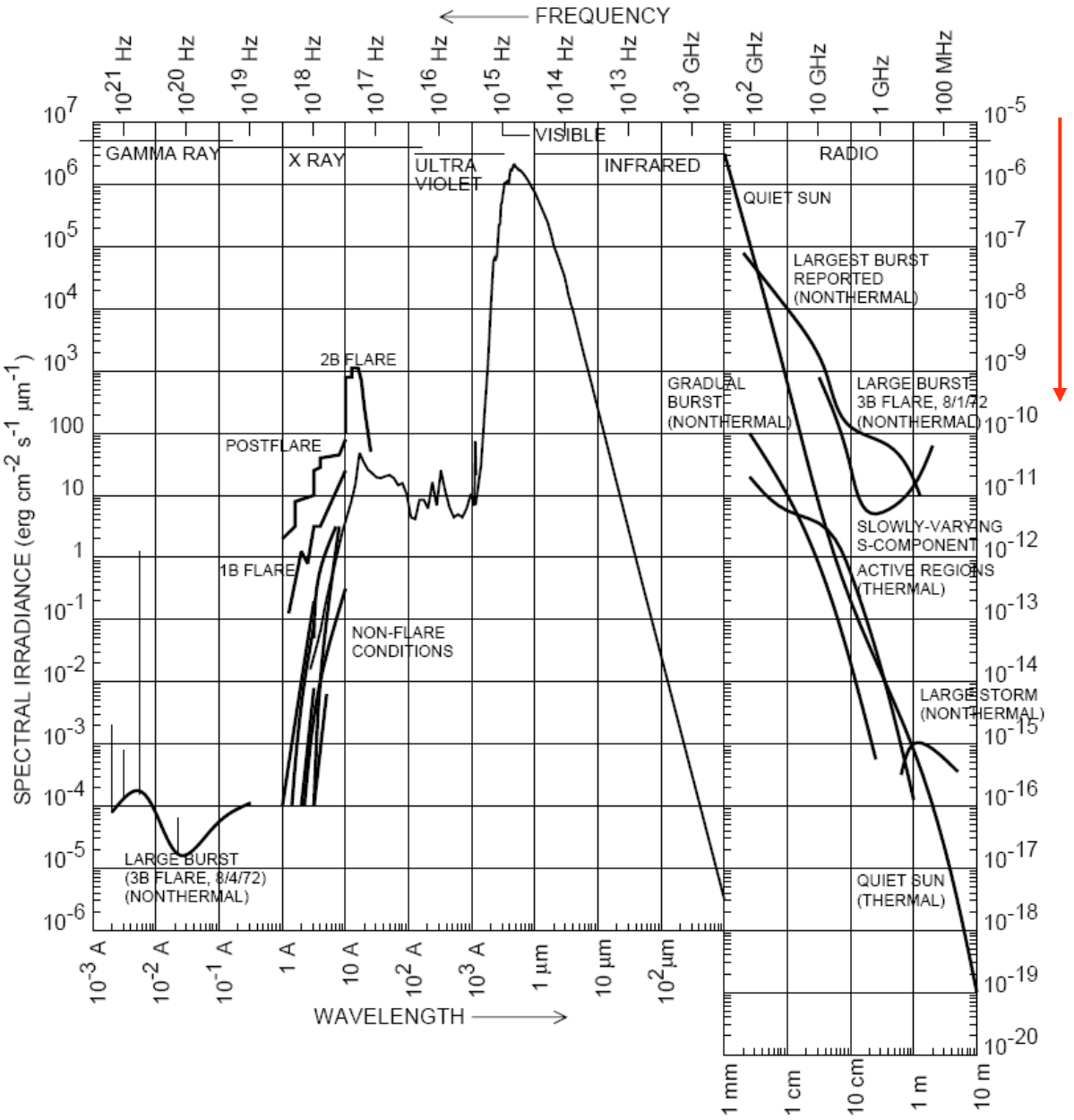

Figure 1.25: The solar irradiance spectrum from gamma-rays to radio waves. The spectrum is shifted by 12 orders of magnitude in the vertical axis at $\lambda = 1$ mm to accommodate for the large dynamic range in spectral irradiance (after Zombeck, 1990 and Foukal, 1990).

Shifted by 12 orders

Solar Irradiance Spectra

Granulation and Sunspot Dynamics

(Solar Swedish Telescope- Hinode)

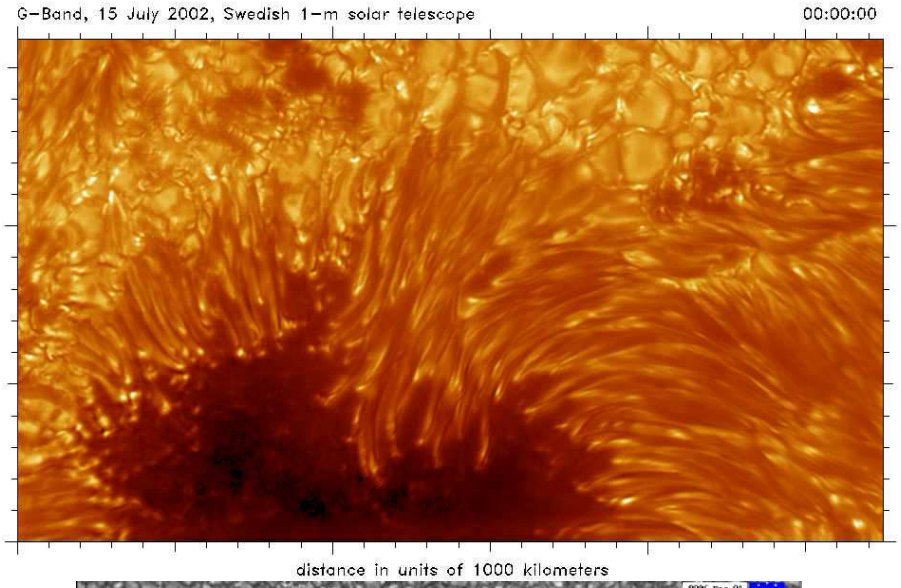

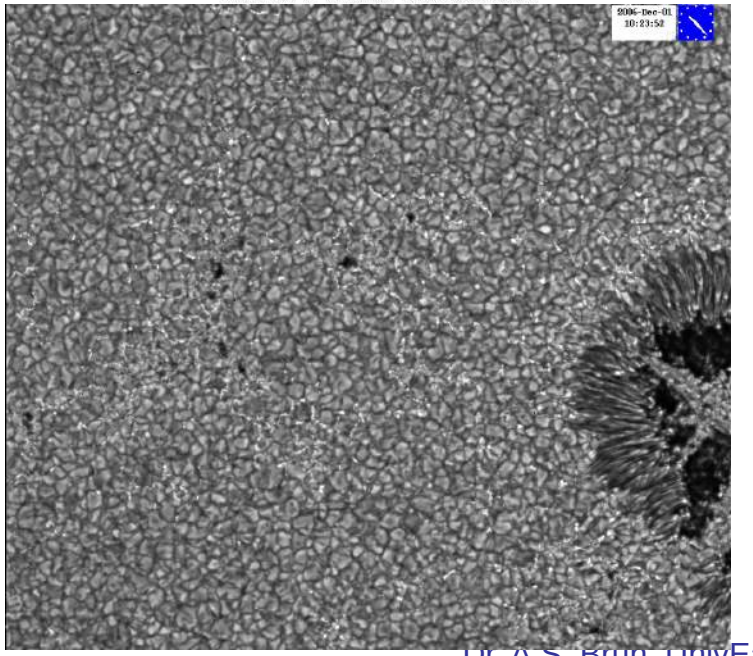

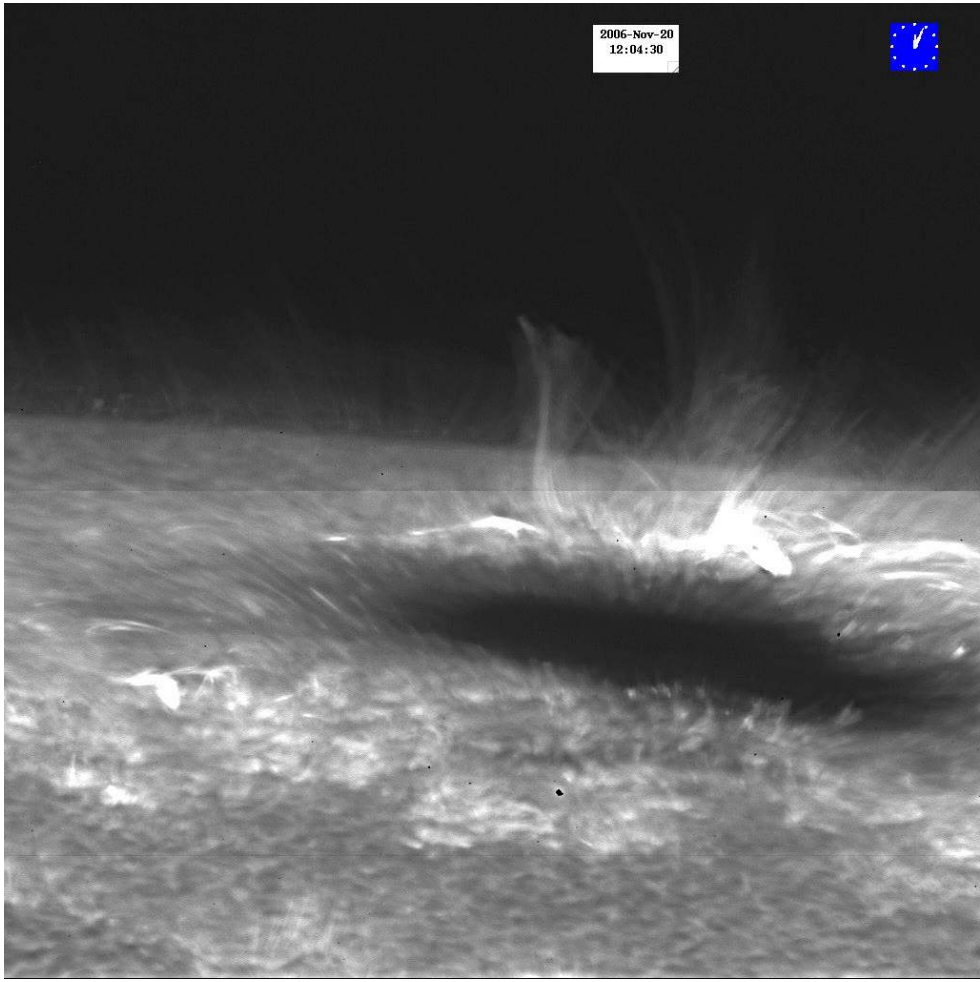

Active Region Classification (Mt. Wilson)

- ALPHA: A single dominant spot, often linked with a plage of opposite magnetic polarity.
- BETA: A pair of dominant spots of opposite polarity (Bipolar, i.e., a leader and a follower).
- GAMMA: Complex groups with irregular distribution of polarities.
- BETA-GAMMA: Bipolar groups which have more than one clear north-south polarity inversion line.
- DELTA: Umbrae of opposite polarity together in a single penumbra.

Transport et génération du champ toroidal Btor

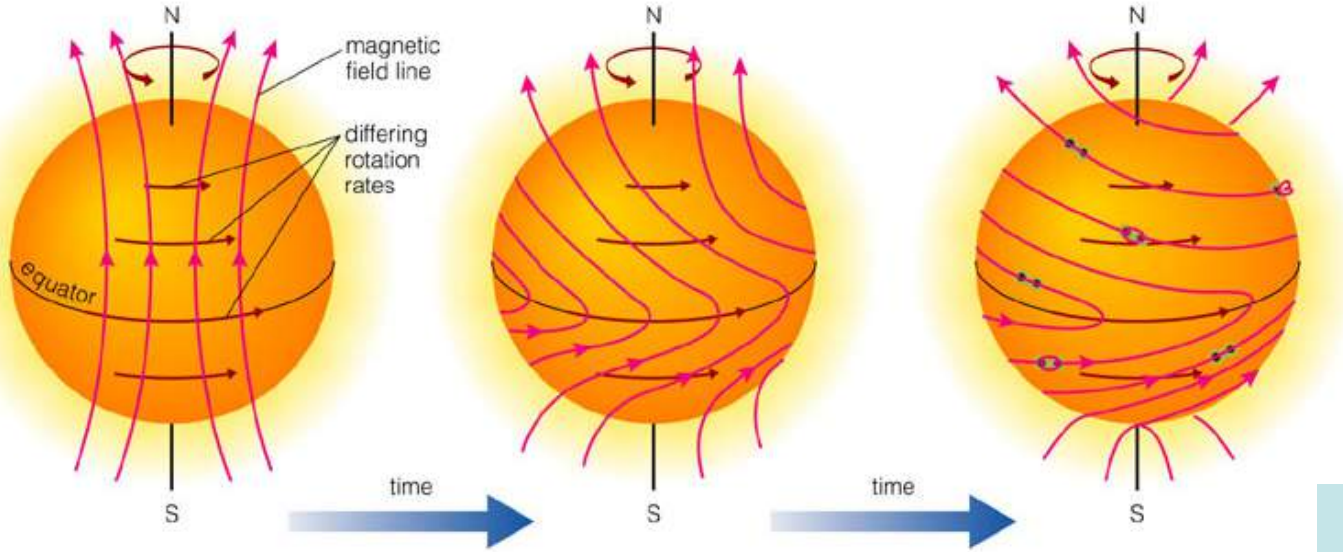

Effet Omega (ω): enroulement des lignes de champ

Go 3-D model

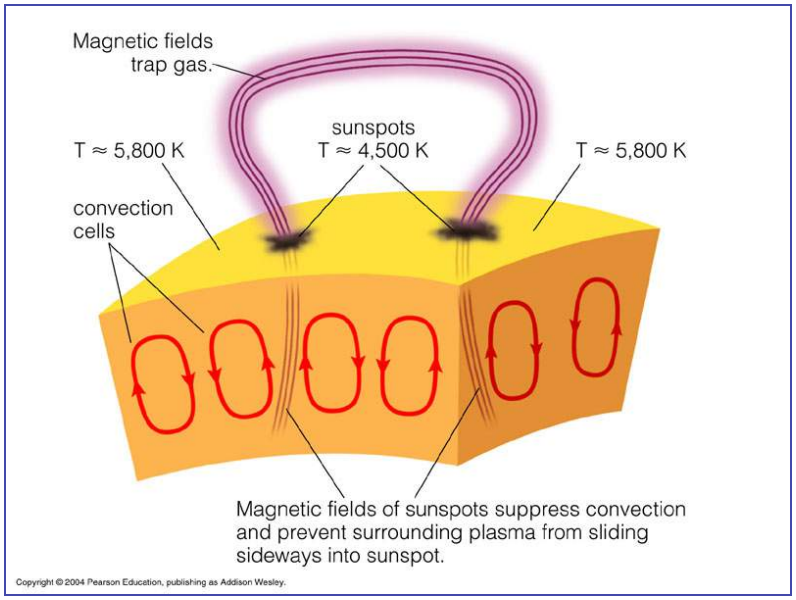

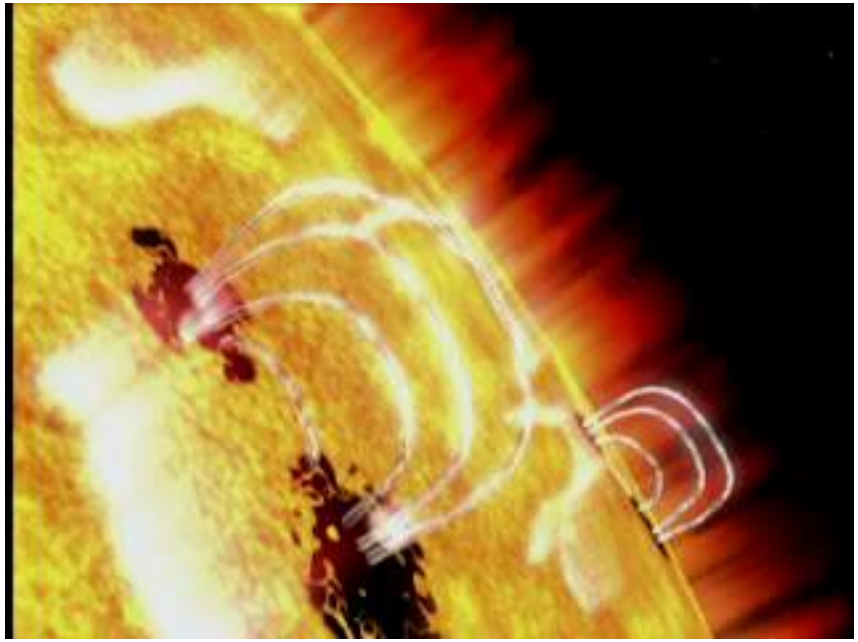

Transport & generation of toroidal field in Convection zone

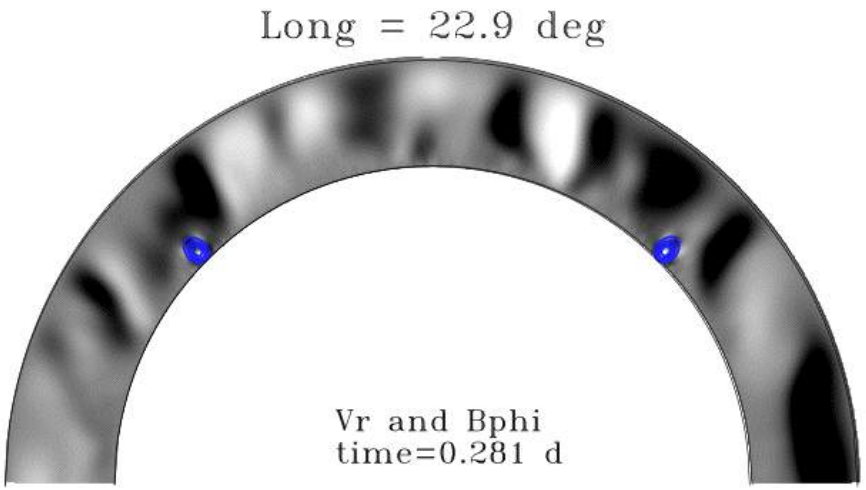

Jouve & Brun 2007 (AN), 2009, 2013, ApJ

Pinto & Brun 2013, ApJ

Field strenght B0 ~5 Beq

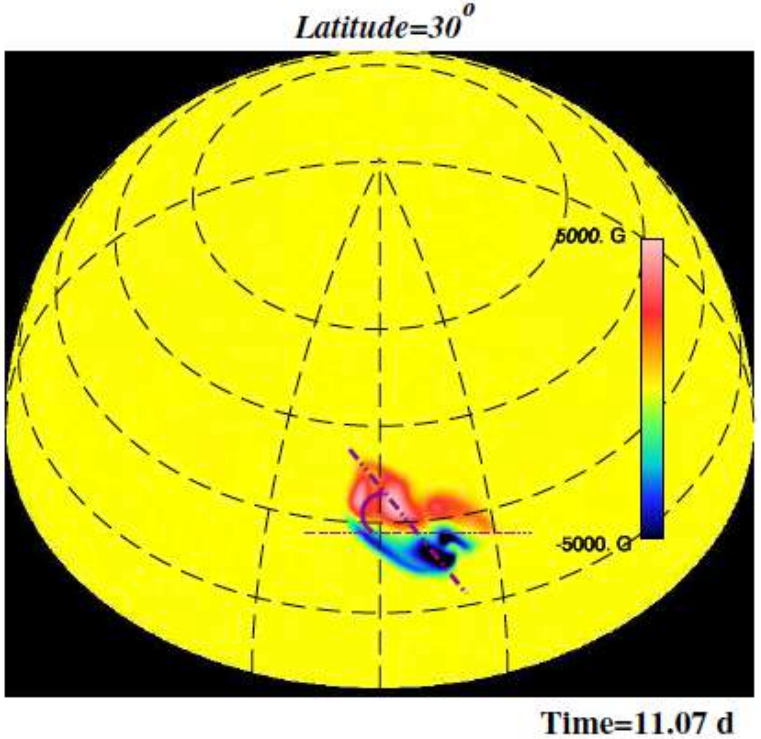

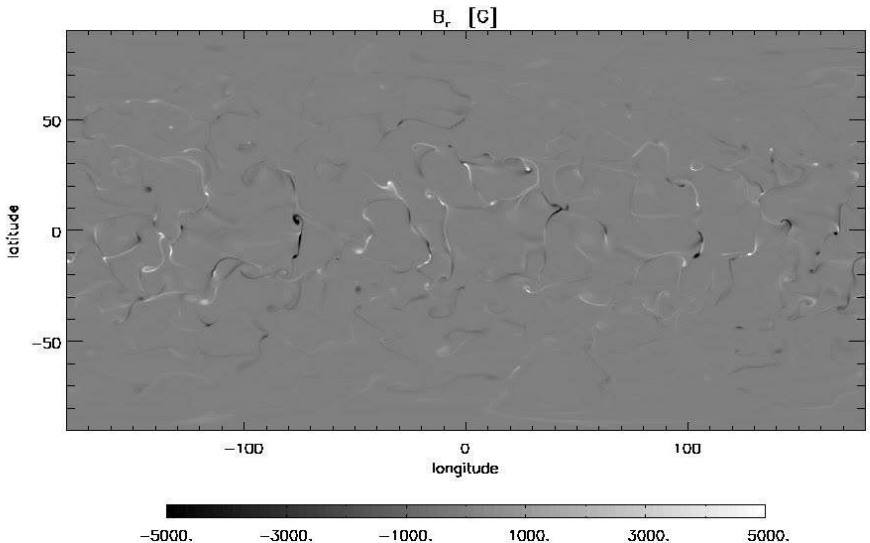

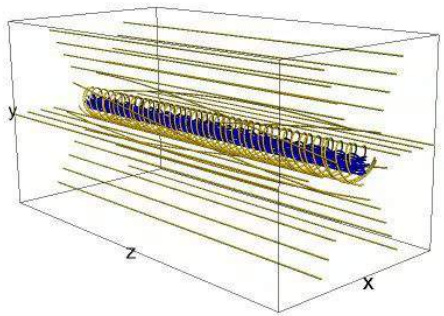

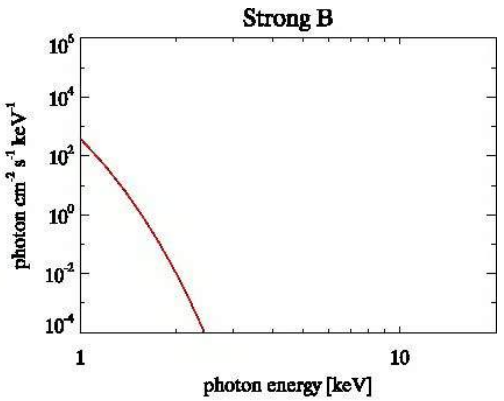

Soft X-ray emission

Pinto, Vilmer, Brunn 2015, A&A

Going Beyond the introduction of flux tube:
Self-consistent buoyant Loops generations

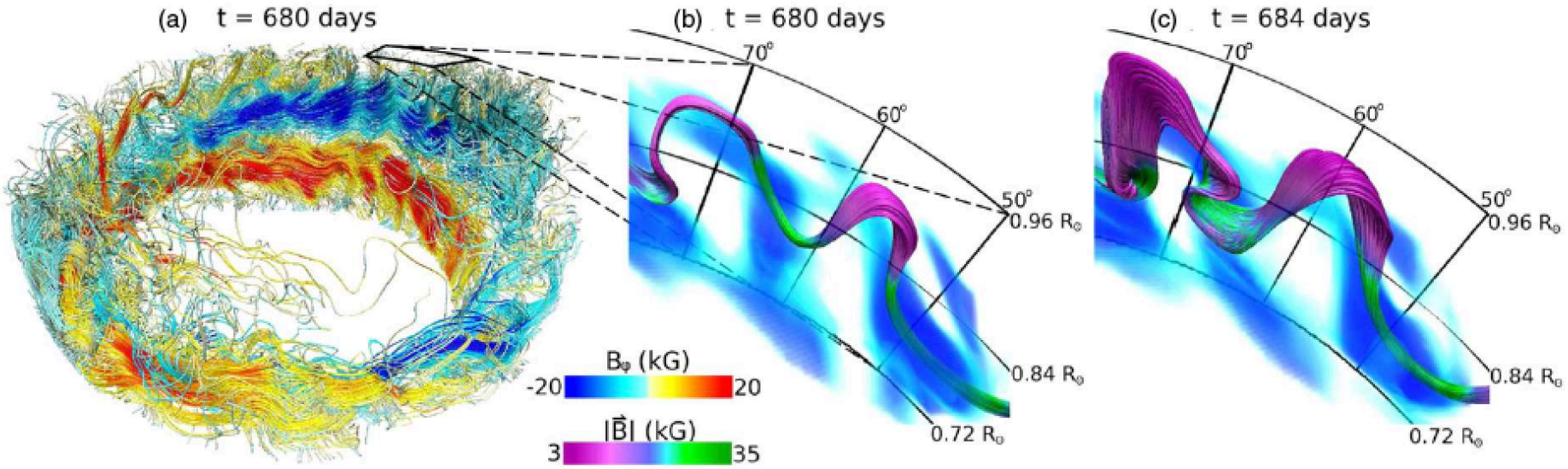

Nelson et al. 2011, 2013a, 2013b

Influence of **B** on the solar atmosphere

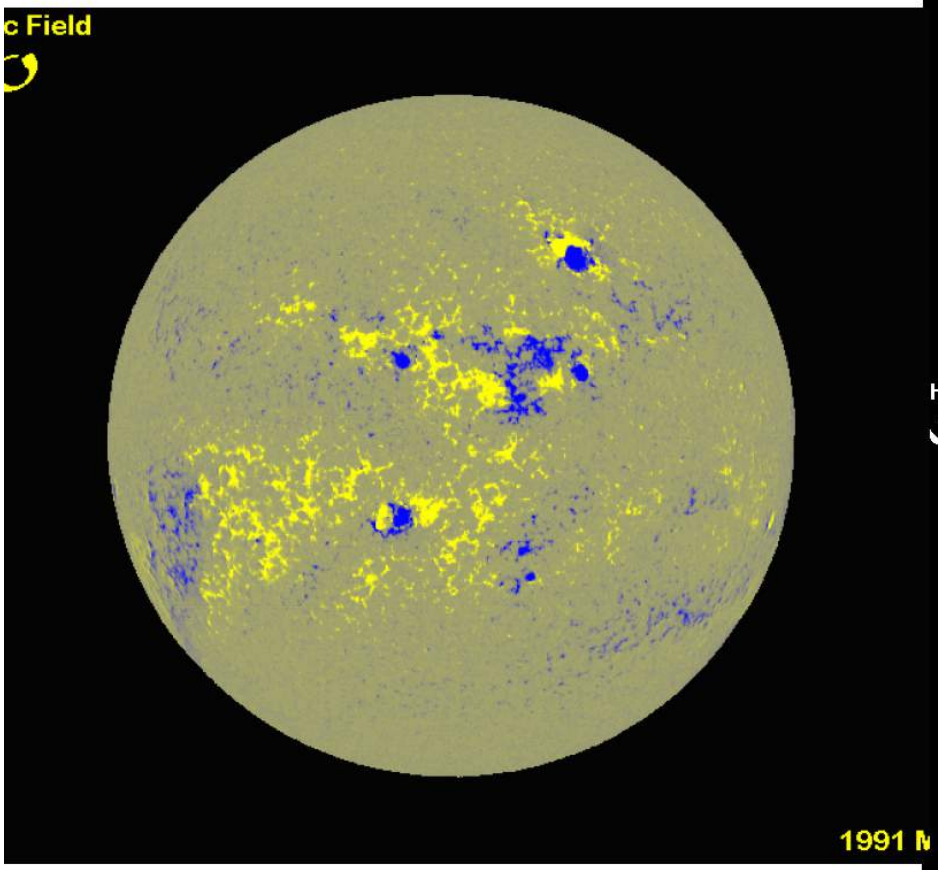

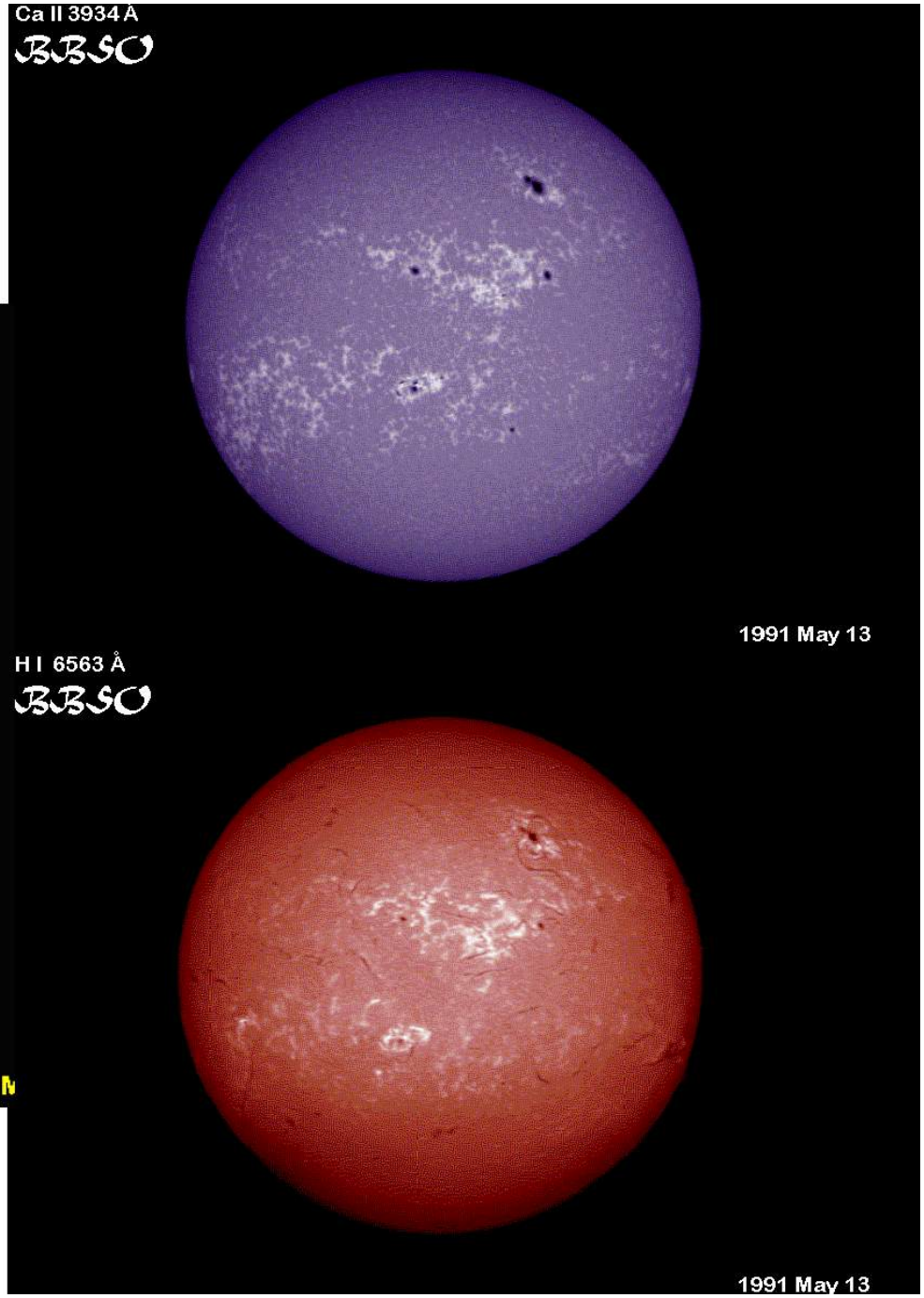

From MSSTA soundingrocket.

Soleil en rayon X (satellite Hidone (Japon))

Loops-Eruptions (TRACE Data)

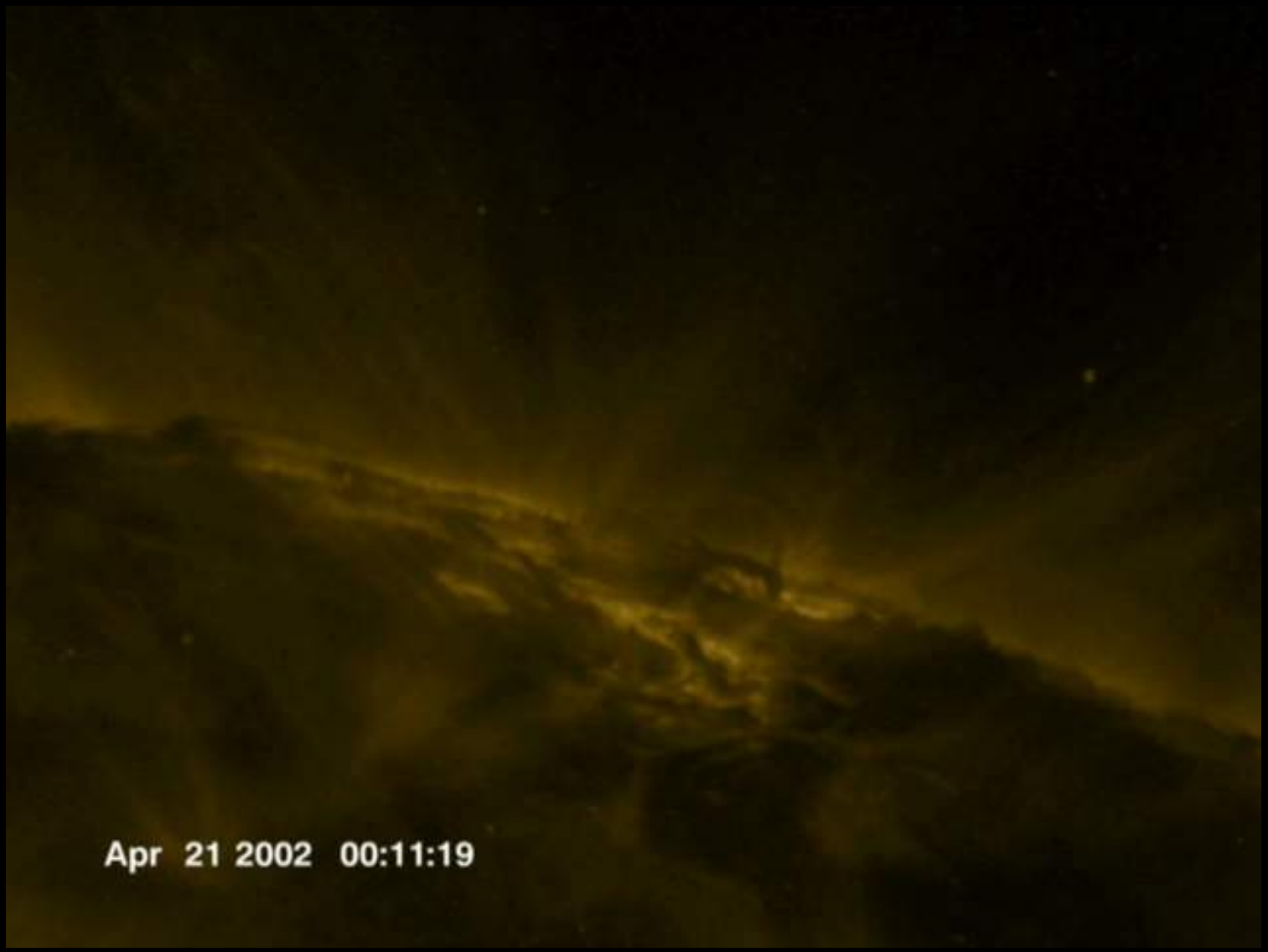

http://vestige.lmsal.com/TRACE/

Flares in Hα & CaH

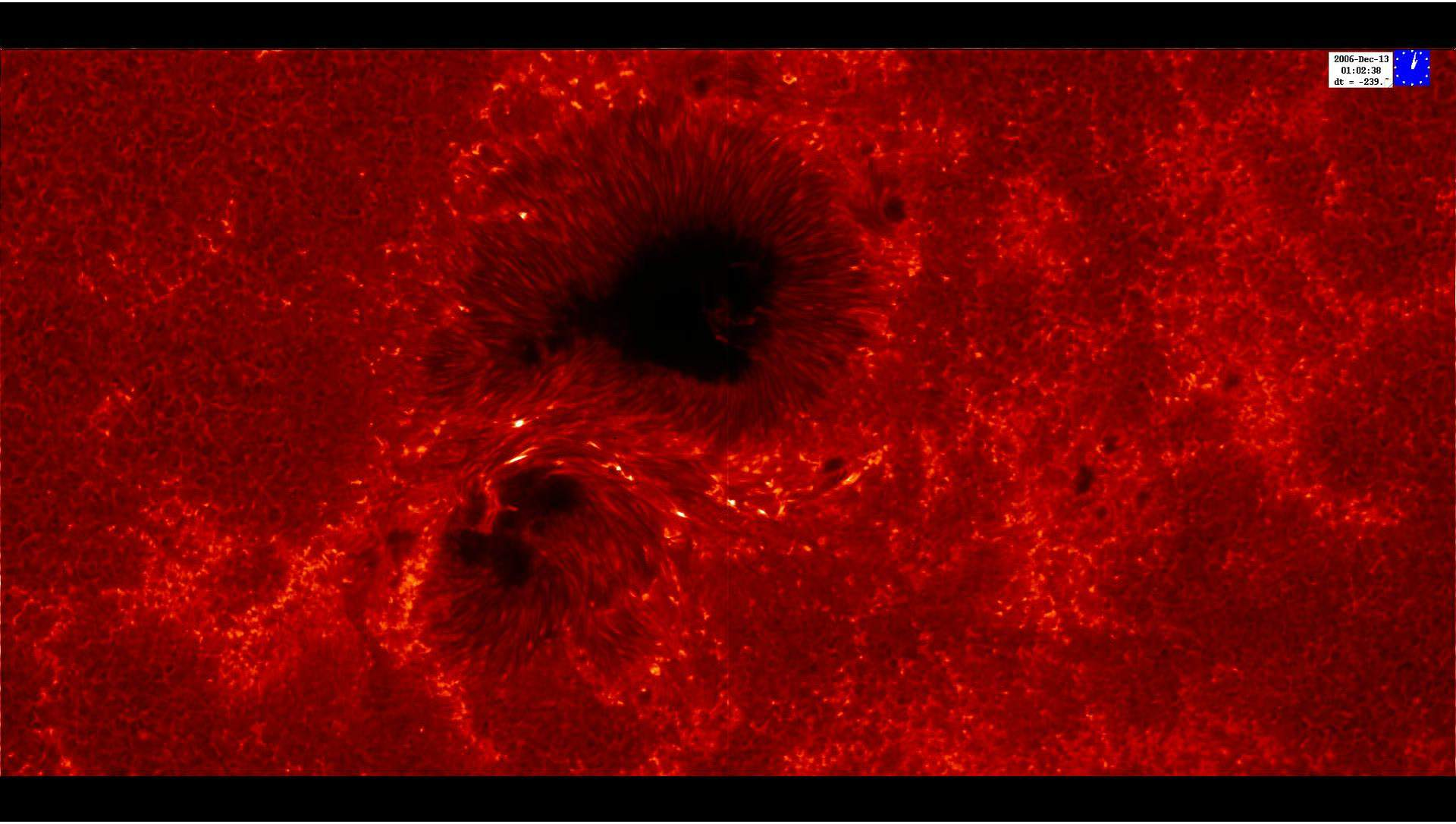

Big Bear Solar Observatory & Hinode satellite

Soft and hard X-ray emission (Rhessi + Trace)

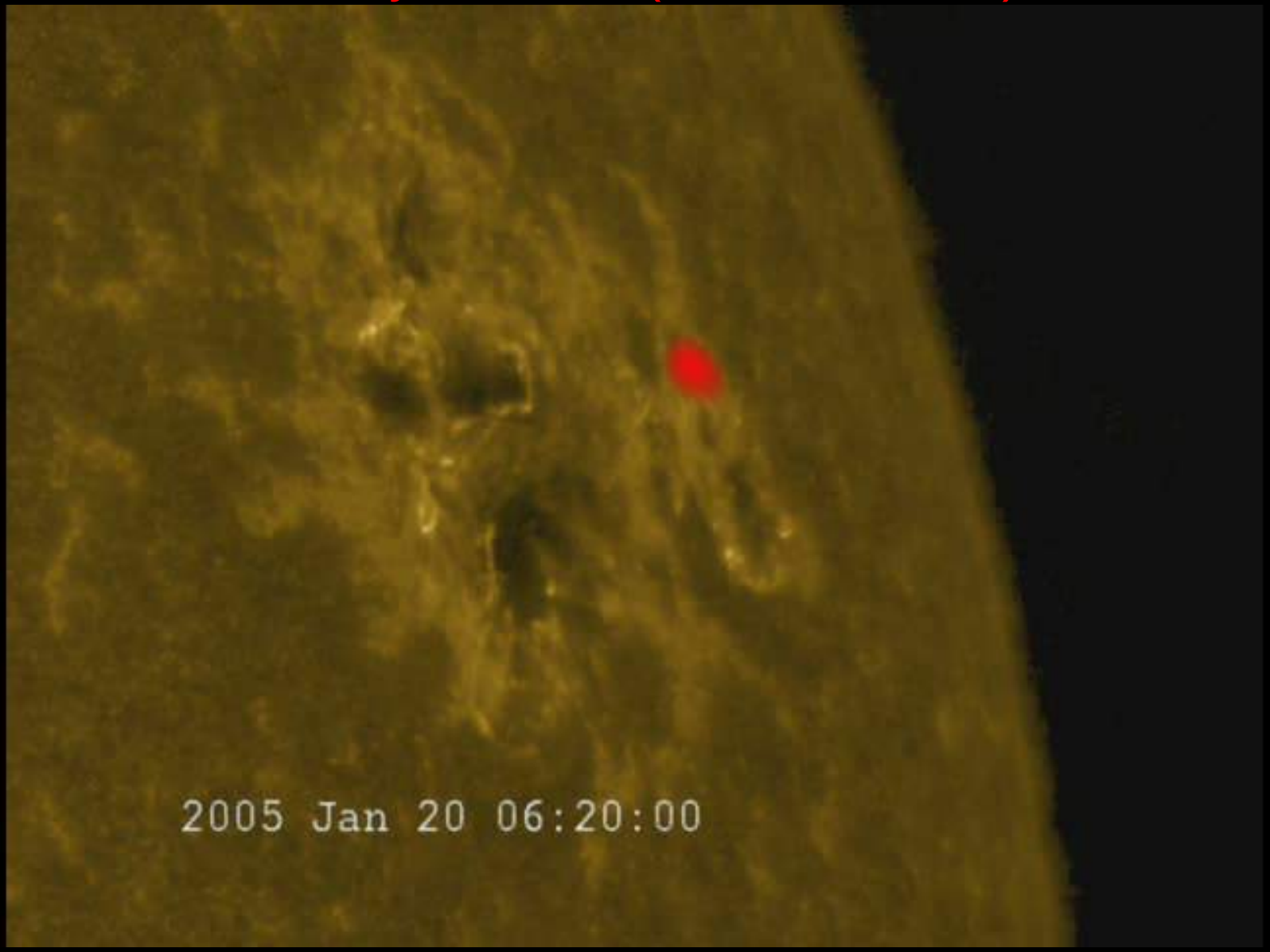

14 July 2000 Flare
TRACE 3 Band Composite Images

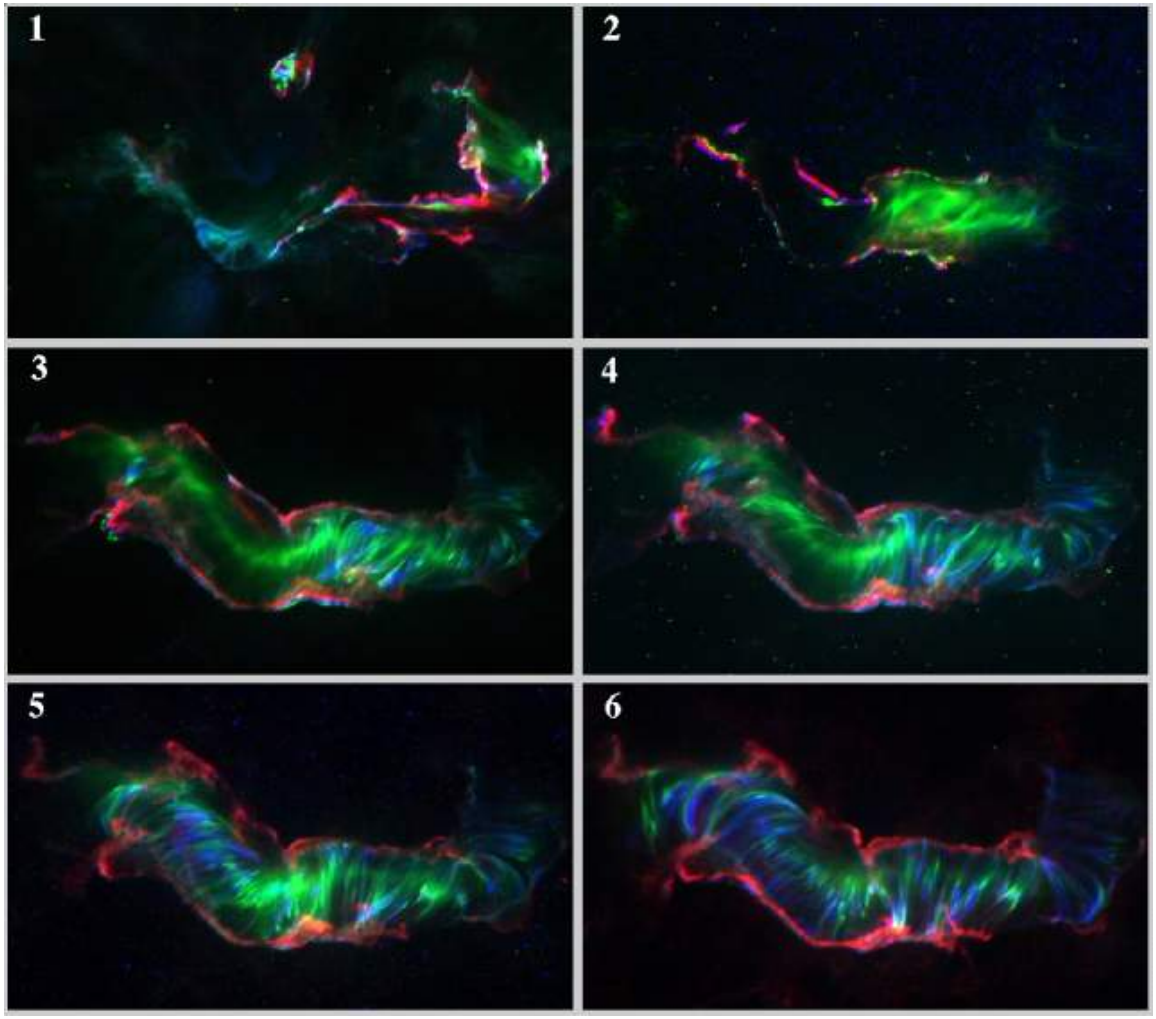

Red: UV continuum

Blue: 171 Å pass band, ~1 MK

Green: 195 Å pass band, >1.5 MK

Post flare loops

Flare Classification Schemes

After Bhatnagar & Livingston 2005

Hα classification			Radio flux at 5000 MHz in s.f.u.	Soft X-ray class	
Importance Class	Area (Sq. Deg.)	Area 10^{-6} solar disk		Importance class	Peak flux in 1-8 Å w/m^2
S	2.0	200	5	A	10^{-8} to 10^{-7}
1	2.0–5.1	200–500	30	B	10^{-7} to 10^{-6}
2	5.2–12.4	500–1200	300	C	10^{-6} to 10^{-5}
3	12.5–24.7	1200–2400	3000	M	10^{-5} to 10^{-4}
4	>24.7	>2400	3000	X	>10^{-4}

Hα sub-classification by brightness: F – faint, N – normal, B – bright

1 s.f.u. = 10^4 jansky = 10^{-2} W m^{-2} Hz^{-1}

Résumé “flare/CME”

“flares”	Taille (L)	Temps de vie(t)	Temps Alfvén(t_A)	t/t_A	Mass éjectée
microflares	10^3 -10^4 km	100-1000sec	1-10 sec	~100	jet/ surge
Impulsive flares	(1-3) x 10^4 km	10 min – 1 hr	10-30 sec	~60-100	X-ray plasmoid/ Spray
Long duration (LDE) flares	(3-10)x 10^4 km	1-10 hr	30-100 sec	~100-300	X-ray plasmoid/ prom. eruption
Giant arcades	10^5 -10^6 km	10 hr – 2 days	100-1000 sec	~100-300	CME/ prom. eruption

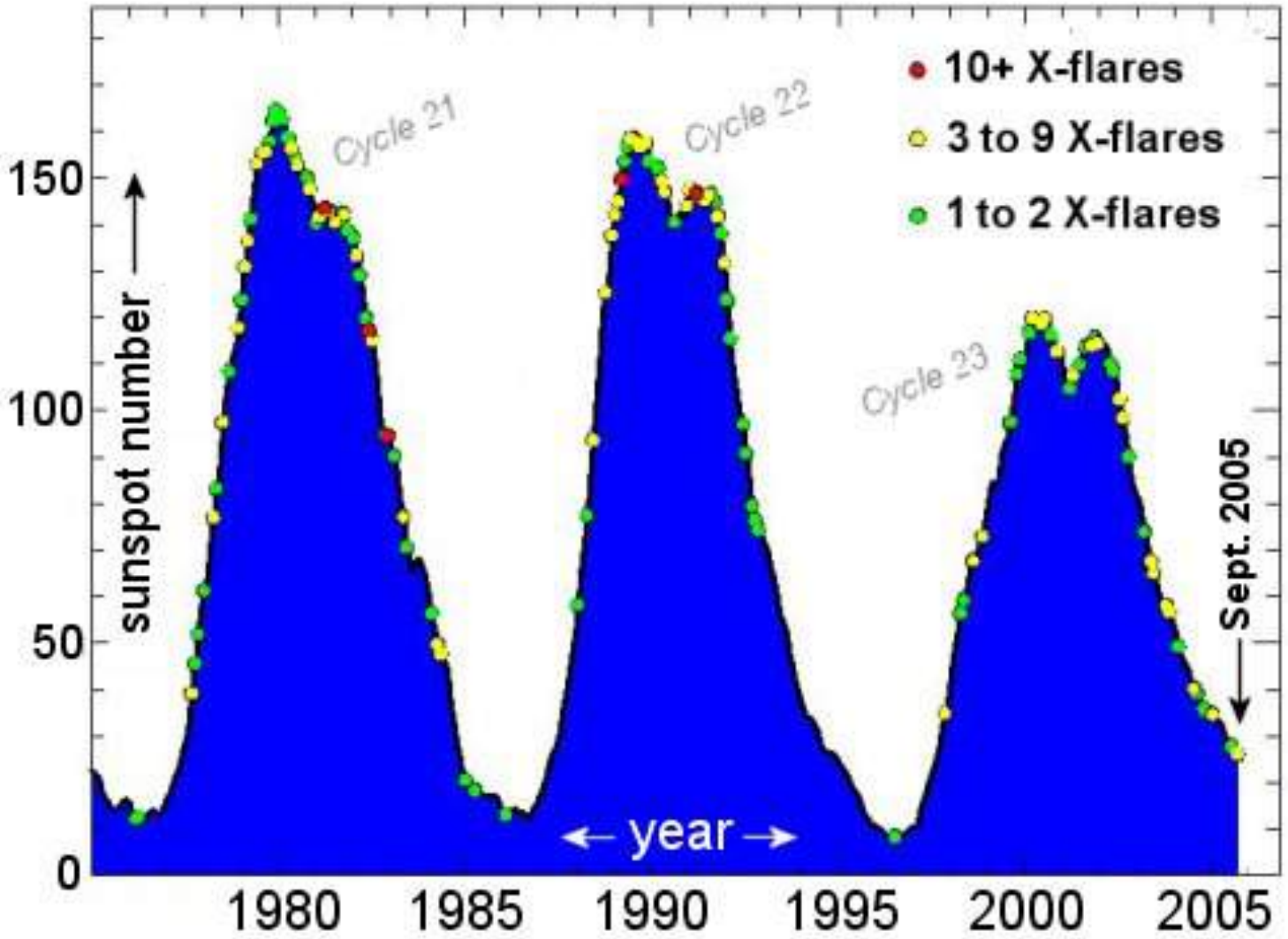
10+ X-flares
3 to 9 X-flares
1 to 2 X-flares
Cycle 21
Cycle 22
Cycle 23
sunspot number
150
100
50
0
year
1980
1985
1990
1995
2000
2005
Sept. 2005

Radiation Mechanisms

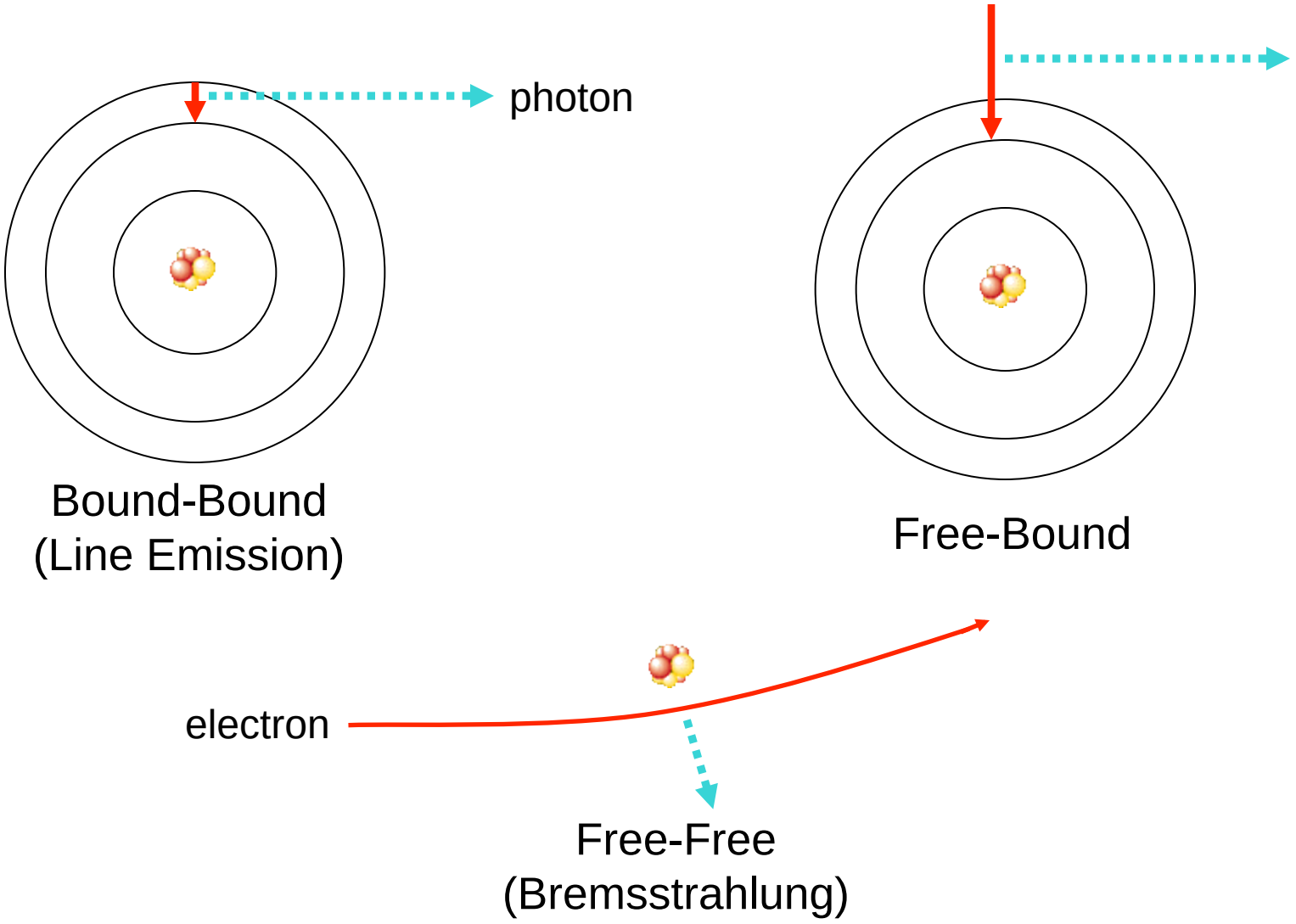

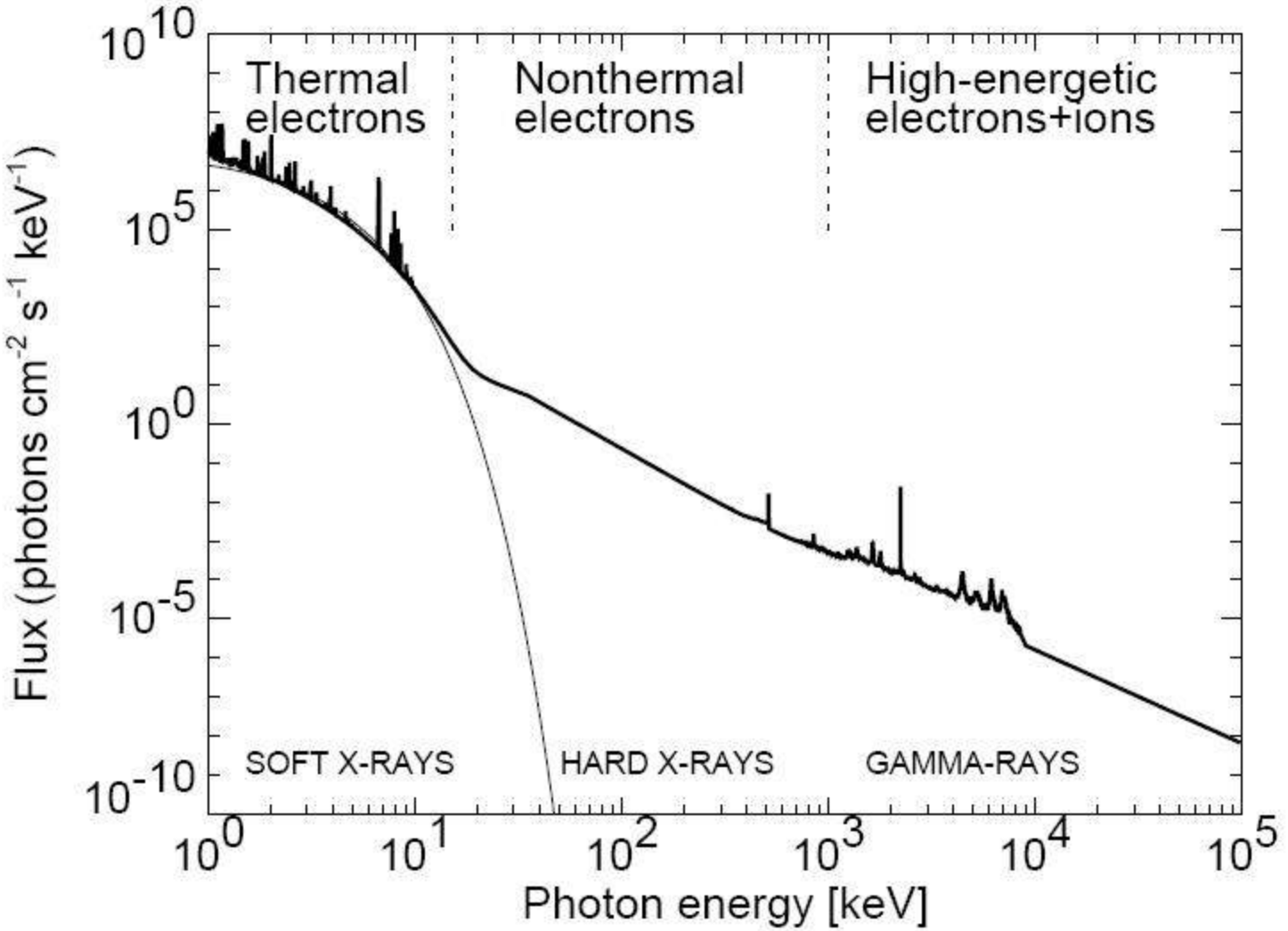

Figure 94. Composite photon spectrum of a large ¤are, extending from soft X-rays (1-10 keV), hard X-rays (10 keV-1 MeV), to gamma rays (1 MeV-10 GeV), mostly produced by thermal, nonthermal (energetic), or high-energetic electrons. Gamma-ray line emission and parts of the gamma-ray continuum is produced by interactions of protons, neutrons, ions, and pion decay.

Field Lines Reconstruction

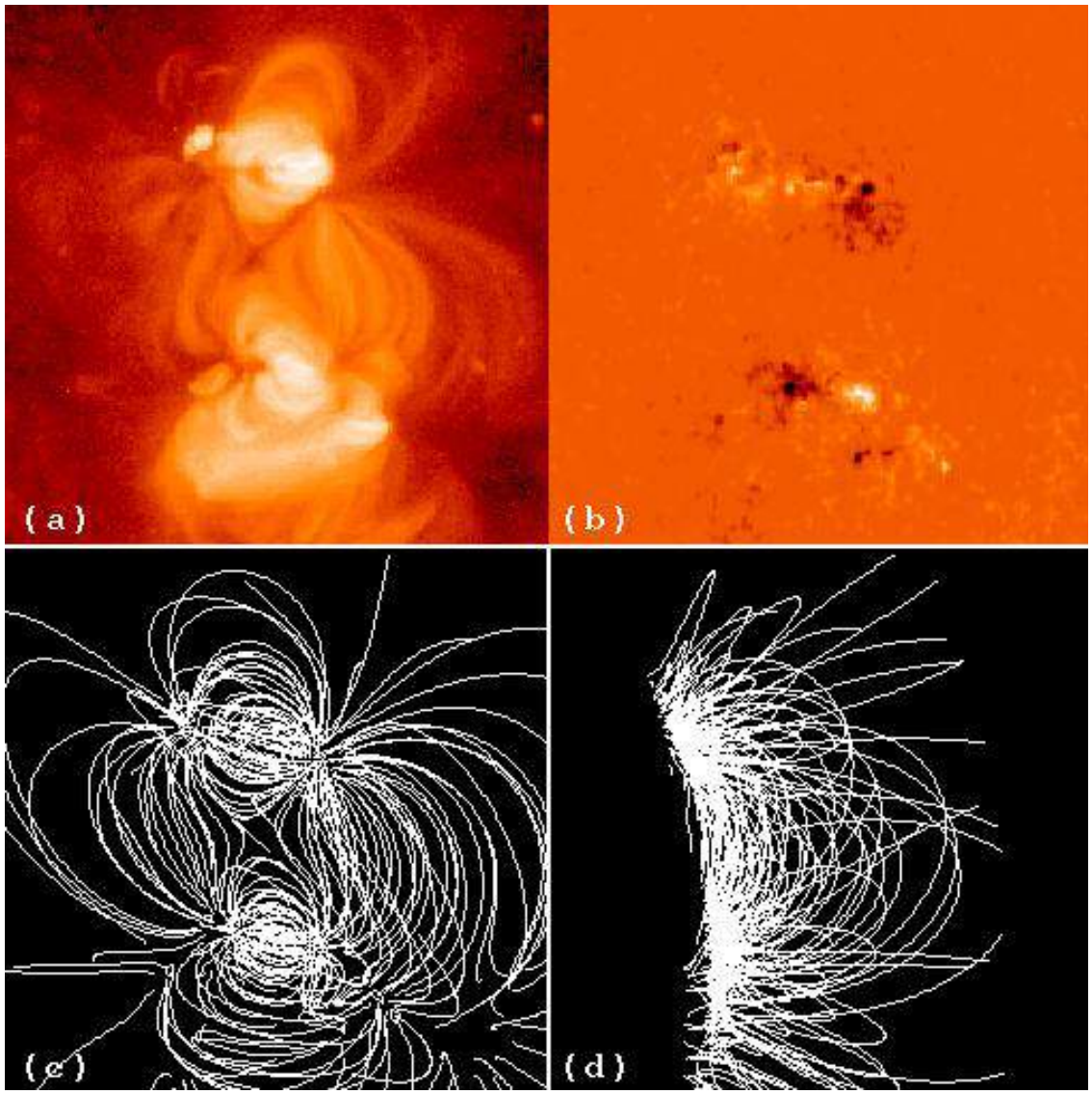

Eruptive event falling back: unguided case

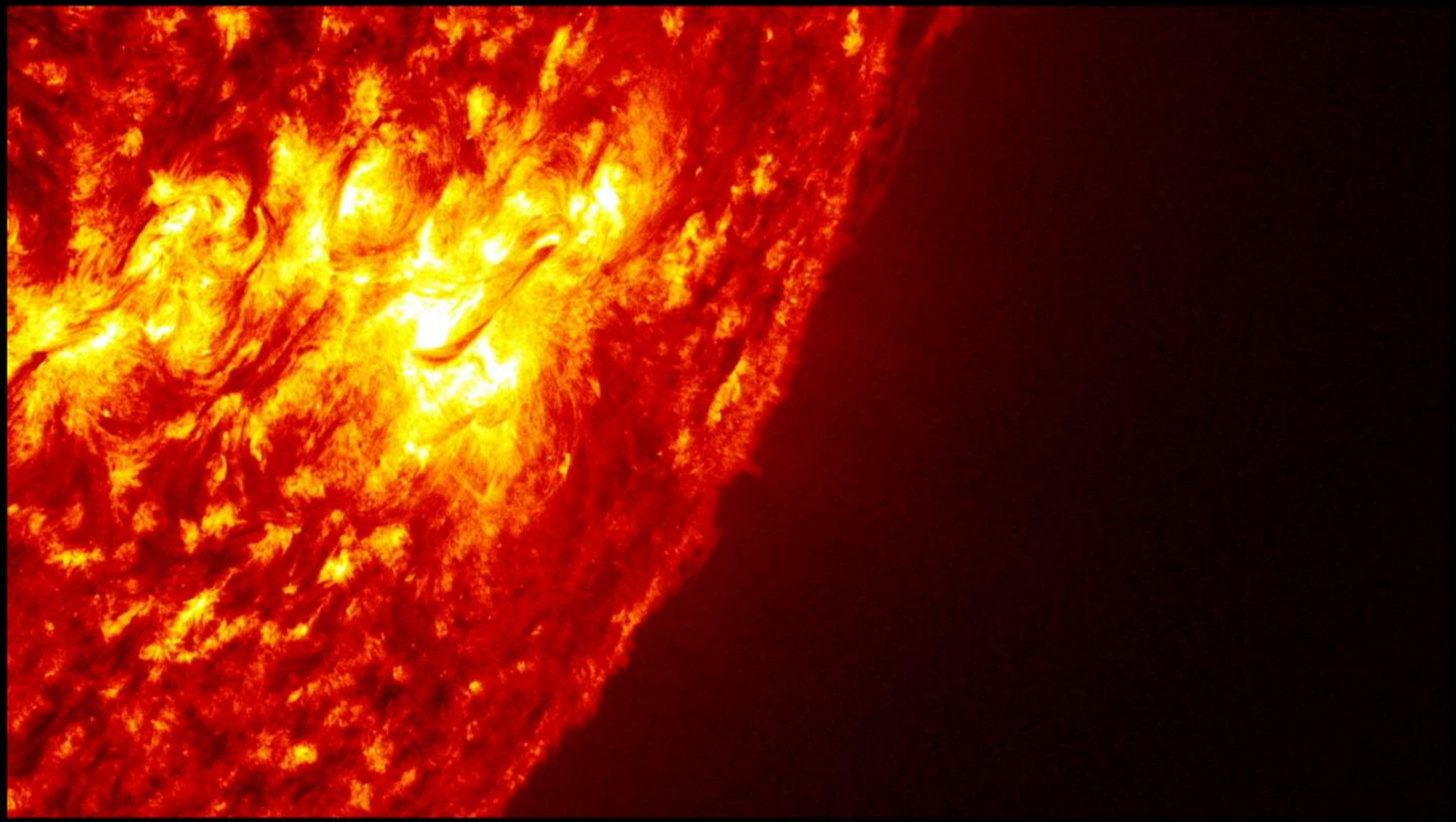

Eruptive event falling back: guided case

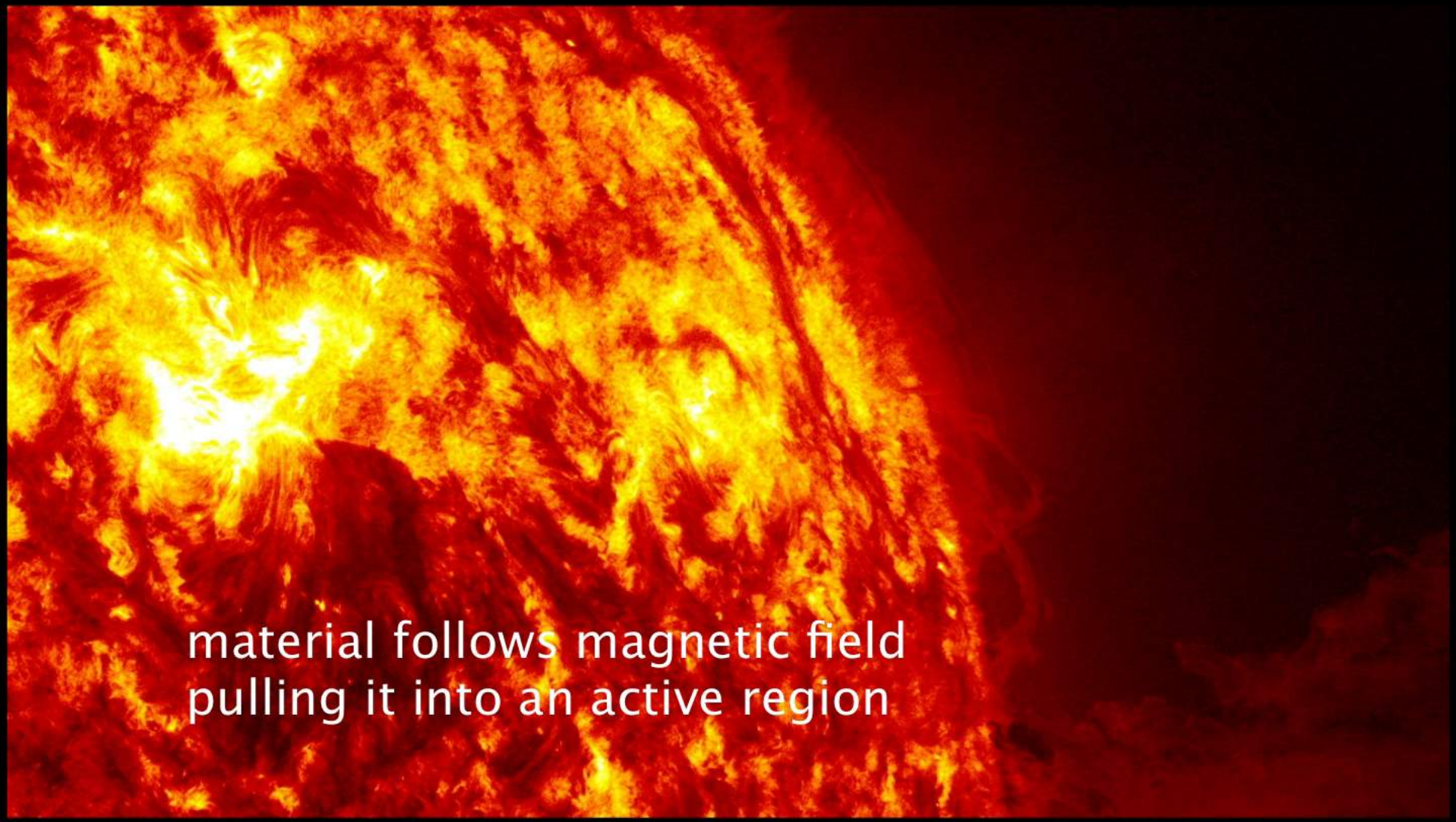

Coronal Mass Ejection (CME)

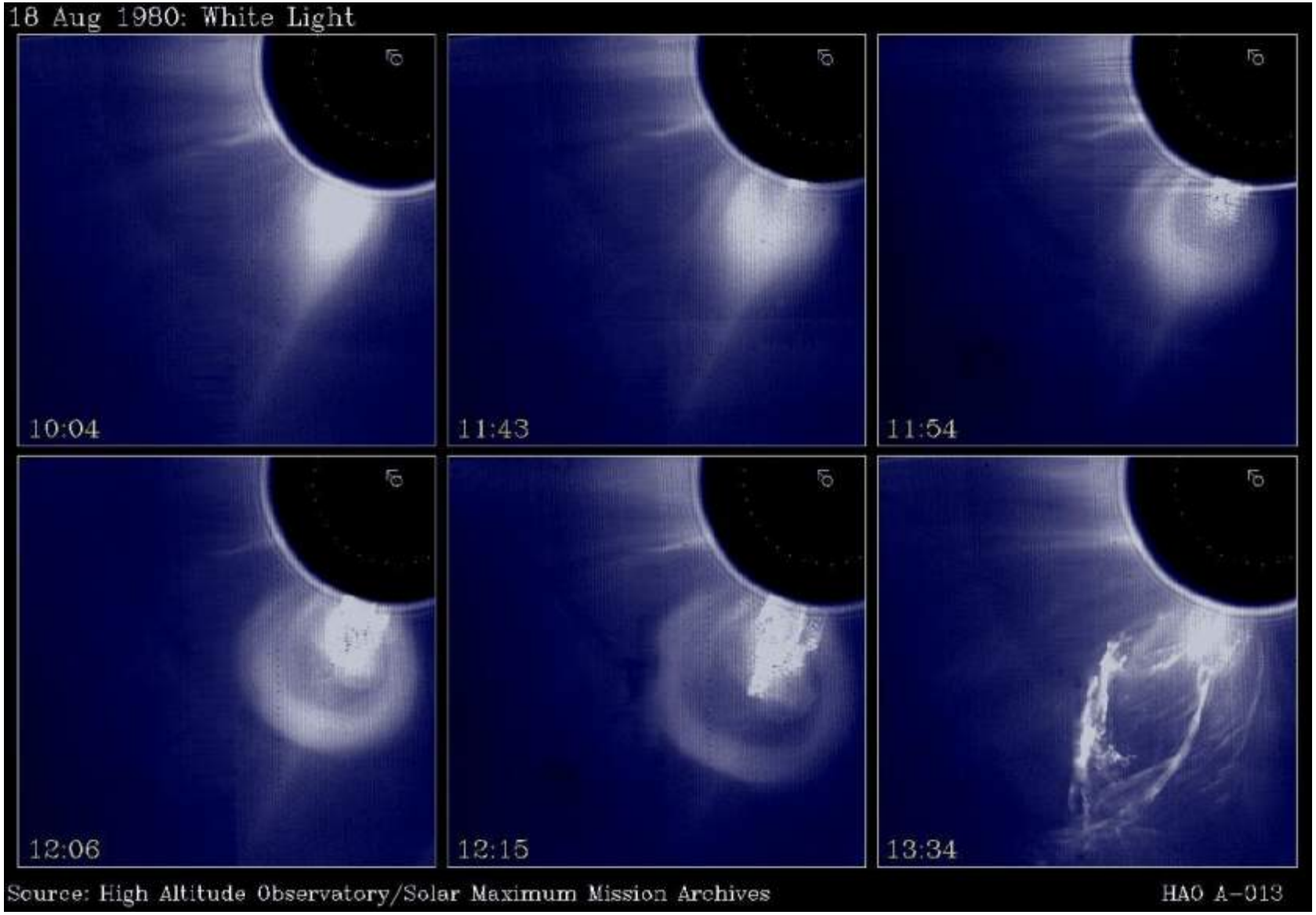

2003 November 18 CME: Enhanced LASCO C2 Images

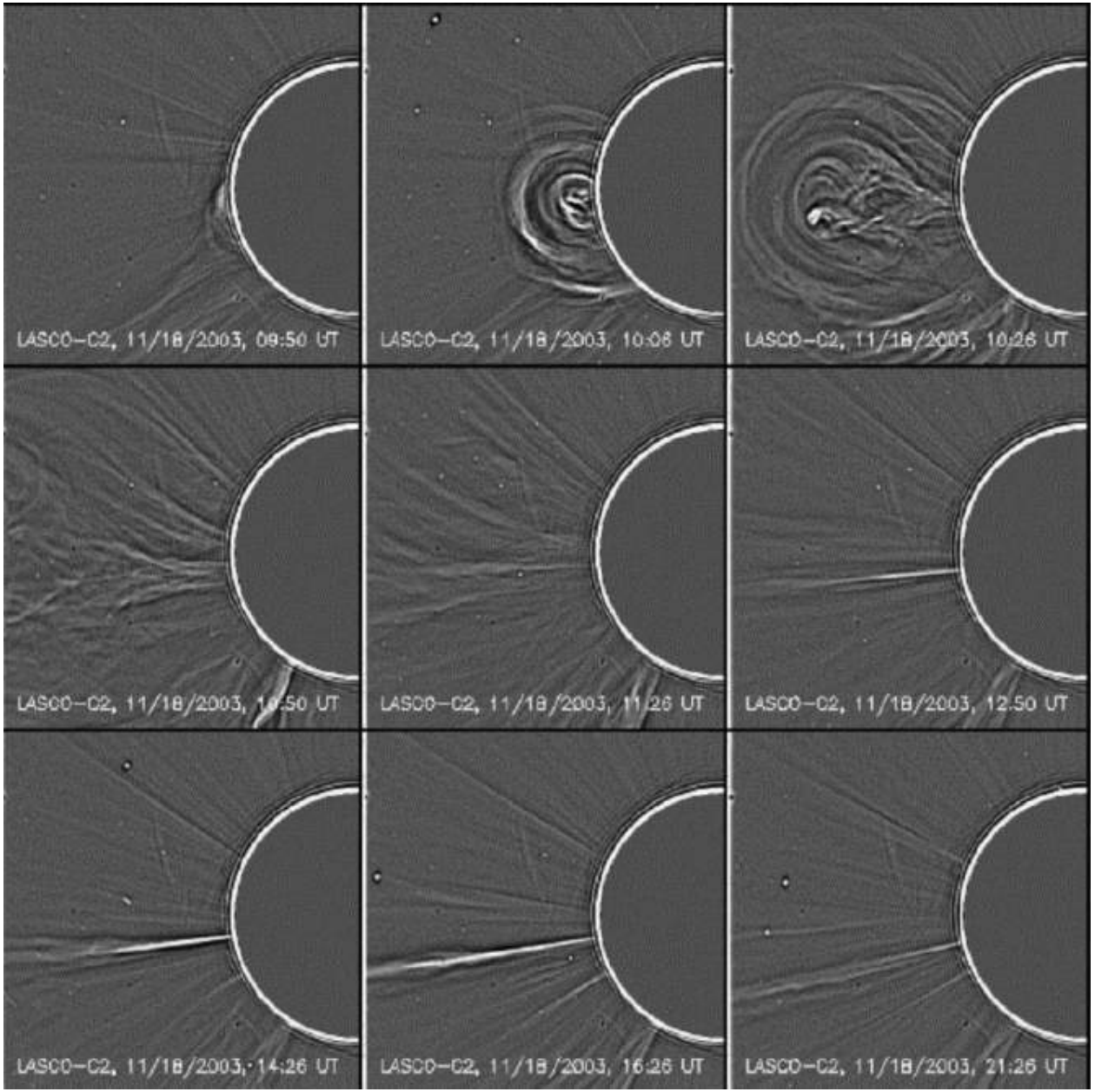

Lin, J., Ko, Y.-K., Sui, L., Raymond, J. C., Steinborg, G. A., Jiang, Y., Zhao, S. & Mancuso, S., 2005, Ap. J. 622, 1251

CME Speed vs. Flare Occurrence

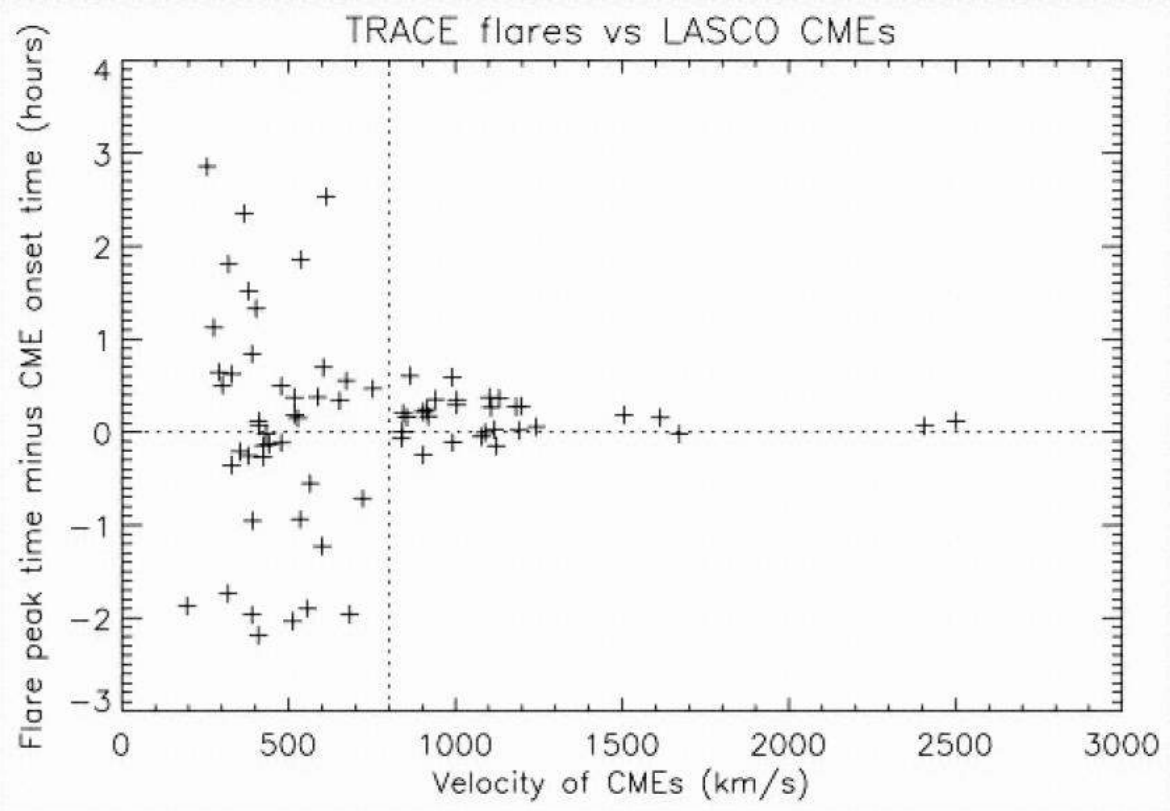

Inverse polarity

Normal polarity

Magnetic Reconnection (2D)

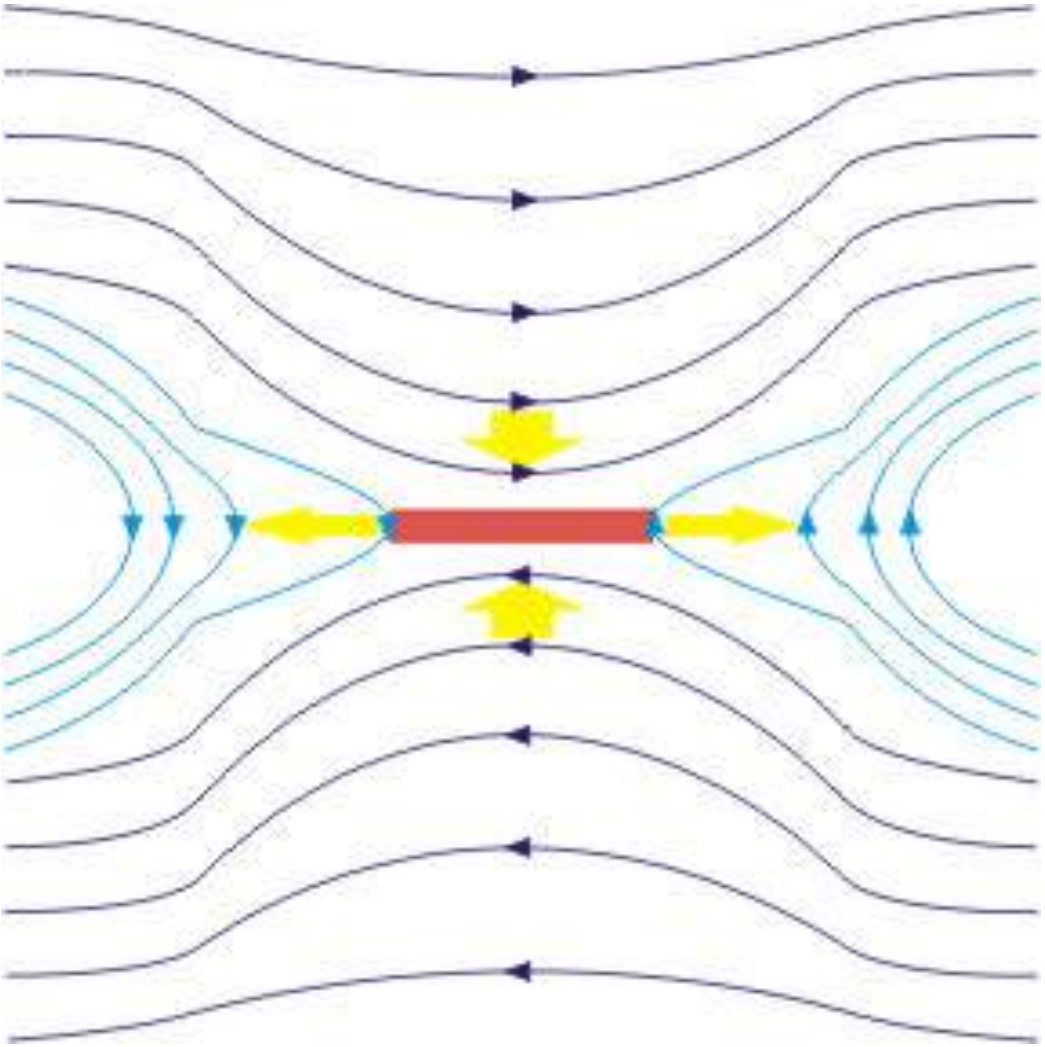

Sweet-Parker

Petschek

Interacting Loops

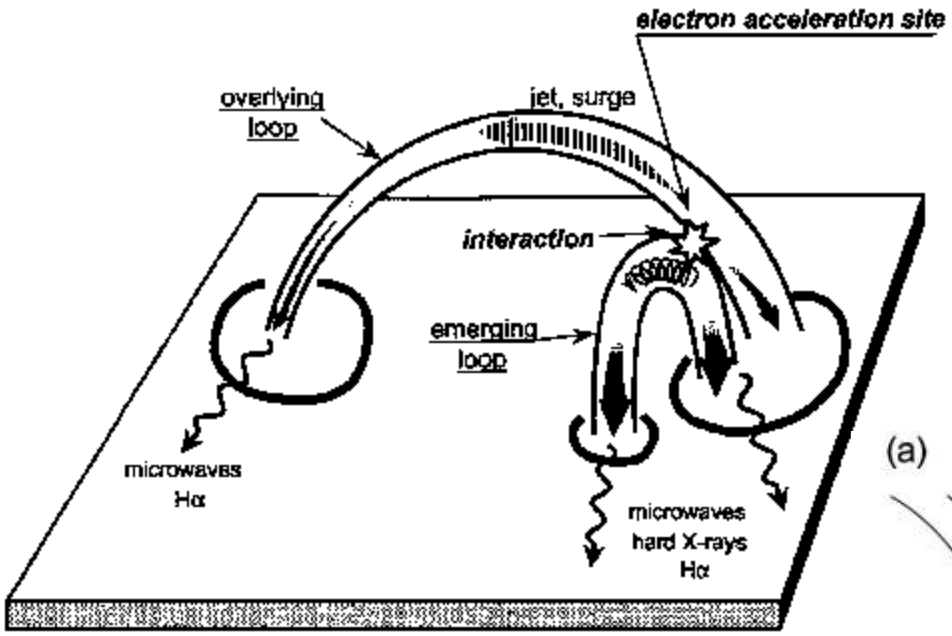

Takasaki et al., *The Astrophysical Journal*, 2004

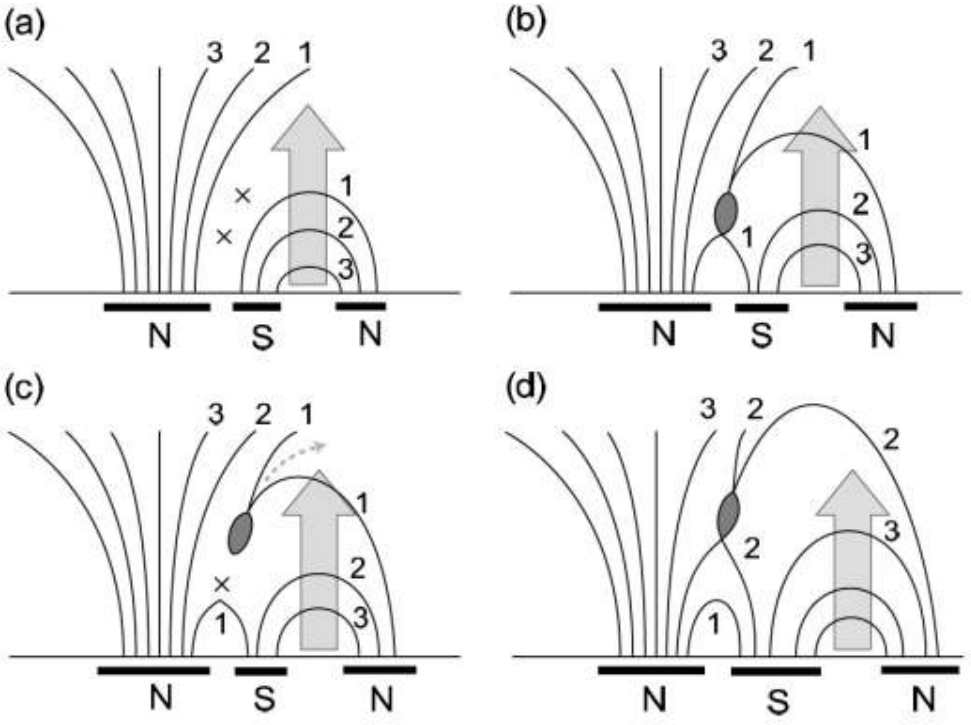

Hanaoka, *Publications of the Astronomical Society of Japan*, 1999

The “Standard” Model for Eruptive Flares

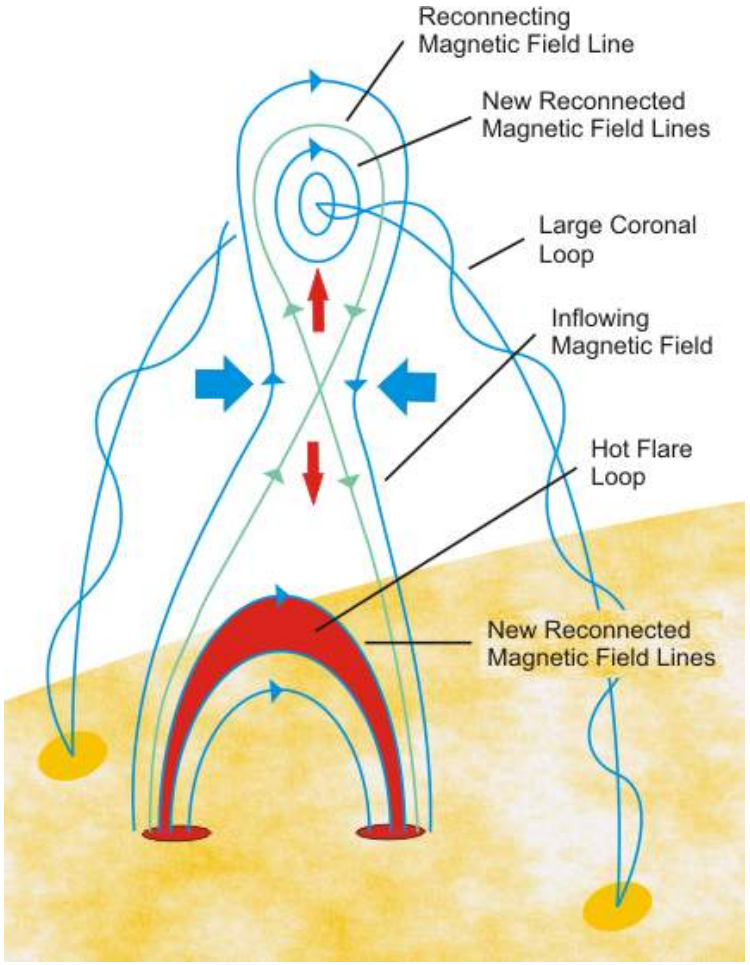

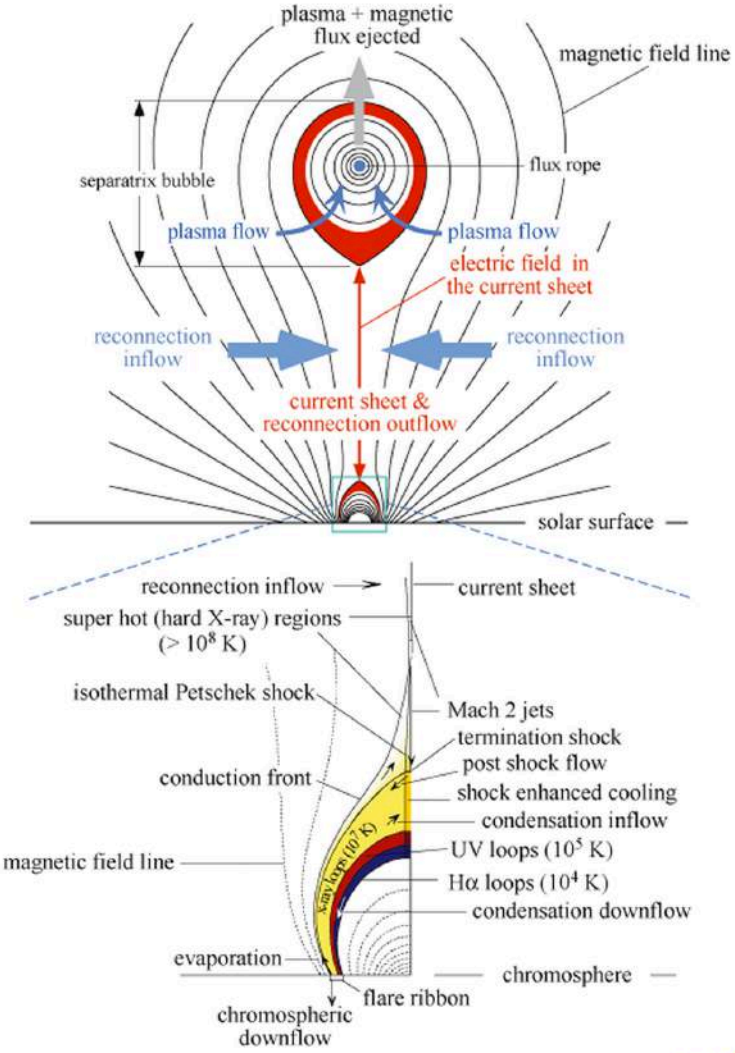

Figure 21: Schematic diagram of a disrupted magnetic field that forms in an eruptive process (Lin, 2004). Catastrophic loss of equilibrium, occurring in a magnetic configuration including a flux rope, stretches the closed magnetic field and creates a Kopp–Pneuman-type structure. This diagram is created by incorporating the traditional two-ribbon flare model (bottom), from Forbes and Acton (1996) with the CME model (top) of Lin and Forbes (2000). Colors denote the different hierarchies of plasma in the configuration. Image reproduced with permission from Lin (2004), copyright by Springer.

15 July 2002 Flare

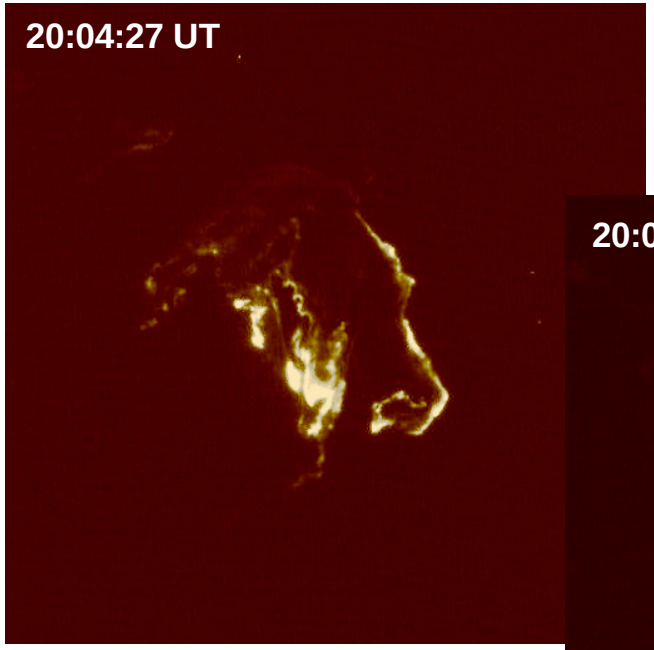

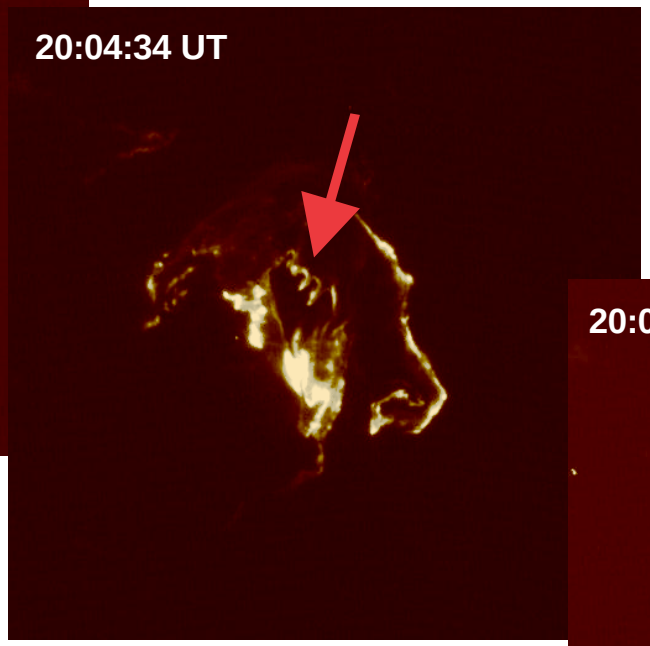

TRACE 1600 Å Images
$T \sim 10^5$ K

Magnetic reconnection
or kink instability?

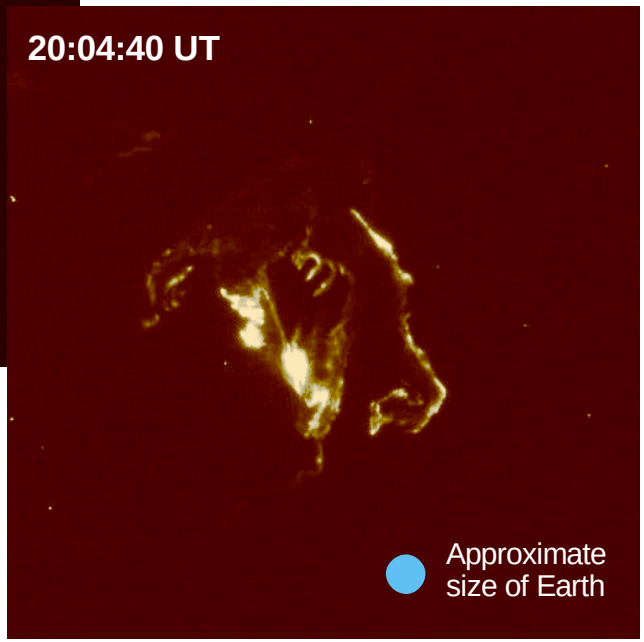

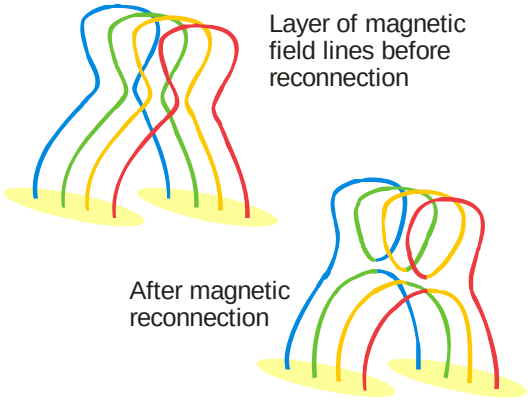

1 possible reconnection model

Thermodynamic MHD simulation of the Bastille Day event

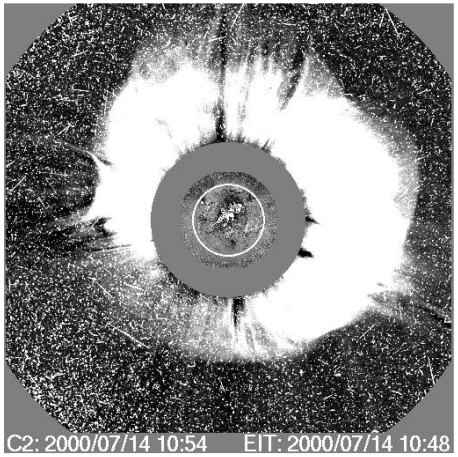

SOHO/LASCO C2

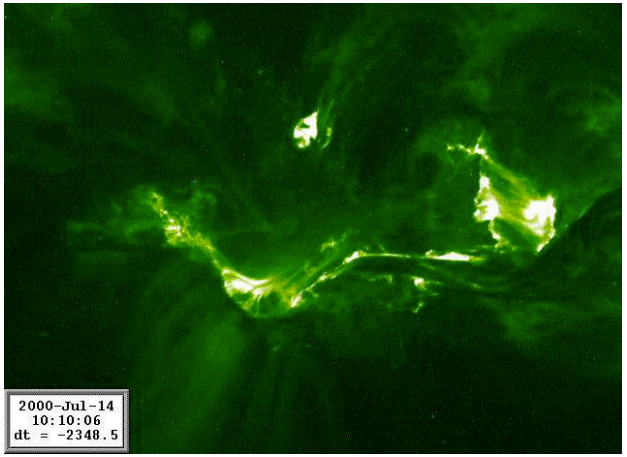

TRACE 195 Å

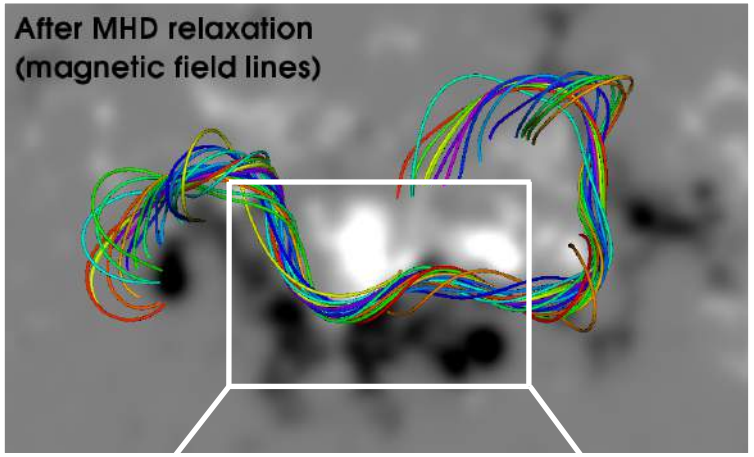

inserted flux rope

X5.7 flare & geo-effective halo CME on 2000 July 14

1.) calculate steady-state corona & solar wind

2.) construct stable flux rope in active region

3.) trigger eruption by ad-hoc converging flows

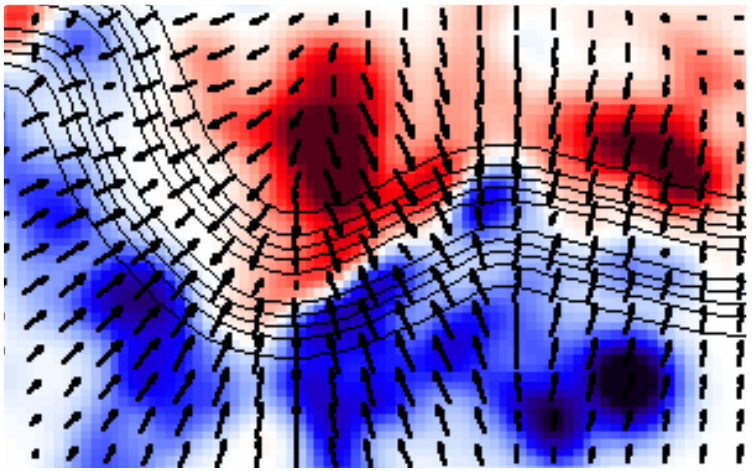

converging flows

Thermodynamic MHD simulation of the Bastille Day event

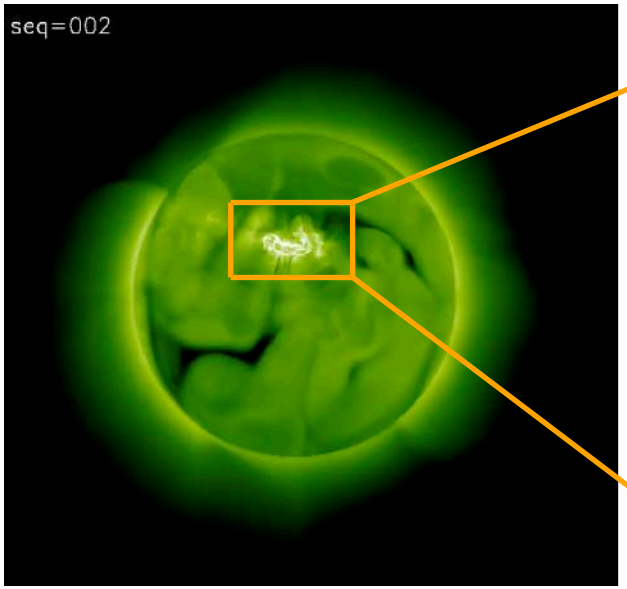

SOHO/EIT 195 Å
(synthetic emission;
full-disk view)

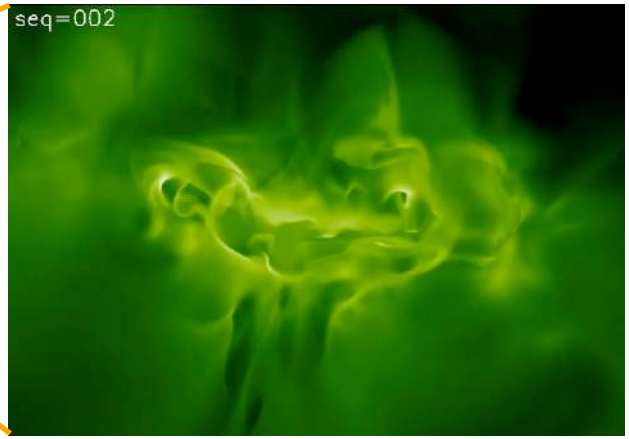

SOHO/EIT 195 Å
(active region)

polarization brightness
running ratio
(synthetic emission;
3-20 solar radii)

Courtesy of T. Torok, Predictive Sciences Inc.

- synthetic satellite images allow direct comparison with observations
- flare arcade and halo-CME morphologies qualitatively reproduced
- CME core speed ≈ 1500 km/s & kinetic energy ≈ 4 x 10^{32} ergs
- provides quantities that cannot be observed directly (e.g. 3D magnetic field, V_a)

Heliospheric simulation of the Bastille Day event

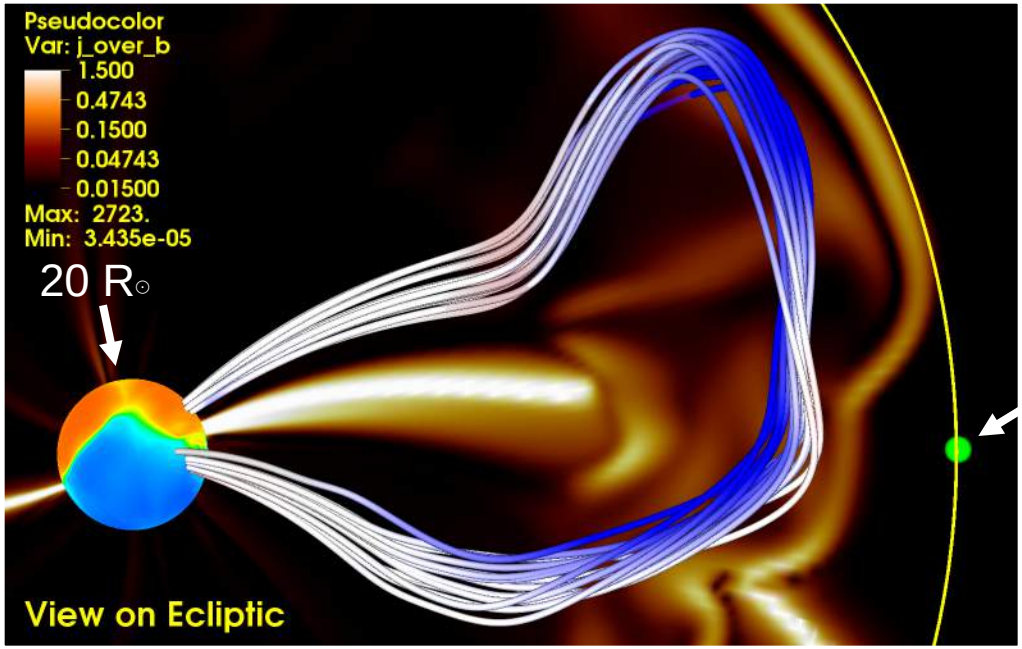

model ICME core & electric currents in ecliptic plane

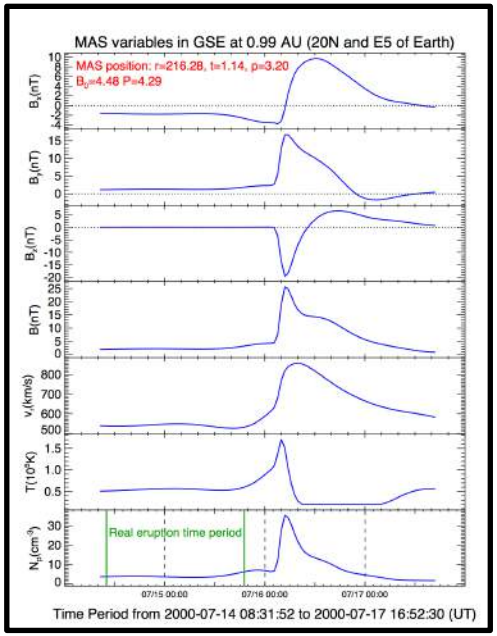

synthetic data at 1 AU

Courtesy of T. Torok, Predictive Sciences Inc.

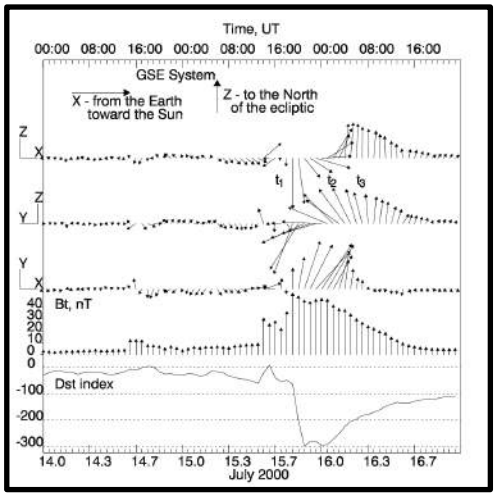

Yurchyshyn *et al.* (2001)

- CME propagated out to 1 AU (simpler equations)
- flux rope structure largely preserved, but front distorted
- comparison simulation to 1 AU data (specifically B_z)

→ difficult to match quantitatively (flux rope distortion)

Idealized model: setup

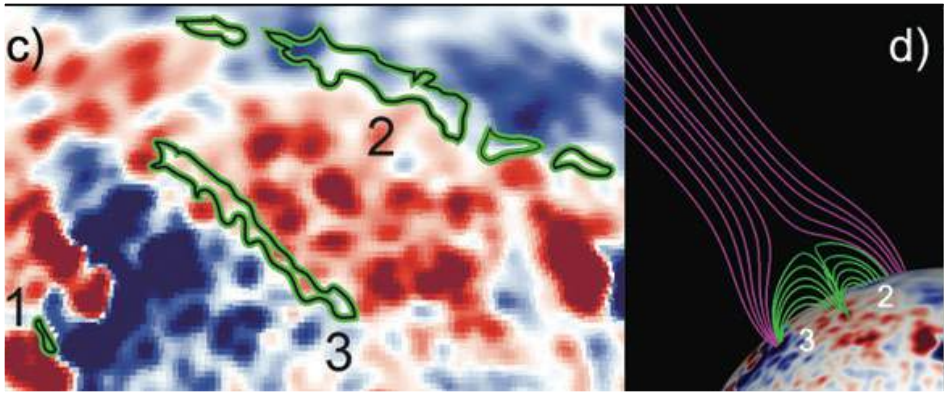

Courtesy of T. Torok, Predictive Sciences Inc.

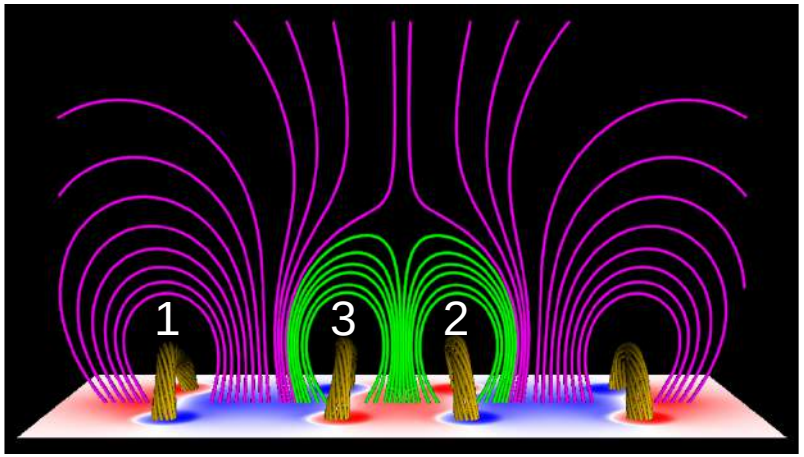

Török *et al.* (2011)
(see also Lynch & Edmondson 2013)

observational constraints:

- filaments approximately aligned, but different in size
- filaments 2 and 3 located in "tri-polar" region within lobes of a pseudostreamer
- order of eruptions different from filament "order" (would expect 1→ 3 → 2)

model simplifications:

- ignore details of magnetogram (e.g., field strengths & exact flux distribution)
- core field (flux ropes) similar & ambient field symmetric
- ignore size, chirality, and exact alignment of filaments
- zero-beta & ideal MHD equations (reconnection only due to num. diffusion)

Idealized model: results

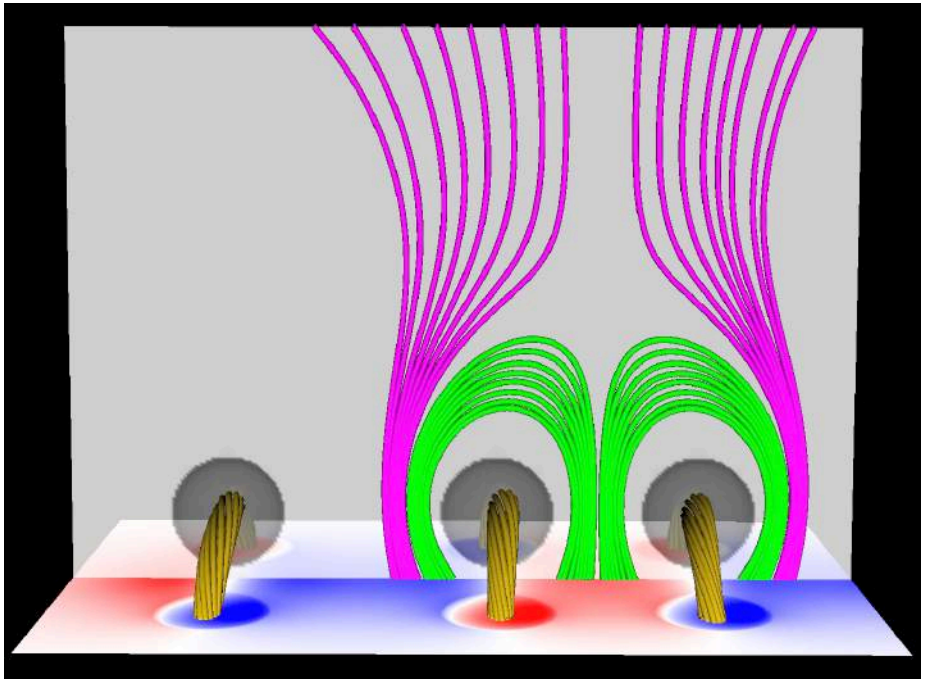

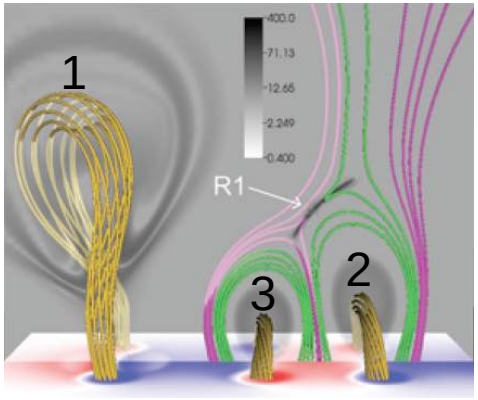

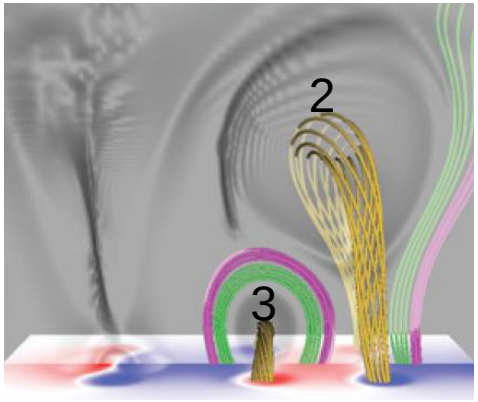

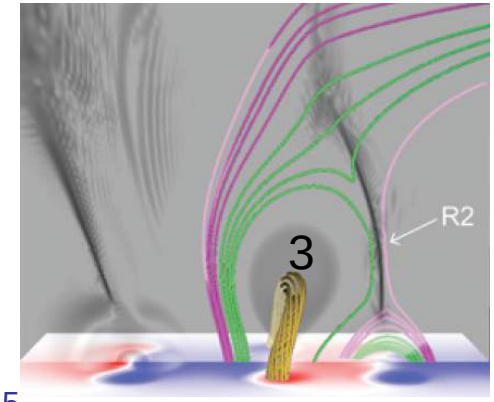

- initiate eruption of flux rope 1 by converging flows (ad-hoc)
- eruption leads to two consecutive reconnection events, each of which triggers a new eruption

R1: “breakout” reconnection at pseudostreamer separator

R2: “flare” reconnection in the wake of erupting FR 2

Idealized model: results

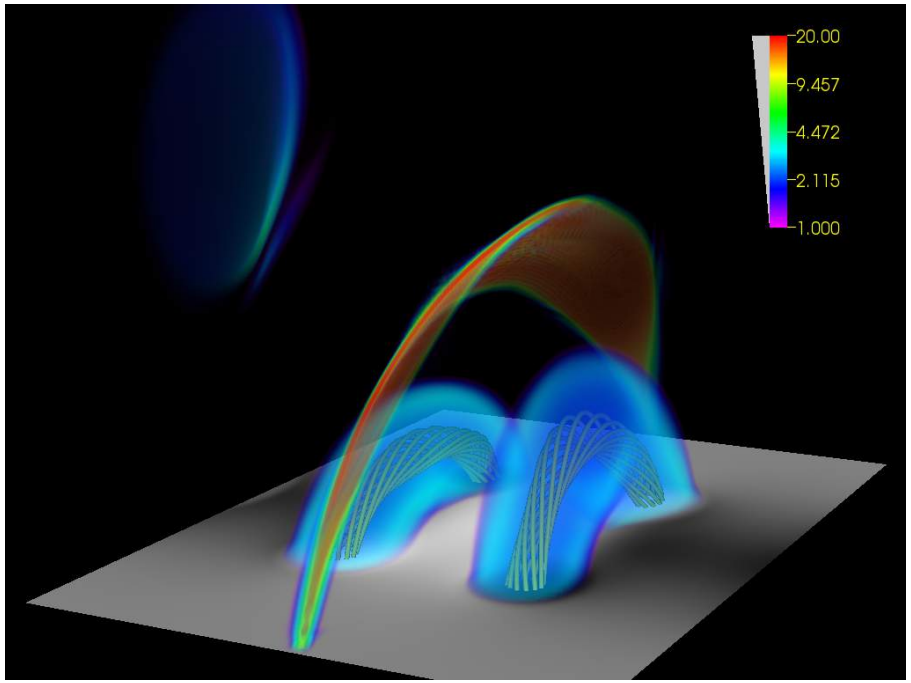

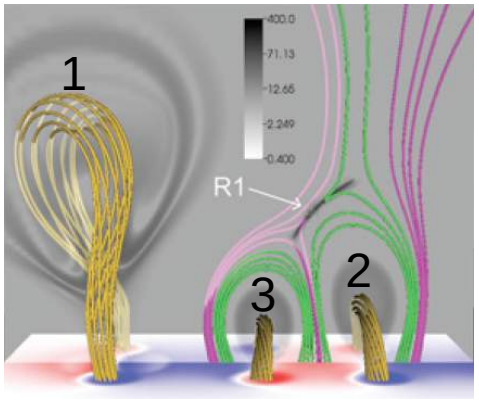

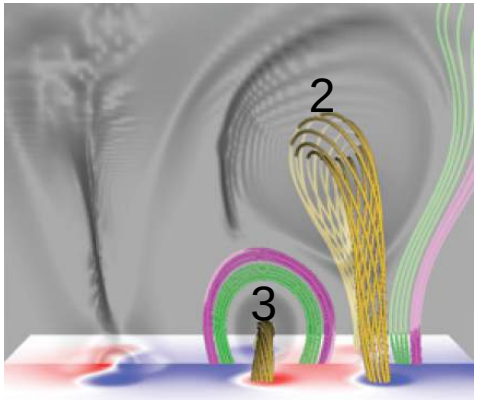

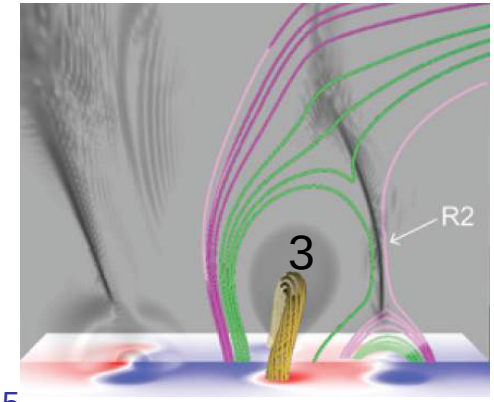

- initiate eruption of flux rope 1 by converging flows (ad-hoc)
- eruption leads to two consecutive reconnection events, each of which triggers a new eruption

R1: “breakout” reconnection at pseudostreamer separator

R2: “flare” reconnection in the wake of erupting FR 2

“Realistic” simulations: 2010 August 1-2 (ongoing)

Courtesy of T. Torok, Predictive Sciences Inc.

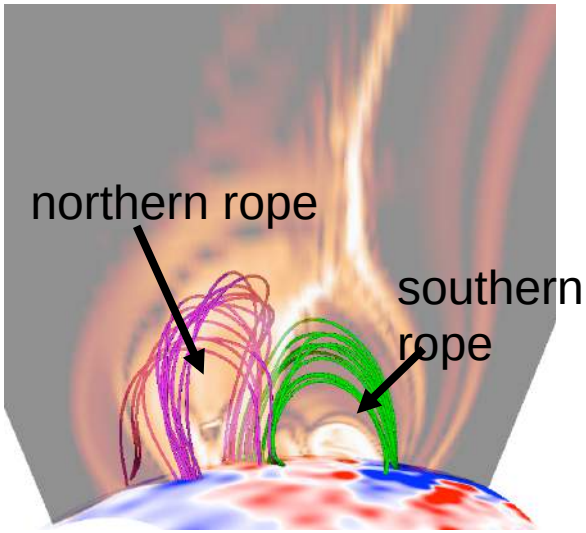

prior to eruption:
flux ropes below PS lobes (magenta and green)

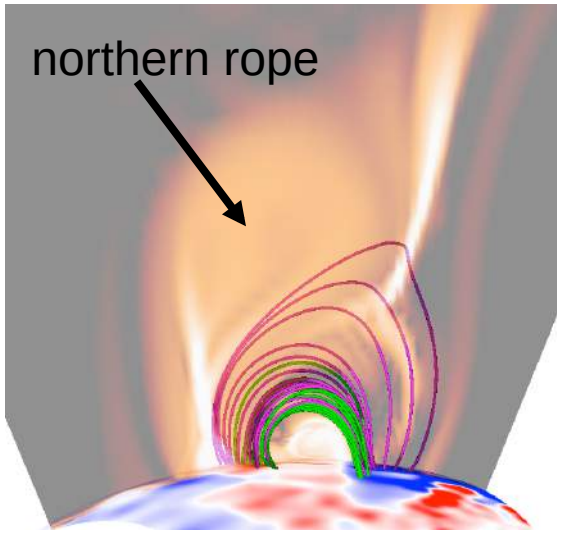

1st eruption (northern):
magenta flux transferred to southern rope

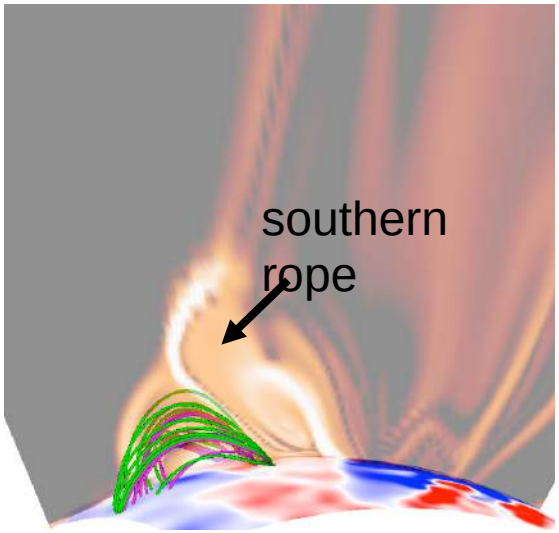

2nd eruption (southern):
magenta (and green) flux transferred back

- supports idealized model scenario (realistic, less symmetric magnetic field)
- next steps: include eruption outside PS and run thermodynamic case

Thermodynamic MHD modeling of the corona

Courtesy of T. Torok, Predictive Sciences Inc.

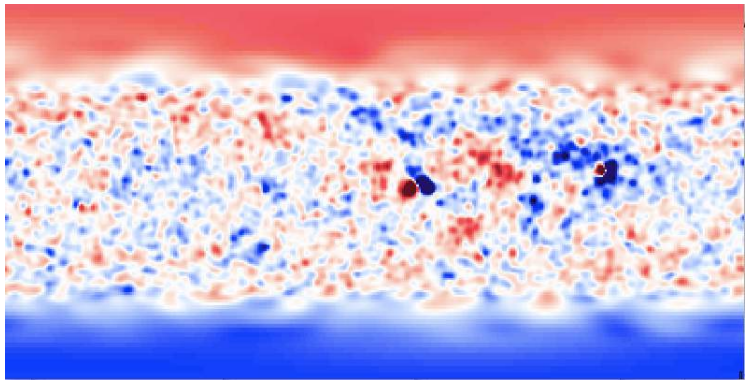

CR 2071 (June 9 - July 6, 2008)

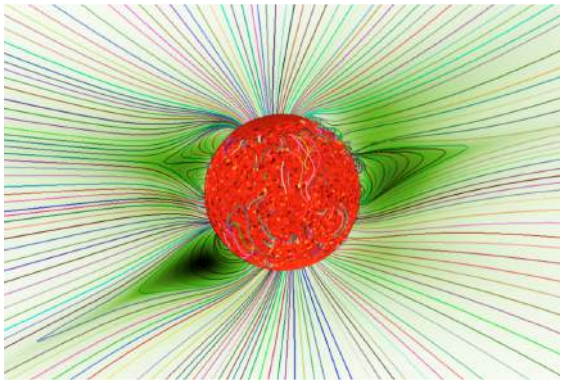

- potential field from (filtered) synoptic map
- MHD relaxation to steady-state including solar wind
- advanced energy equation:
  - parallel thermal conduction
  - radiative losses
  - coronal heating (empirical)

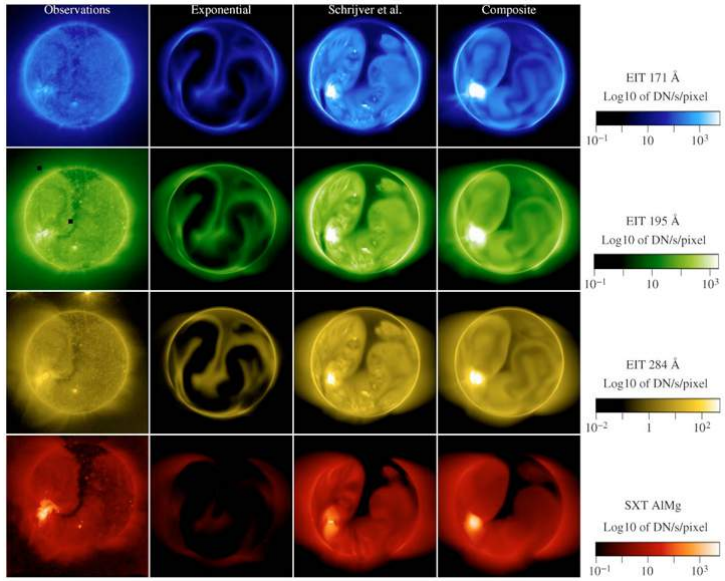

Lionello *et al.* (2009)

→ realistic coronal density & temperature

Forecasting in the Solar Case: CME's

CMEs and Sigmoid Features

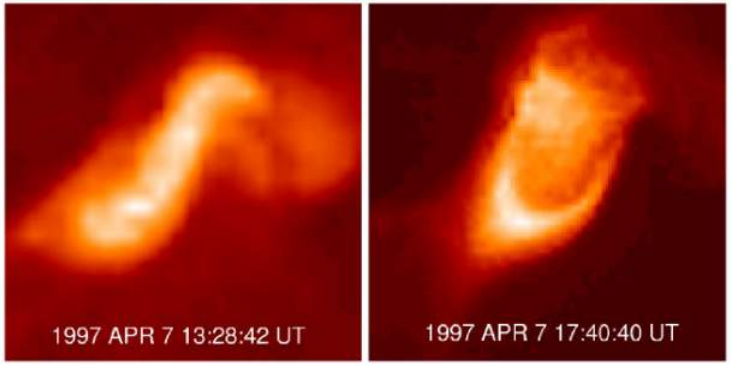

1. Sigmoid structures are often seen in Soft X-Rays (SXRs) prior to the onset of CMEs.
2. They are more apparent in SXT (SXR) than EIT (EUV) images (hotter features).
3. Regions sigmoid prior to the eruption evolve into un-sheared arcades or cusp after the eruption.
4. The position of the footpoints changes after the eruption.
5. Dimming regions associated with the sigmoid-feature eruptions are seen in and the associated mass is an order of magnitude (or more) less than of a typical CME.

Key Questions

1. Not all front-side CMEs are associated with sigmoids or other SXR event.
2. It is still not possible to know if a sigmoid is going to produce a CME or not. Or when it is going to erupt.
3. Another outstanding question is whether the sigmoid regions are sources for the entire CME, or only for one portion of the structure.

The Process

1. The magnetic field stores energy via helicity, producing S-shaped loops called a *sigmoid*.
2. At some point, this sigmoid becomes unstable and erupts. Losing some of its complexity or even disappearing completely.

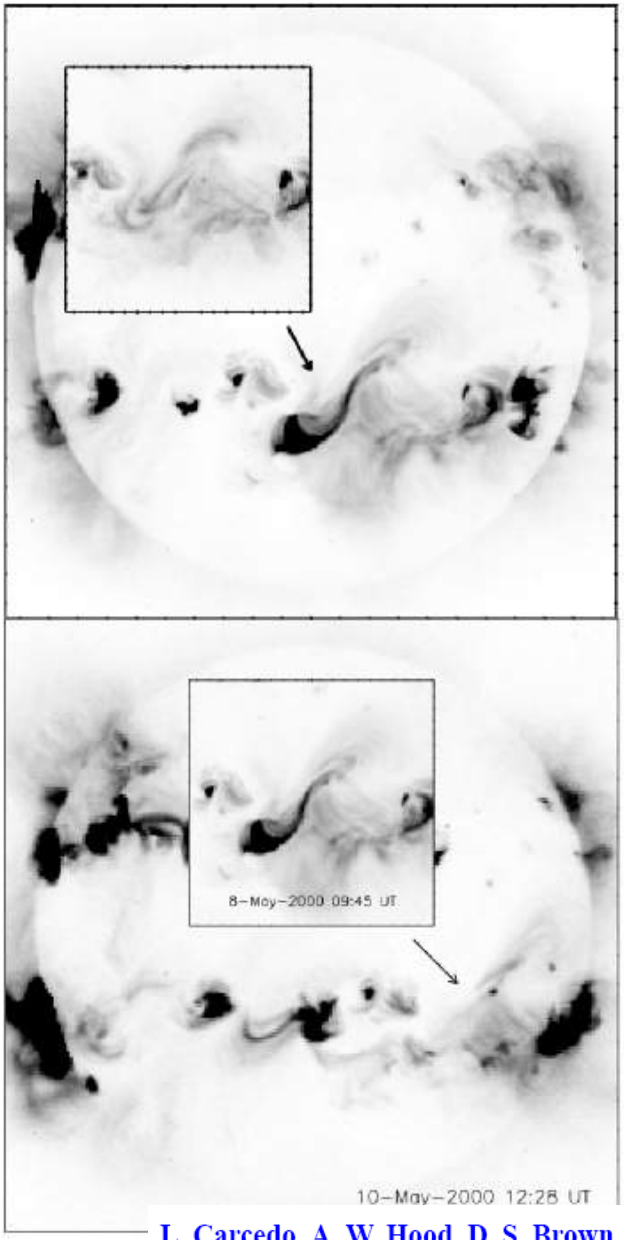

L. Carcedo, A. W. Hood, D. S. Brown

Forecasting in the Solar Case: Coronal Holes

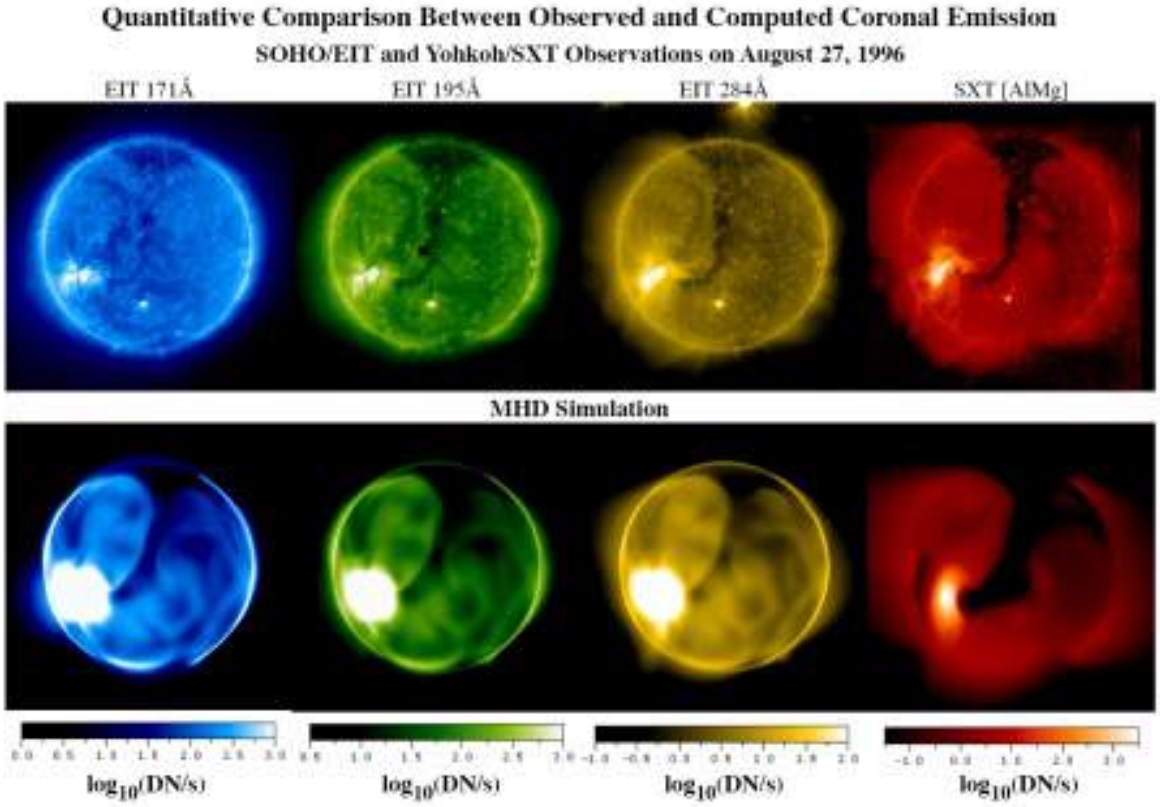

Mikic et al. 2006 (Whole Month Sun 3)

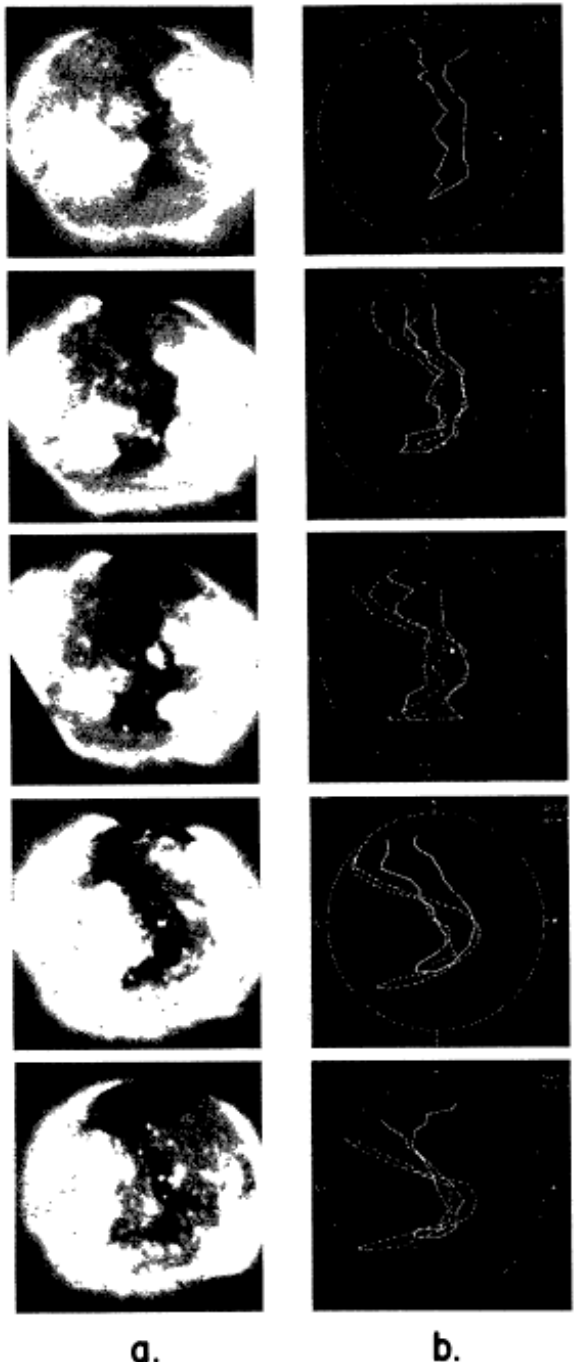

Fig. 9. Comparison of the position of CH1 as seen (a) in soft X-ray wavelengths 3–32 Å and 44–54 Å and (b) its extrapolated position calculated using the Newton and Nunn (1951) differential sunspot rotation rates. Images are shown in five successive rotations for: (i) June 1, 1973; (ii) June 28, 1973; (iii) July 25, 1973; (iv) August 21, 1973; and (v) September 28, 1973. The solid line on each schematic represents the outline of the hole as measured on that rotation, the dotted line shows the extrapolated position of the hole measured on the first rotation and rotated through the appropriate time interval.

Timothy et al. 1975

Well-studied example: 2010 August 1-2

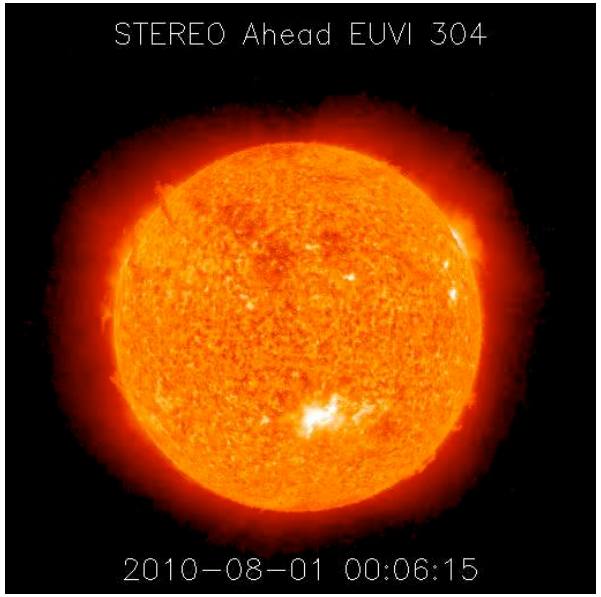

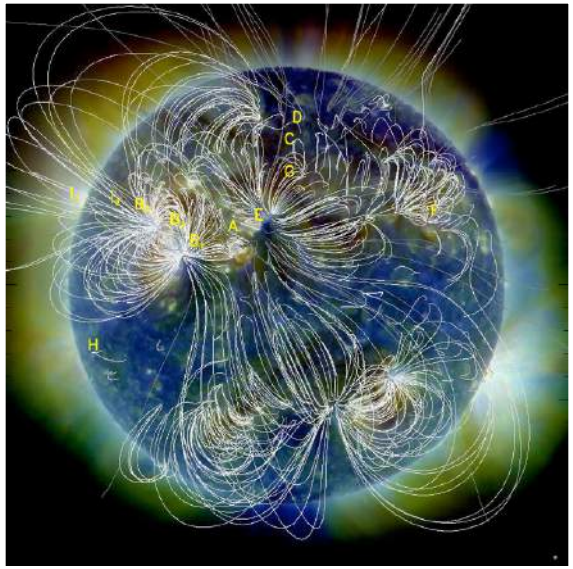

SDO/AIA composite + PFSS

Schrijver & Title (2011)

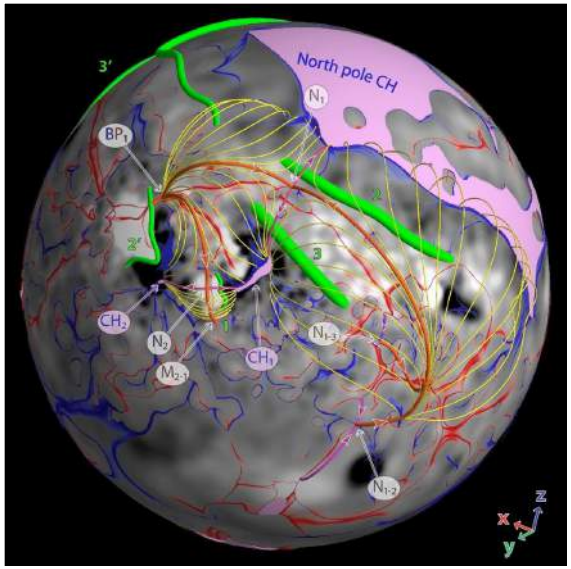

Titov *et al.* (2012)

Courtesy of T. Torok, Predictive Sciences Inc.

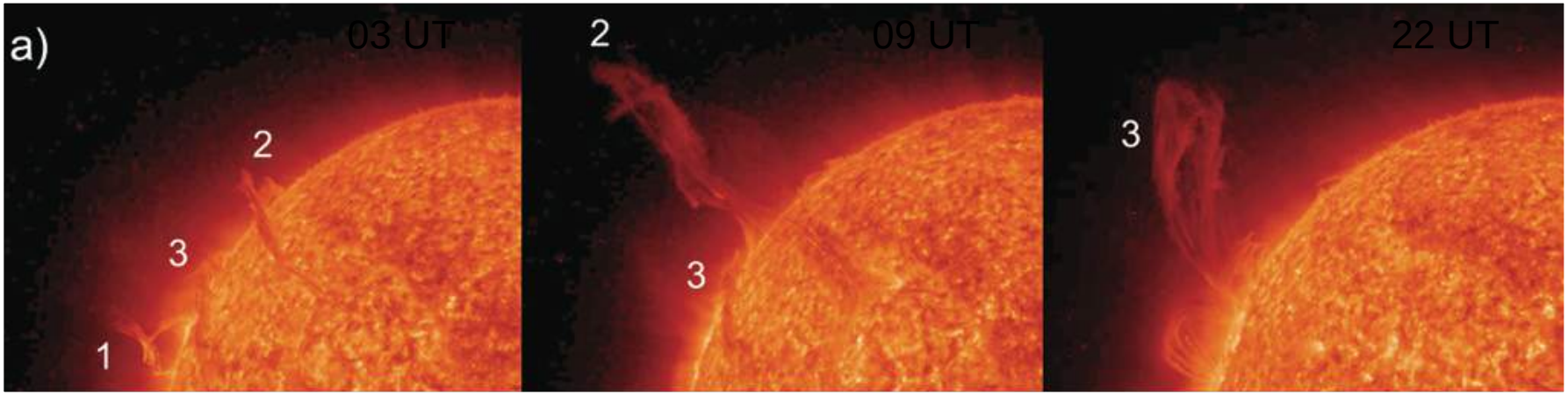

“Realistic” simulations: 2010 August 1-2 (ongoing)

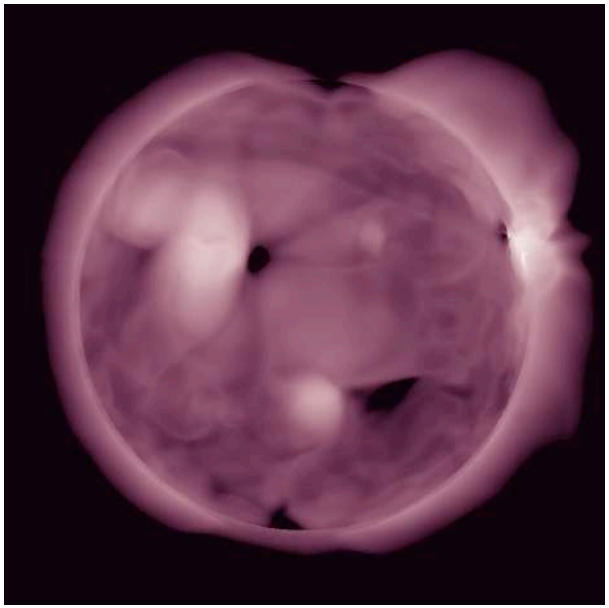

SDO/AIA 211 Å
(simulated emission)

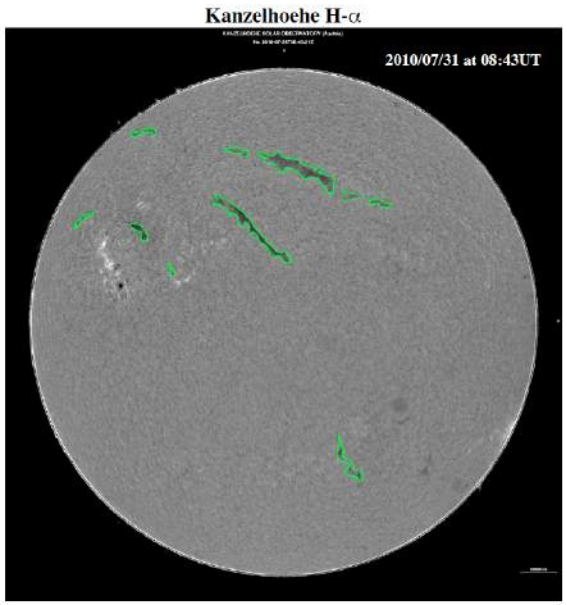

Hα filaments

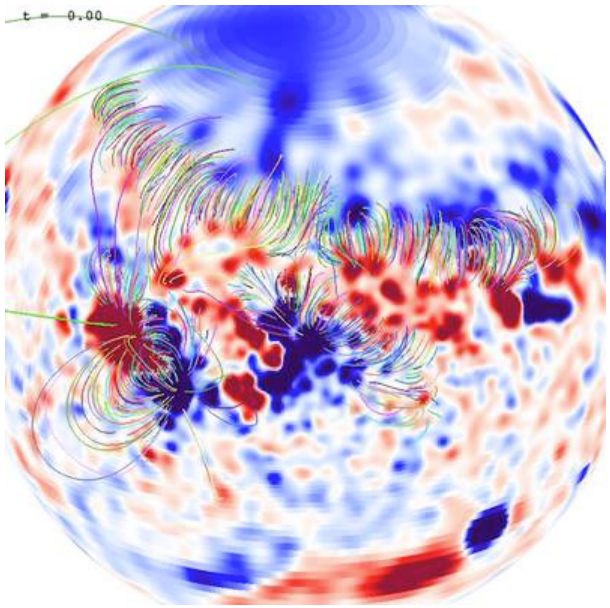

Flux rope eruptions
(so far zero-beta)

Courtesy of Zoran Mikić (PSI)
Courtesy of T. Torok, Predictive Sciences Inc.

- produce thermodynamic MHD solution of corona based on magnetograms
- construct stable flux ropes in regions involved in sequence (complicated!)
- northern flux-rope eruption initiated ad-hoc (via flux cancellation)
- southern flux-rope eruption triggered, but a bit too wimpy so far

Are (some) solar eruptions coupled ("sympathetic") ?

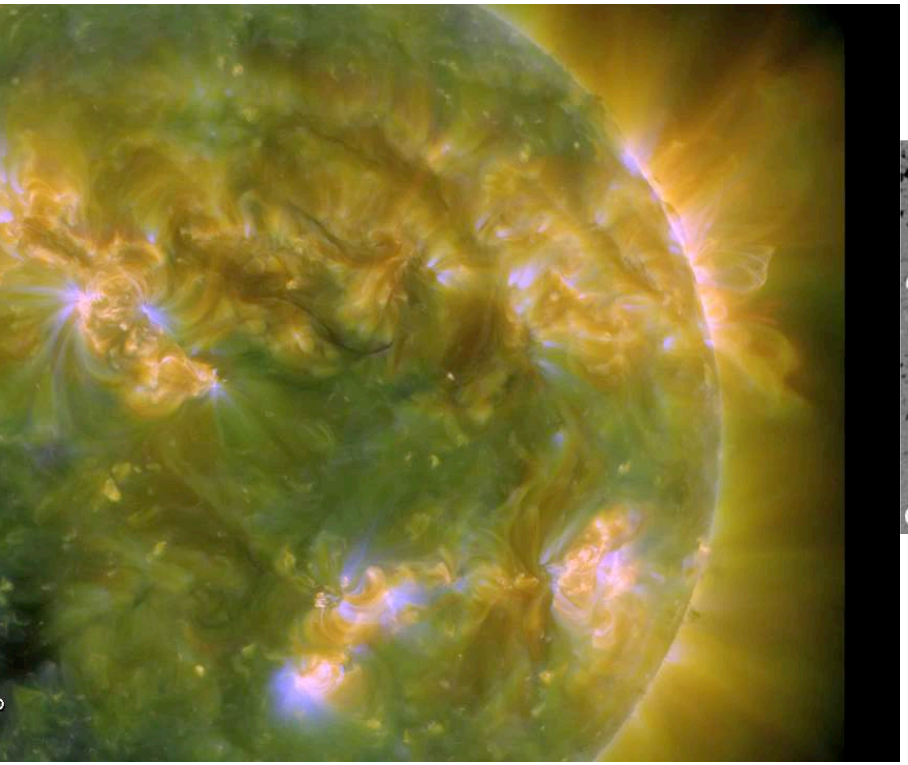

AIA observations on 25 December 2011
(courtesy of C. Schrijver)

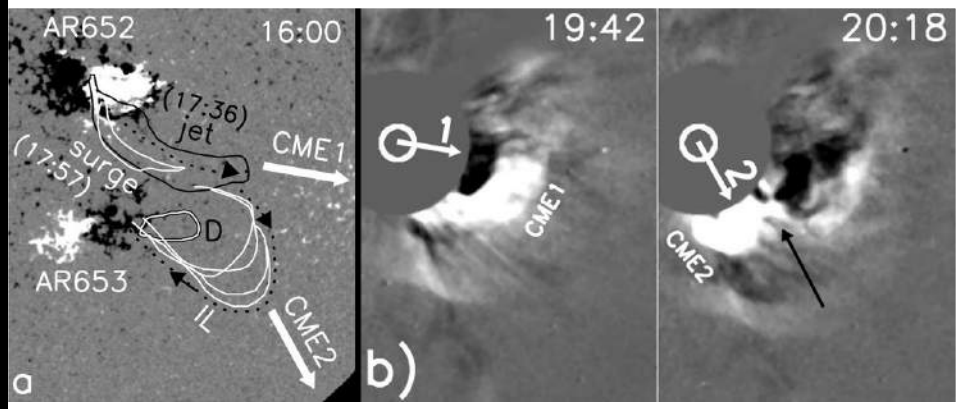

Jiang *et al.* (2008)

Courtesy of T. Torok, Predictive Sciences Inc.

- sympathetic eruptions: near-simultaneous events from different source regions
- statistical studies indicate that such eruptions are sometimes causally linked
  (Wheatland, Moon, et al.)
- various linking mechanisms were suggested (waves, magnetic reconnection, surges, sub-surface connection...), but no models were developed

“Realistic” simulations: 2011 February 15 (ongoing)

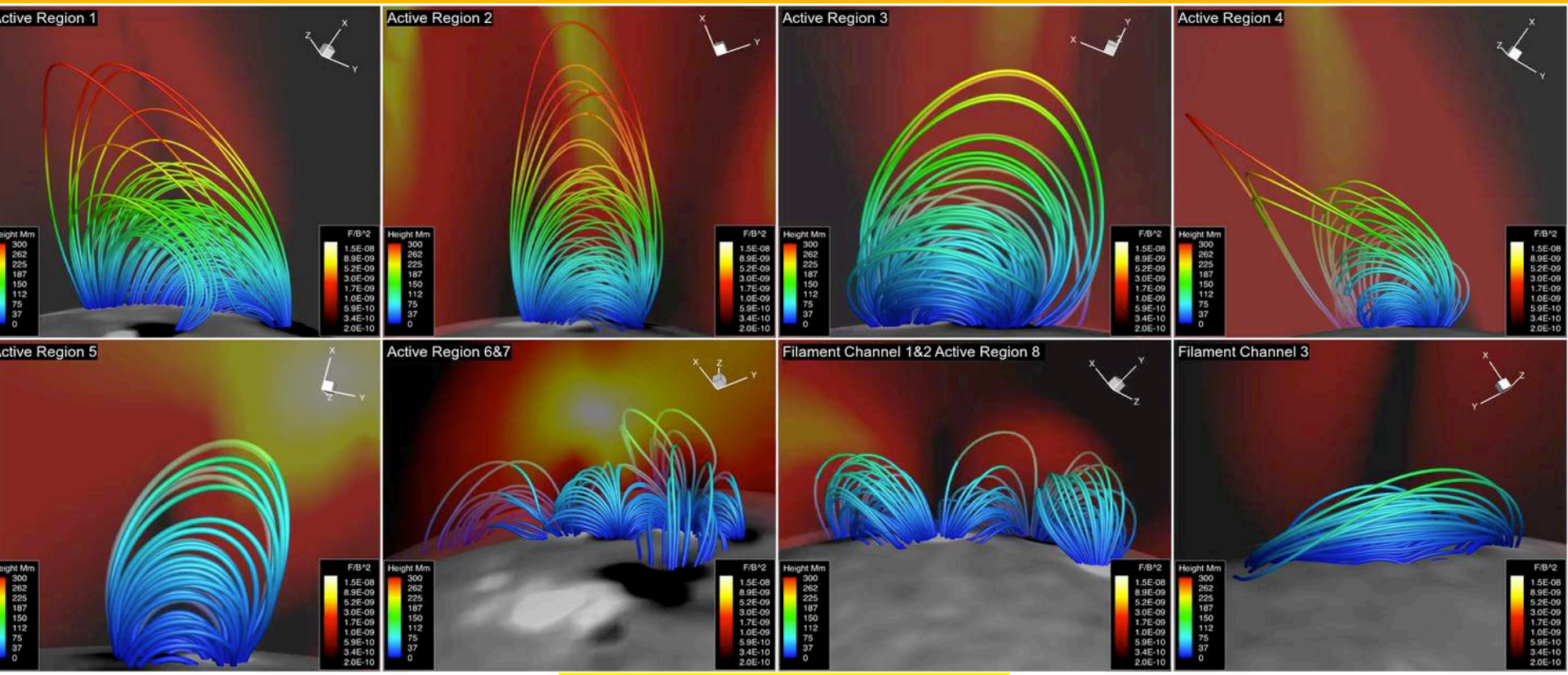

Courtesy of Meng Jin (LMSAL)

Courtesy of T. Torok, Predictive Sciences Inc.

- study impact of CME on those close and remote areas (no flux ropes inserted yet)
- quantify impact using various parameters (decay index, distance, field strength, etc.)
- try to deduce empirical “impact formula” (potential forecast ability)

Éjections Solaires (CME's)

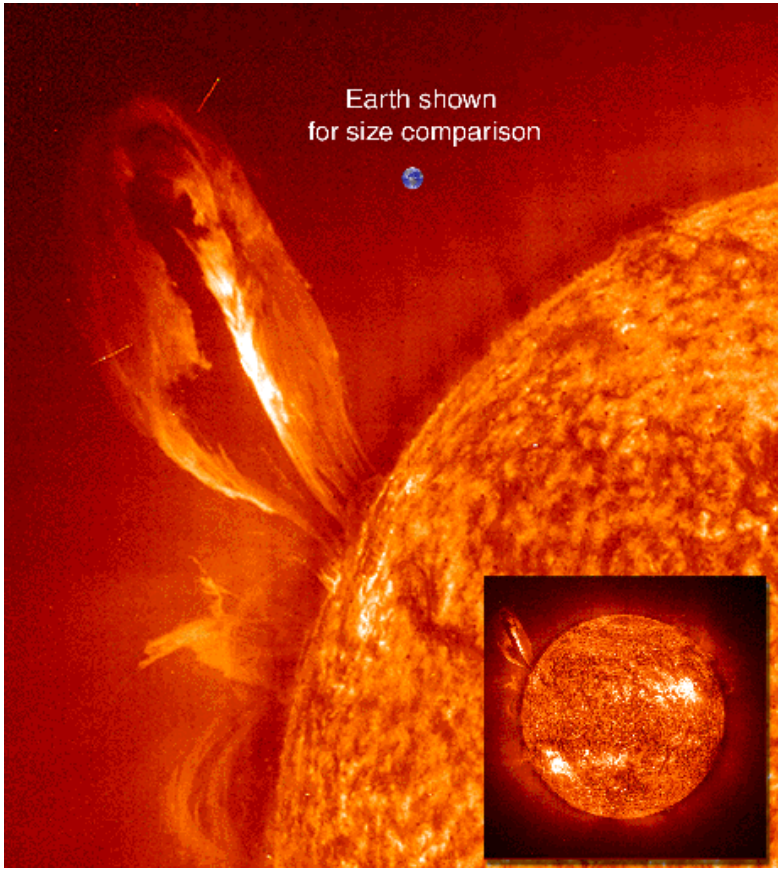

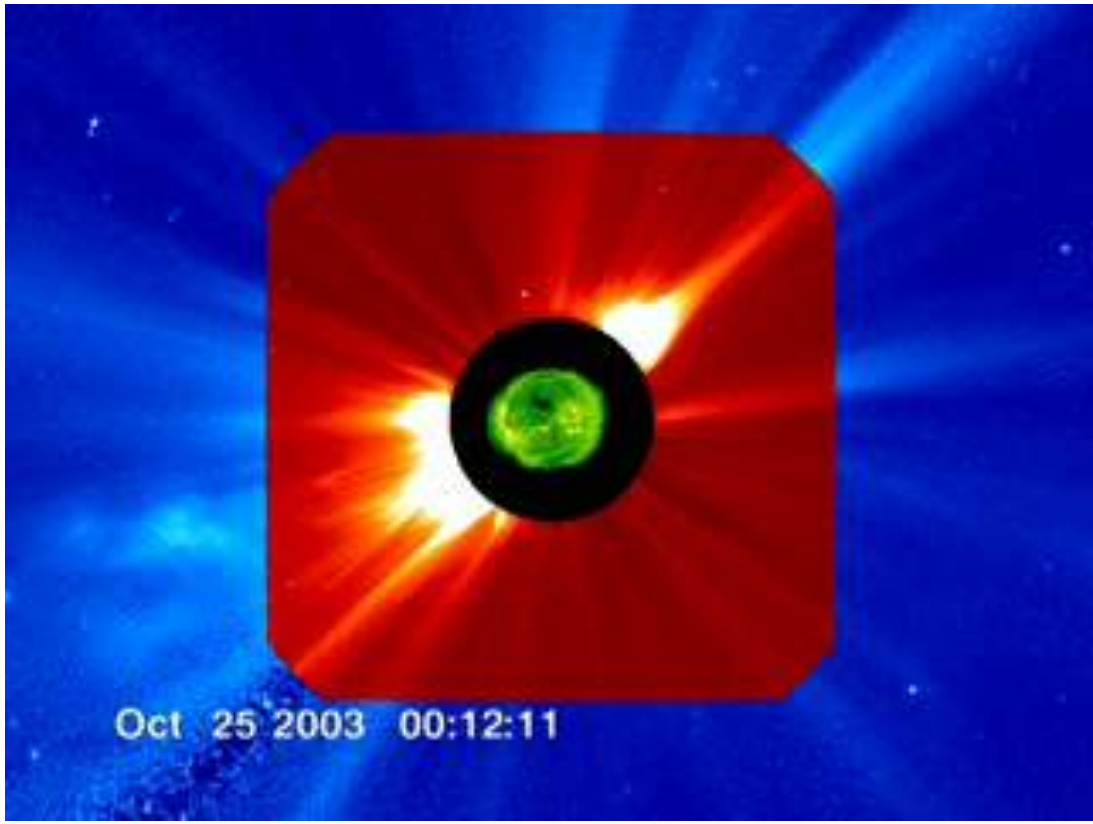

SoHO-EIT & Lasco

“Realistic” simulations: 2011 February 15 (ongoing)

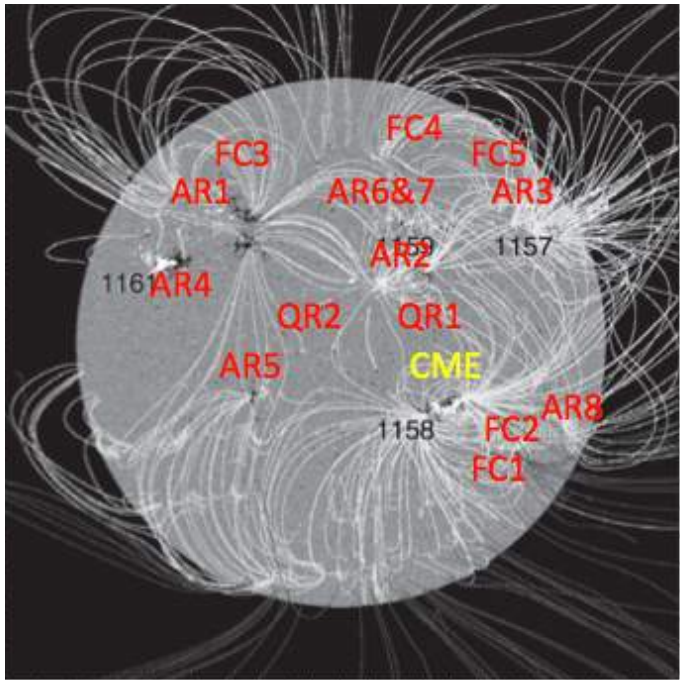

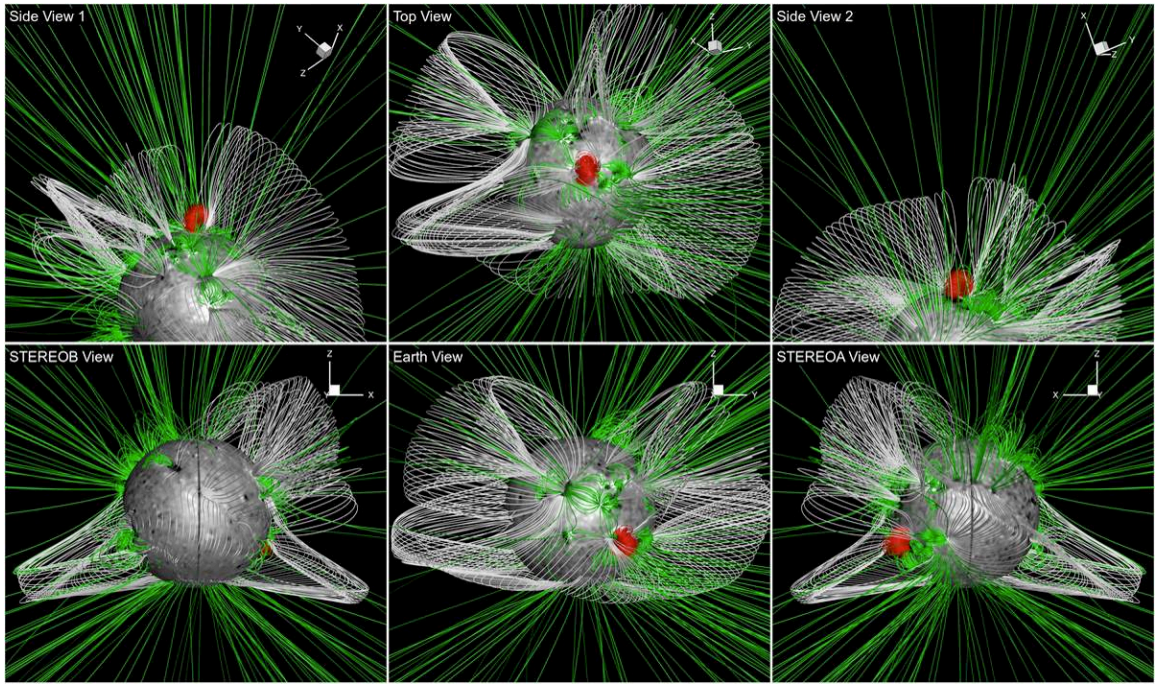

Courtesy of Meng Jin (LMSAL)

- produce thermodynamic MHD solution of corona based on magnetograms
- model eruption in AR 11158 (out-of-equilibrium Gibson-Low flux rope)
- identify coronal regions that are directly or only indirectly affected by CME

Une superflare peut elle partir du Soleil actuel?

Réponse immédiate:

A priori non, car l eSoleil est une étoile dans la force de l'âge en rotation faible.

Mais Schaefer et al. (2000) ont découvert 9 superflares dans des jumeaux solaires tournant lentement!

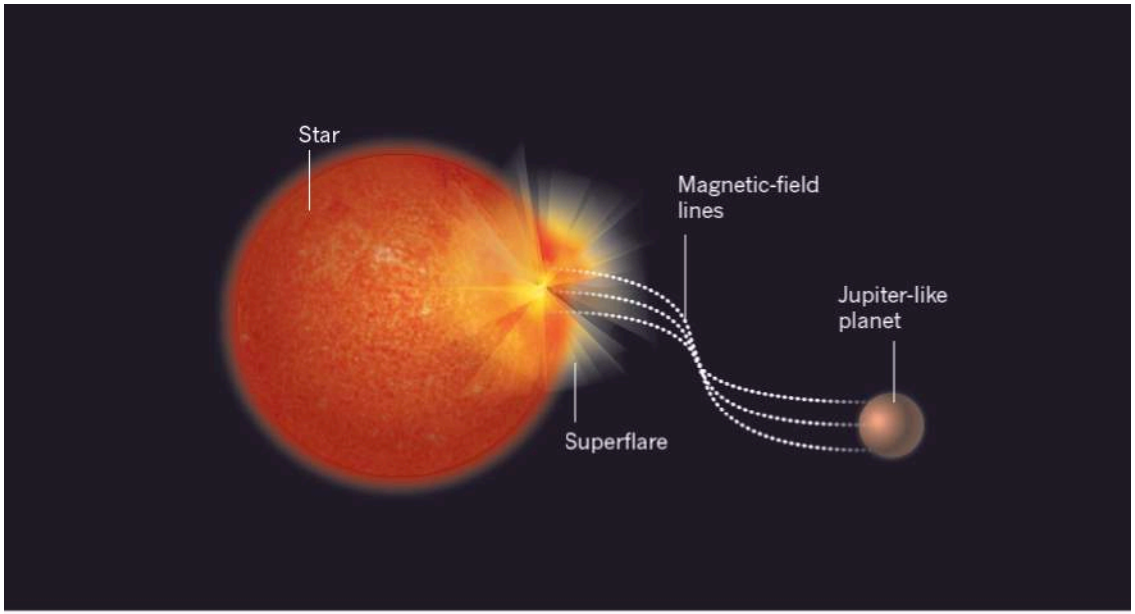

Figure 1 | Magnetic connection. One idea to explain the superflares observed by Maehara *et al.*[2] invokes the presence of intense magnetic fields that connect the star with a Jupiter-like planet in very close orbit around the star. The magnetic-field lines will become twisted and amplified by the orbital motion of the planet, and at some time the lines will be strained and twisted to the point of breaking. The broken lines will accelerate particles to very high energy and release this energy in an explosive event, similar to what happens in ordinary solar flares seen on the Sun.

Ils invoquent la présence de Jupiter Chauds

Est ce toujours nécessaire?

Exo-flares

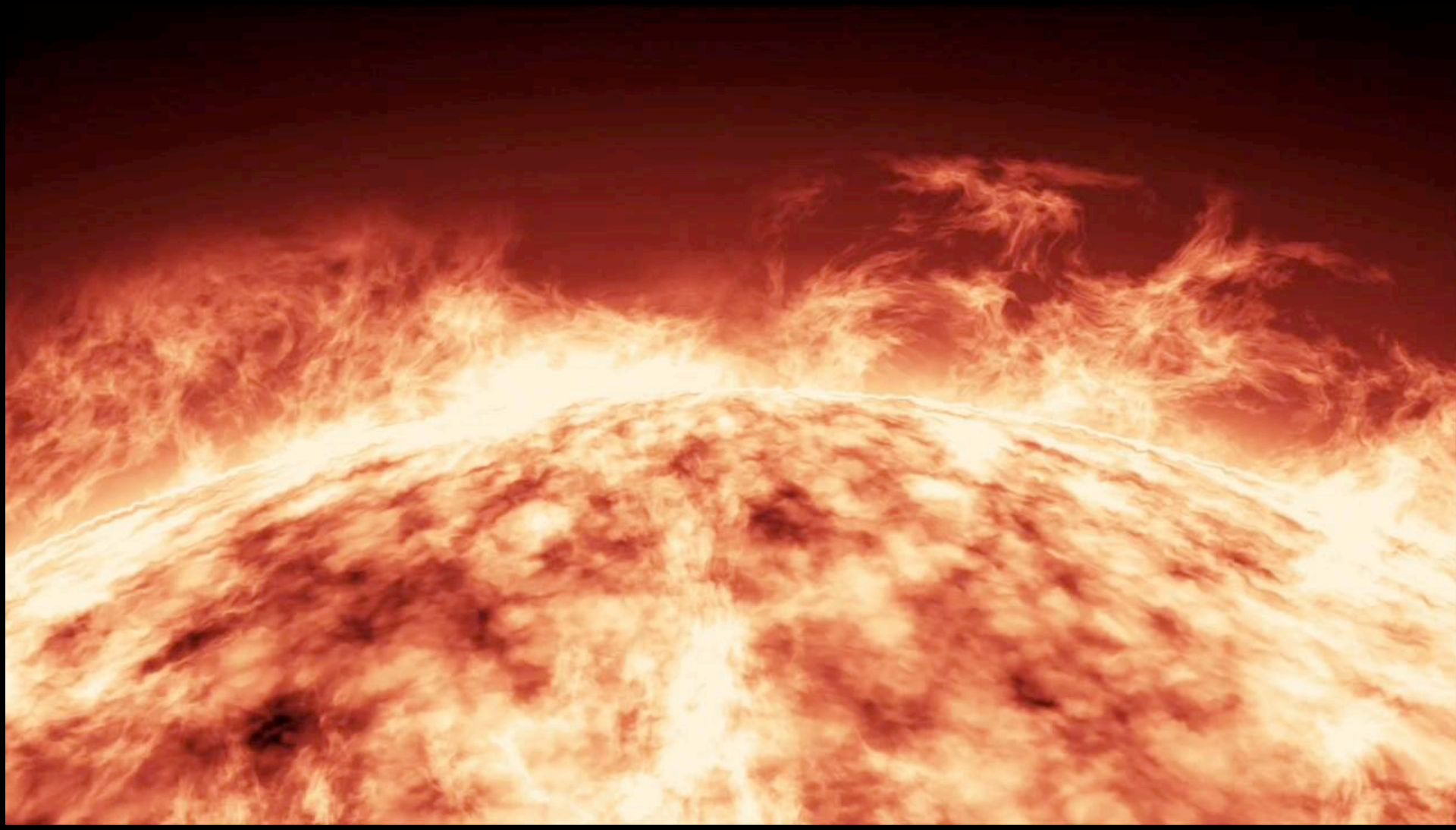

Une superflare observée par le satellite *Kepler*

Maehara et al. (2012)

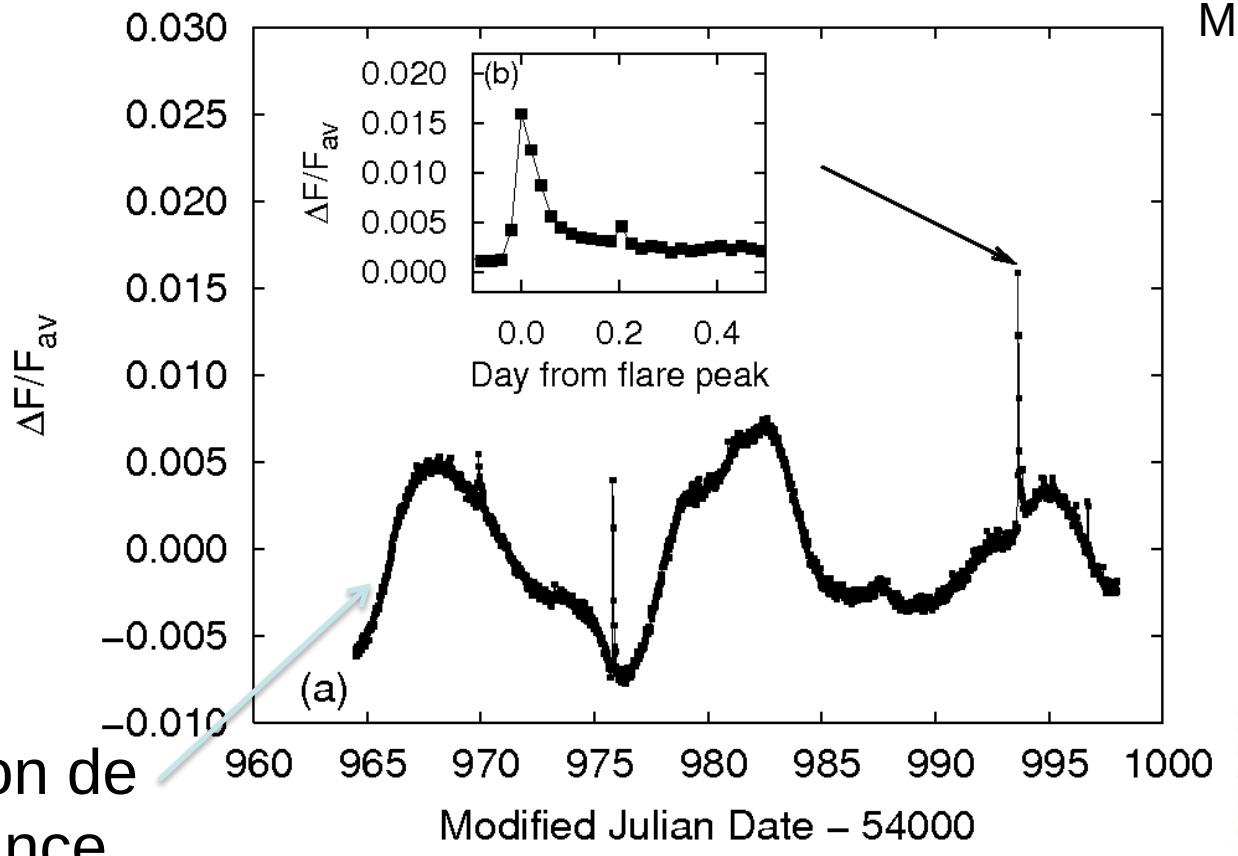

Energie totale
~ 10^35 erg

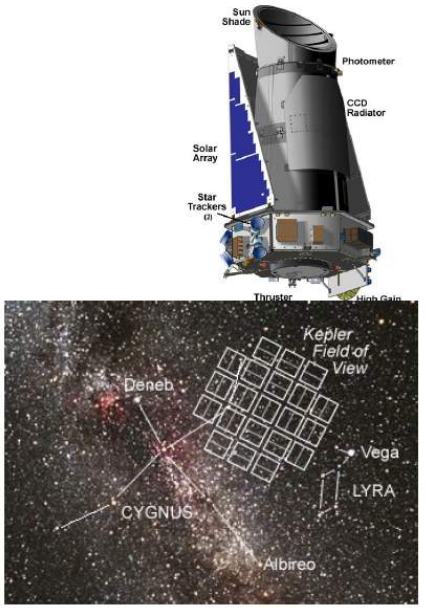

Variation de la brillance de l'étoile et apparition d'une éruption

Temps (jour)

Slide: adapté de Shibata et al. 2012, IAU GA XXVIII

Observations d'une eruption stellaire avec Kepler

Soleil actif

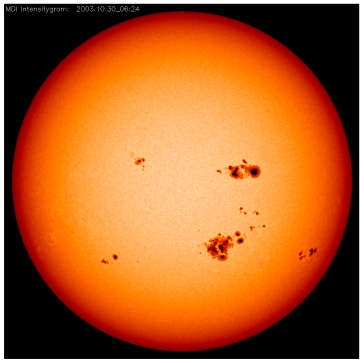

Étoile super active (vue d'artiste)

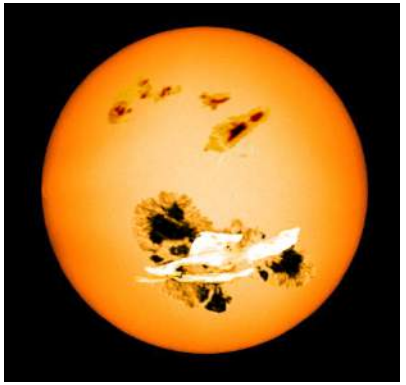

Brillance d'une étoile et d'une éruption

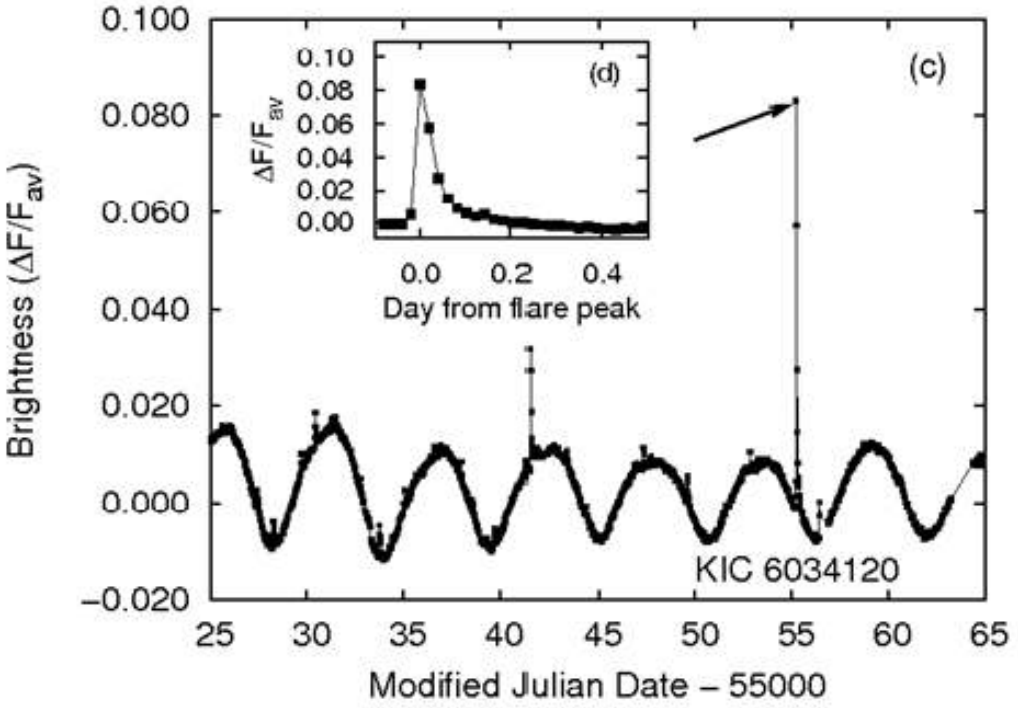

Énergie totale ~ 10^36 erg

Slide: adapté de Shibata et al. 2012, IAU GA XXVIII

Maehara et al. (2012)

Origine de la variation de luminosité? La présence d'un gros complexe actif (tache stellaire) en rotation

Energie des éruption vs rotation

Slide: adapté de Shibata et al. 2012, IAU GA XXVIII

Analyse étendue voir Notsu et al. 2013

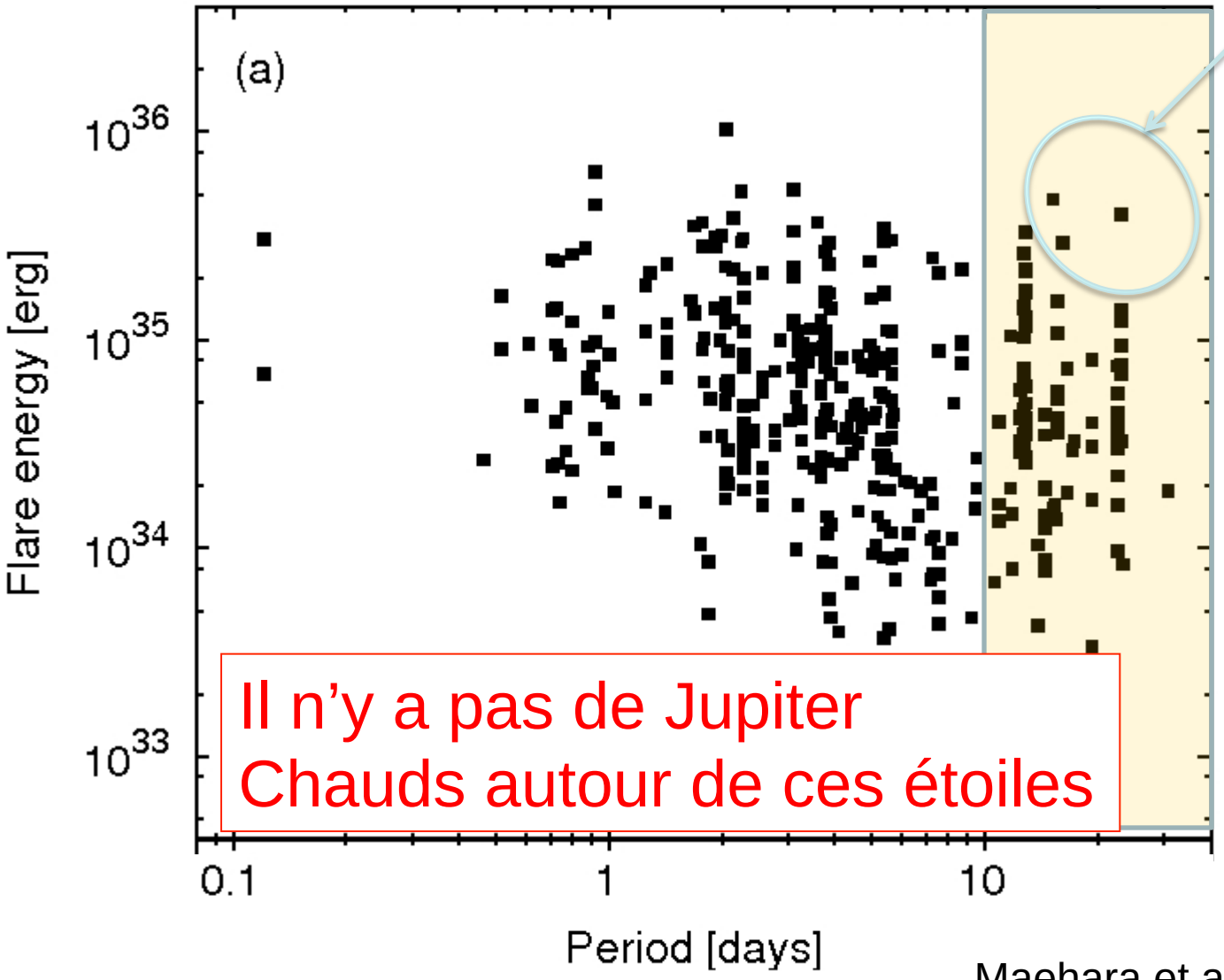

Peu d'étoiles à la position incertaine

Etoiles avec période de rotation > 10j

P_{sol} ~ 28j

Il n'y a pas de Jupiter Chauds autour de ces étoiles

Maehara et al. (2011)

Comparaison des éruptions vs loi d'échelles

Slide: adapté de Shibata et al. 2012, IAU GA XXVIII

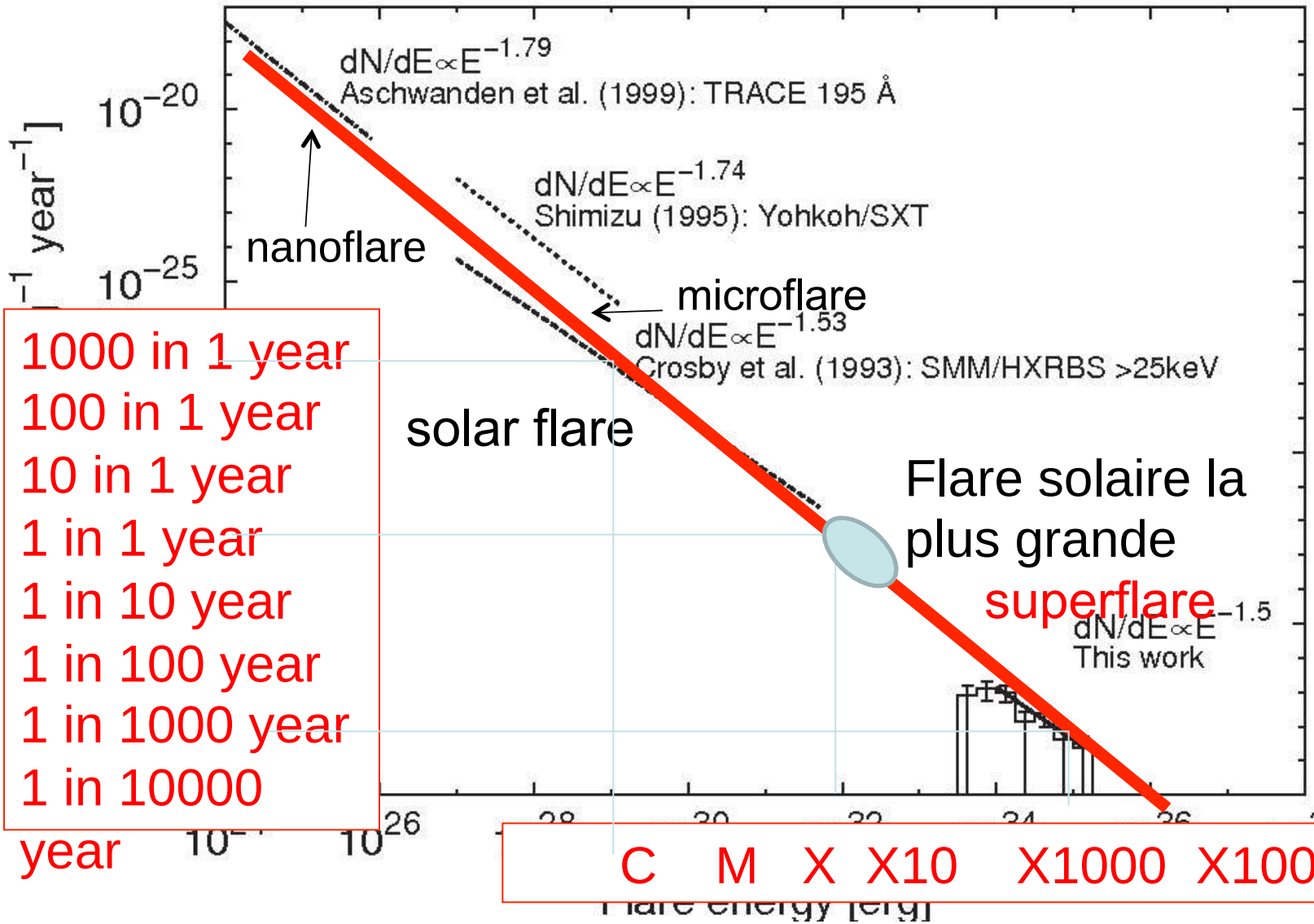

Tache solaire la plus grosse

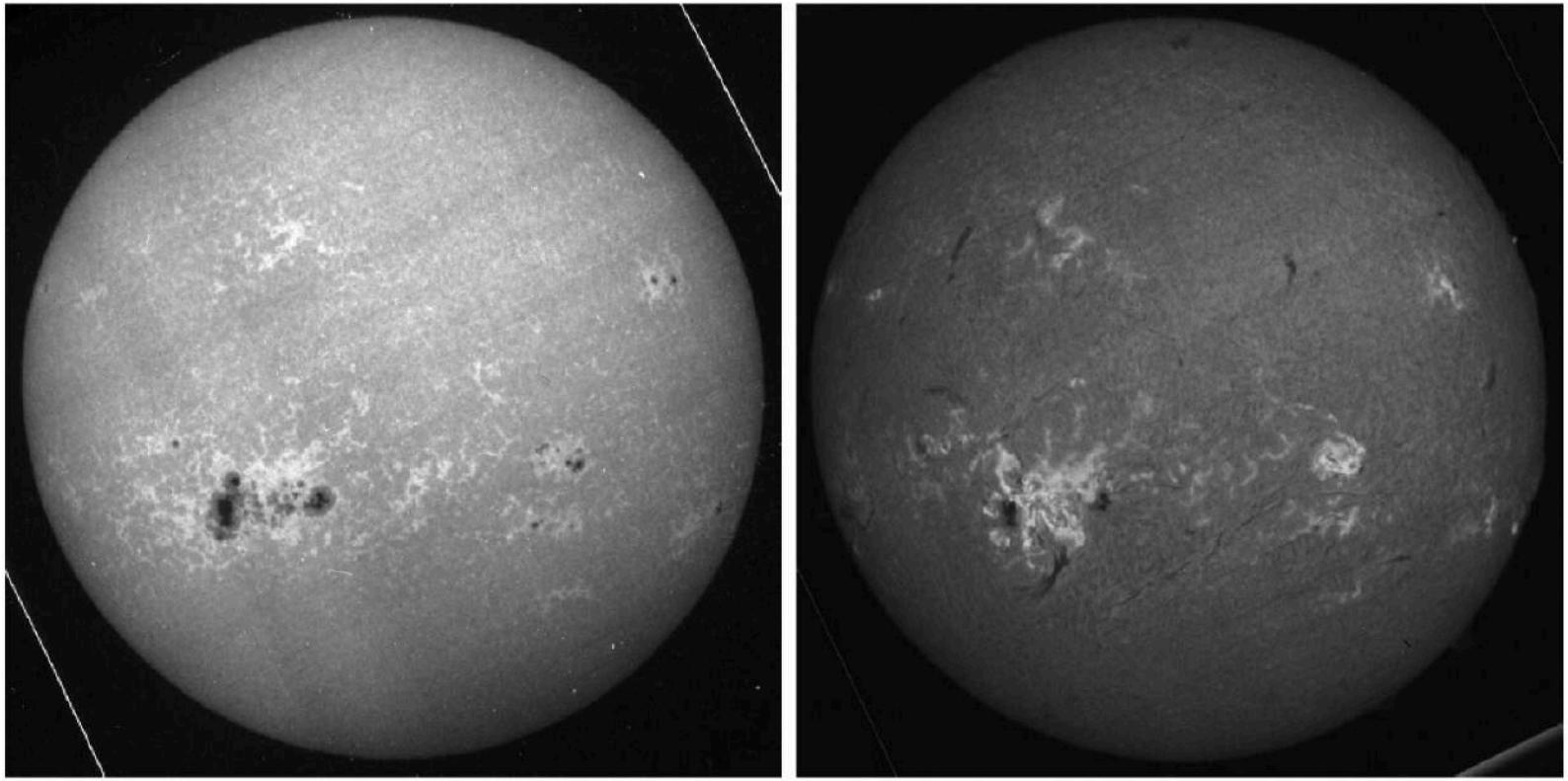

Fig. 3. The largest sunspot group ever reported since the end of the nineteenth century, as observed in April 5, 1947 in Ca II K1v (*left*) and Hα (*right*) by the Meudon spectroheliograph.

Etude critique du travail Maehara et al. 2012

Aulanier et al. 2013 (A&A)

Valeur max qqle 10^34 erg
avec tache de 1947

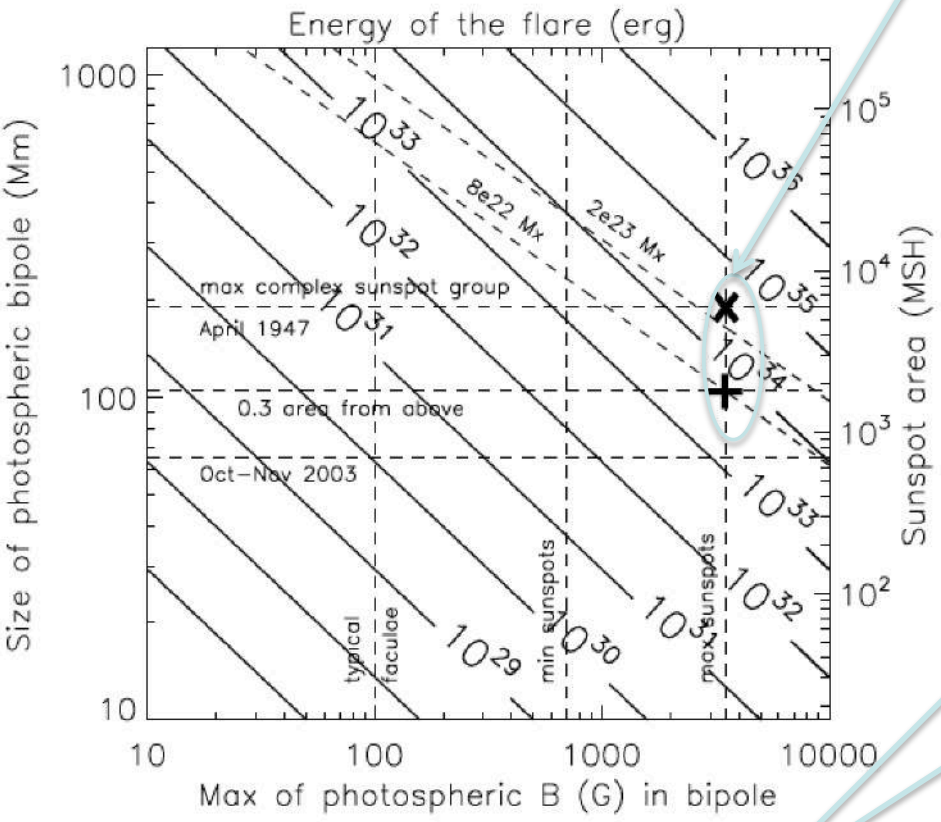

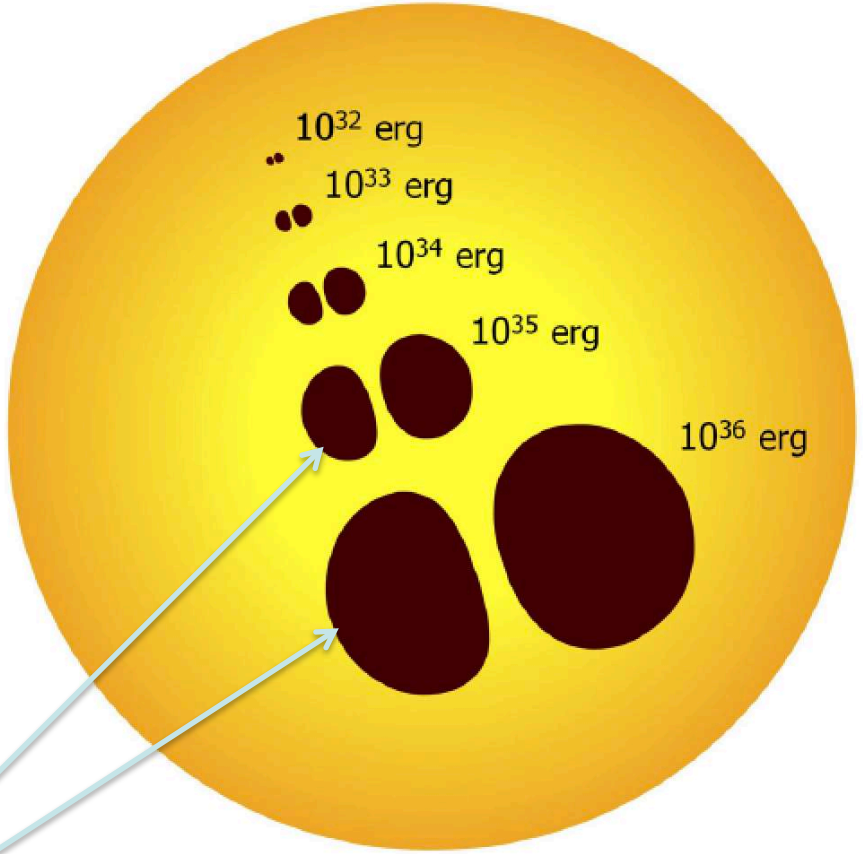

. Schematic representation of several modeled sunspot pairs on the solar disk, with their corresponding modeled flare energies. Note that our estimations state that in the real Sun, a given pair will often be embedded in a much larger sunspot group, from which only the bipole that is shown here will be involved in the flare.

La taille de ces taches
est (trop?) énorme

Winds and stellar evolution gyrochronology

Rotation Models

Gallet & Bouvier 2013

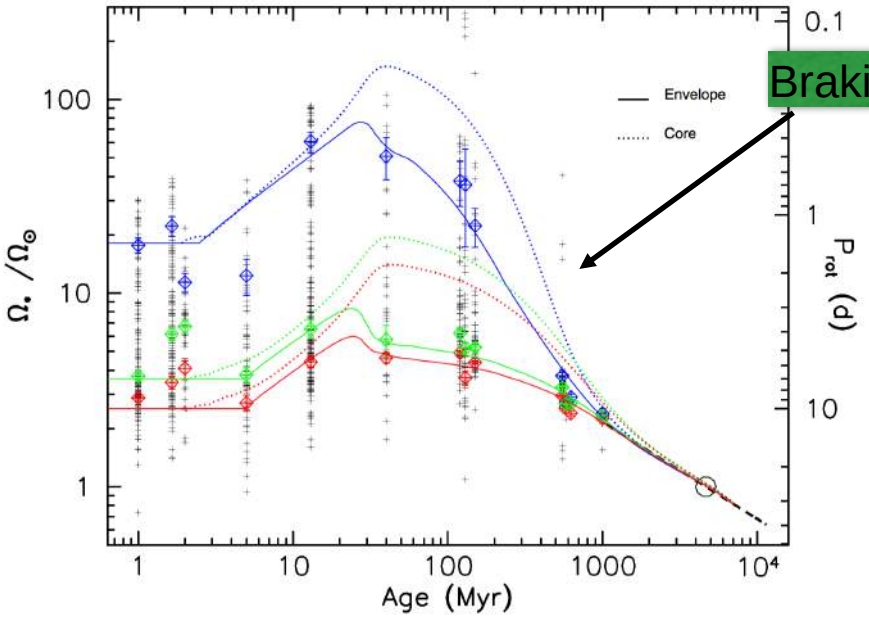

Braking models

dynamo

wind

Magnetic Activity

De Rosa, Brun, Hoeksema 2012

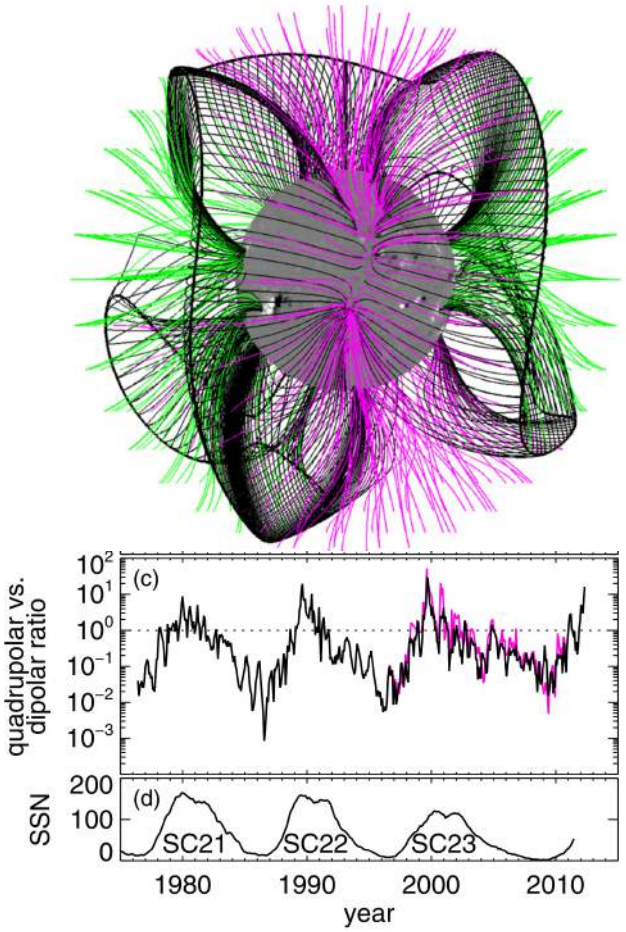

Skumanich's law: $\Omega_* \propto t^{-1/2}$

Relations Soleil-Terre

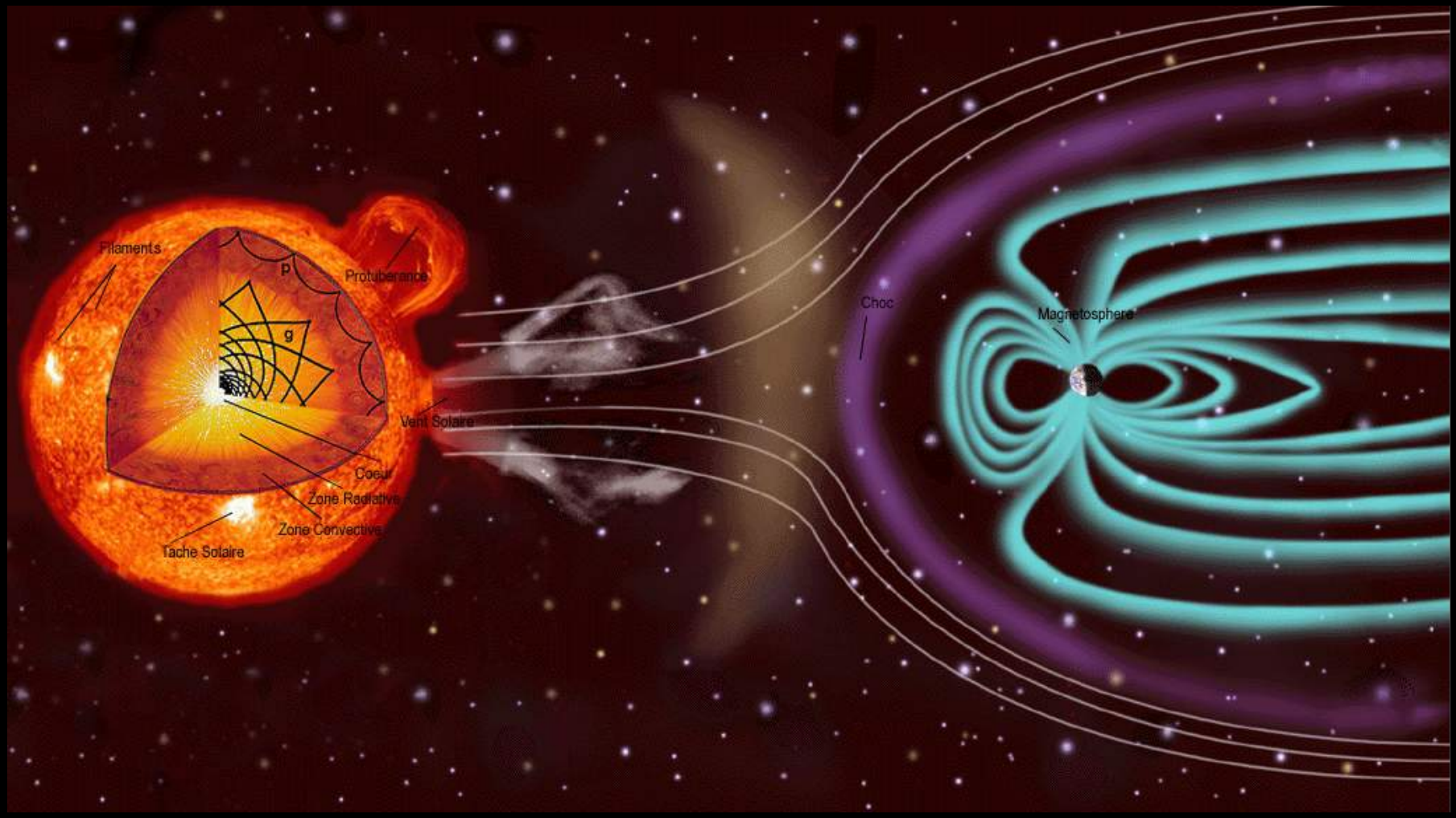

Relations Soleil-Terre

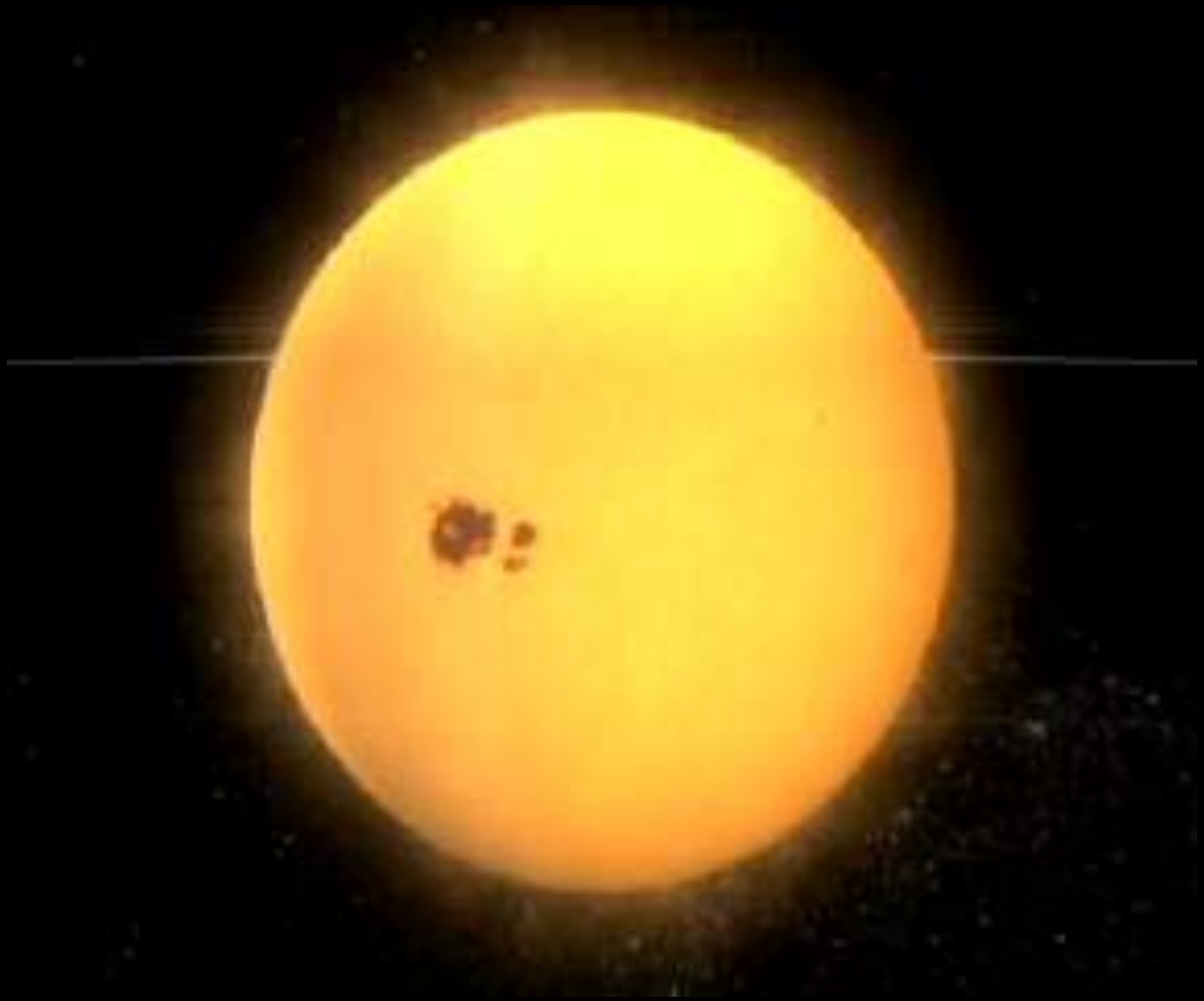

Dose de Radiations en Avion: un exemple pratique Osaka-Paris

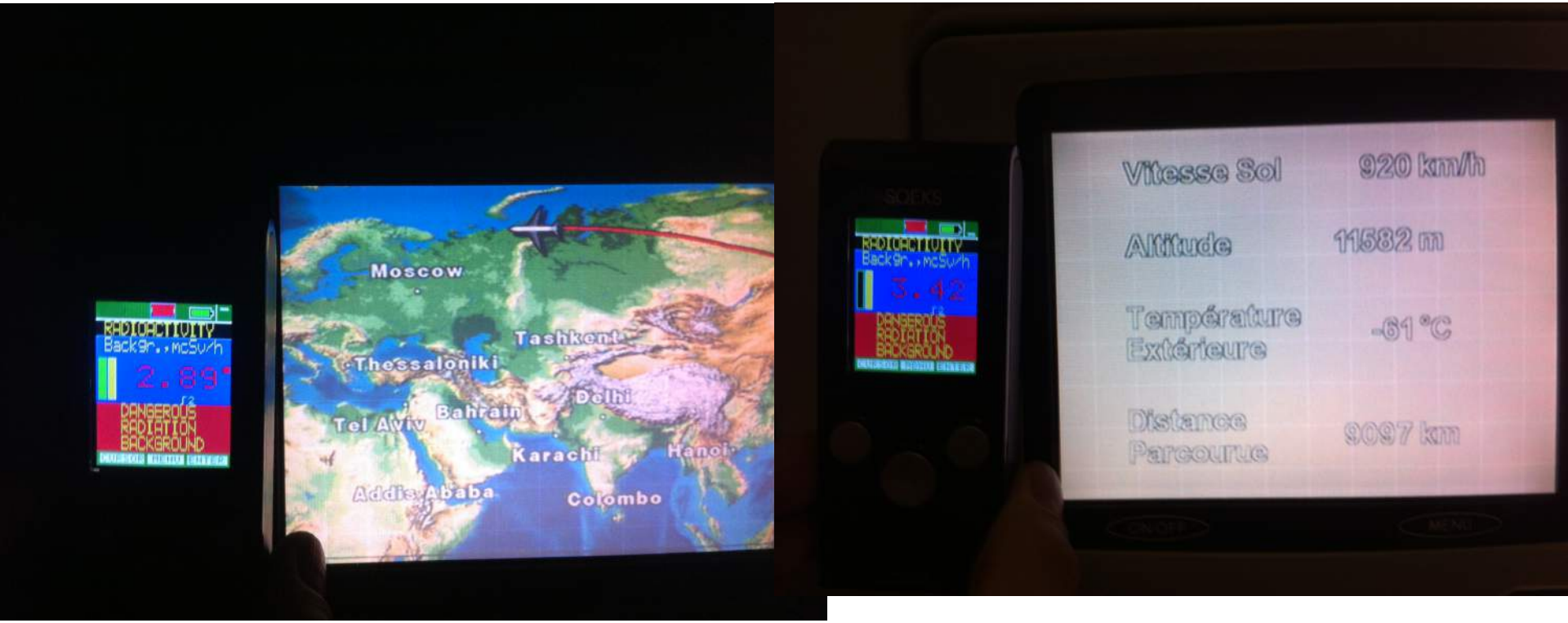

La Comète Enckel rencontre une CME

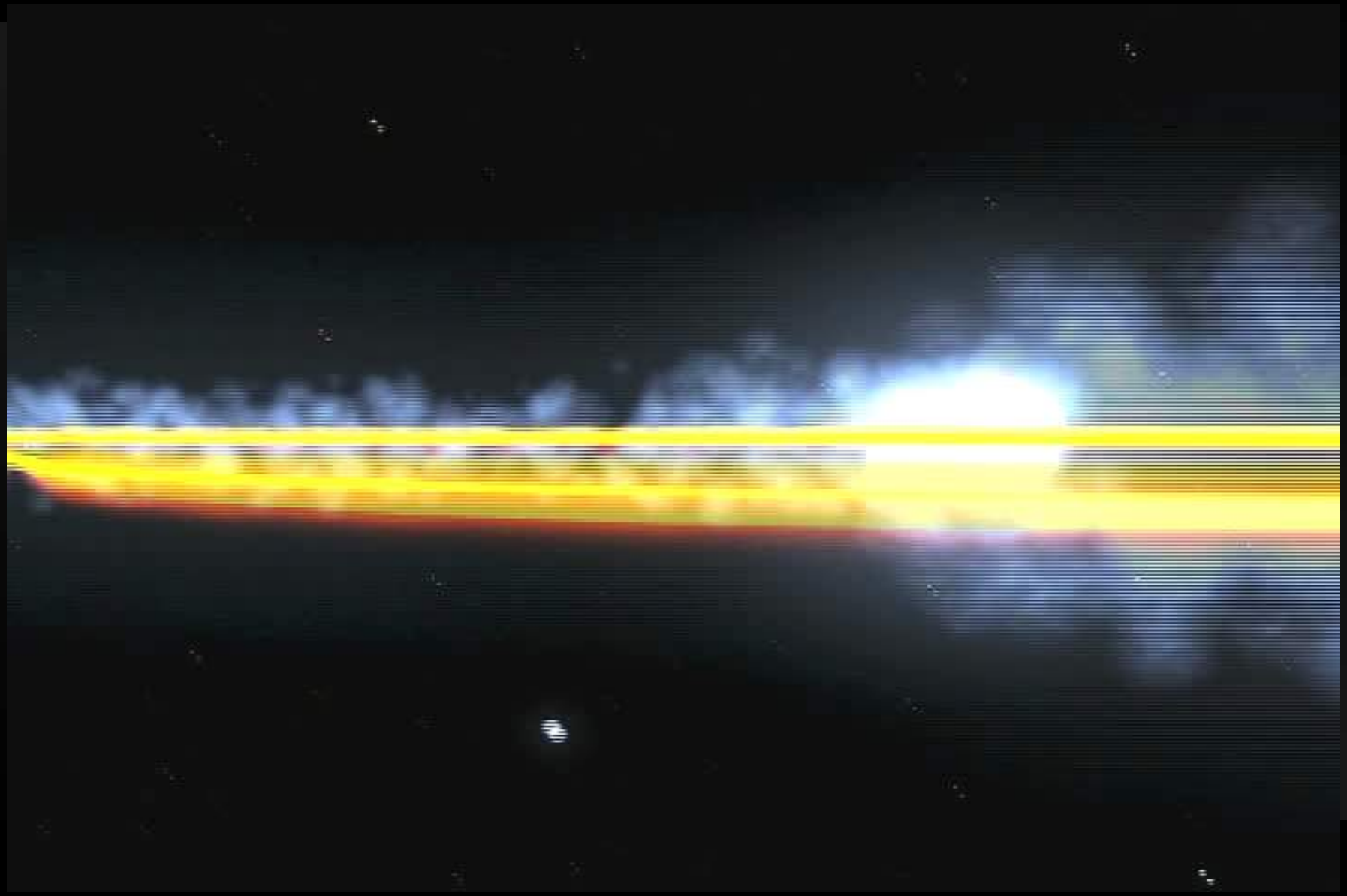

Relations Soleil-Terre

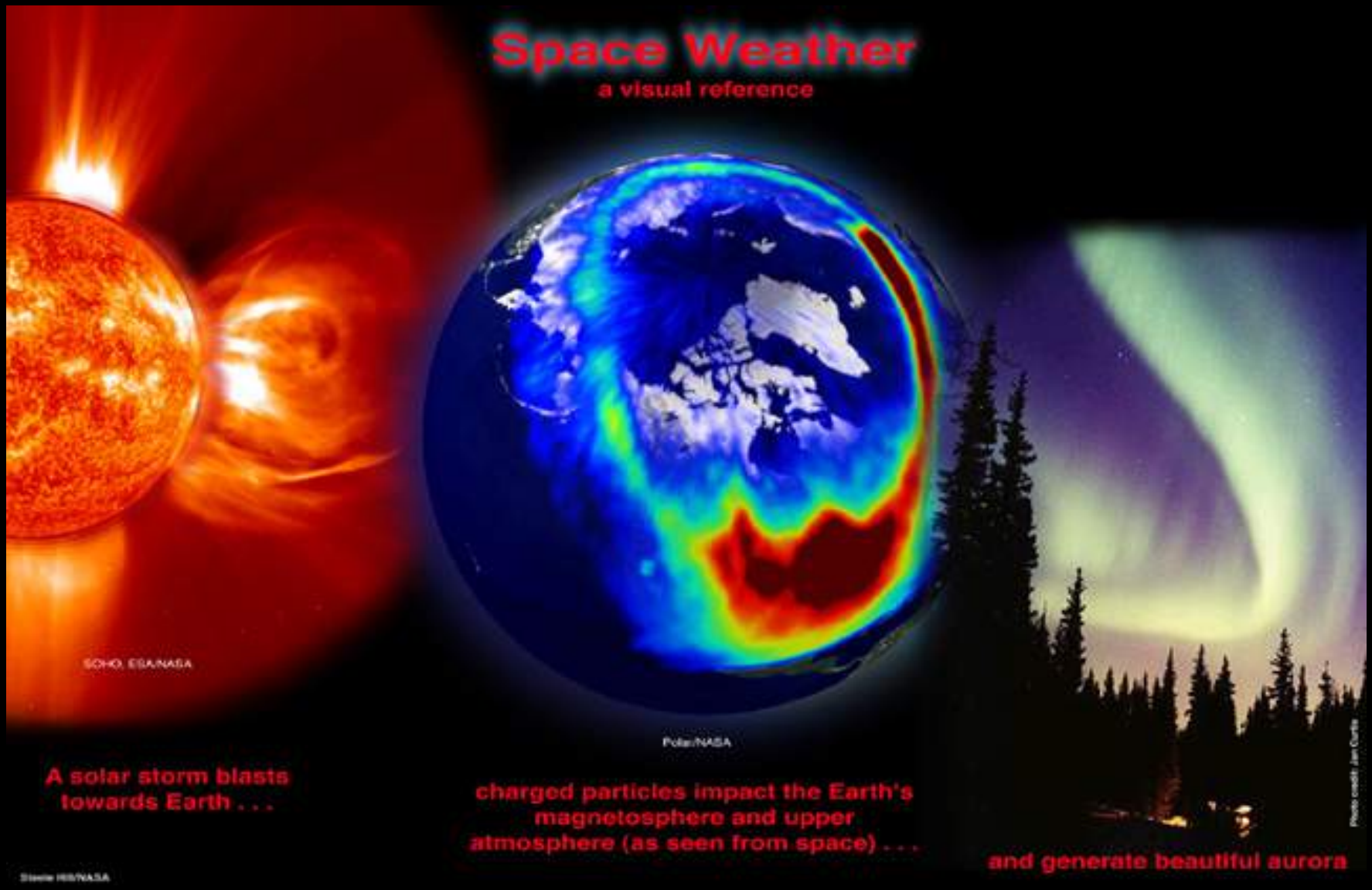

Aurores boréales

CME and Planet Earth

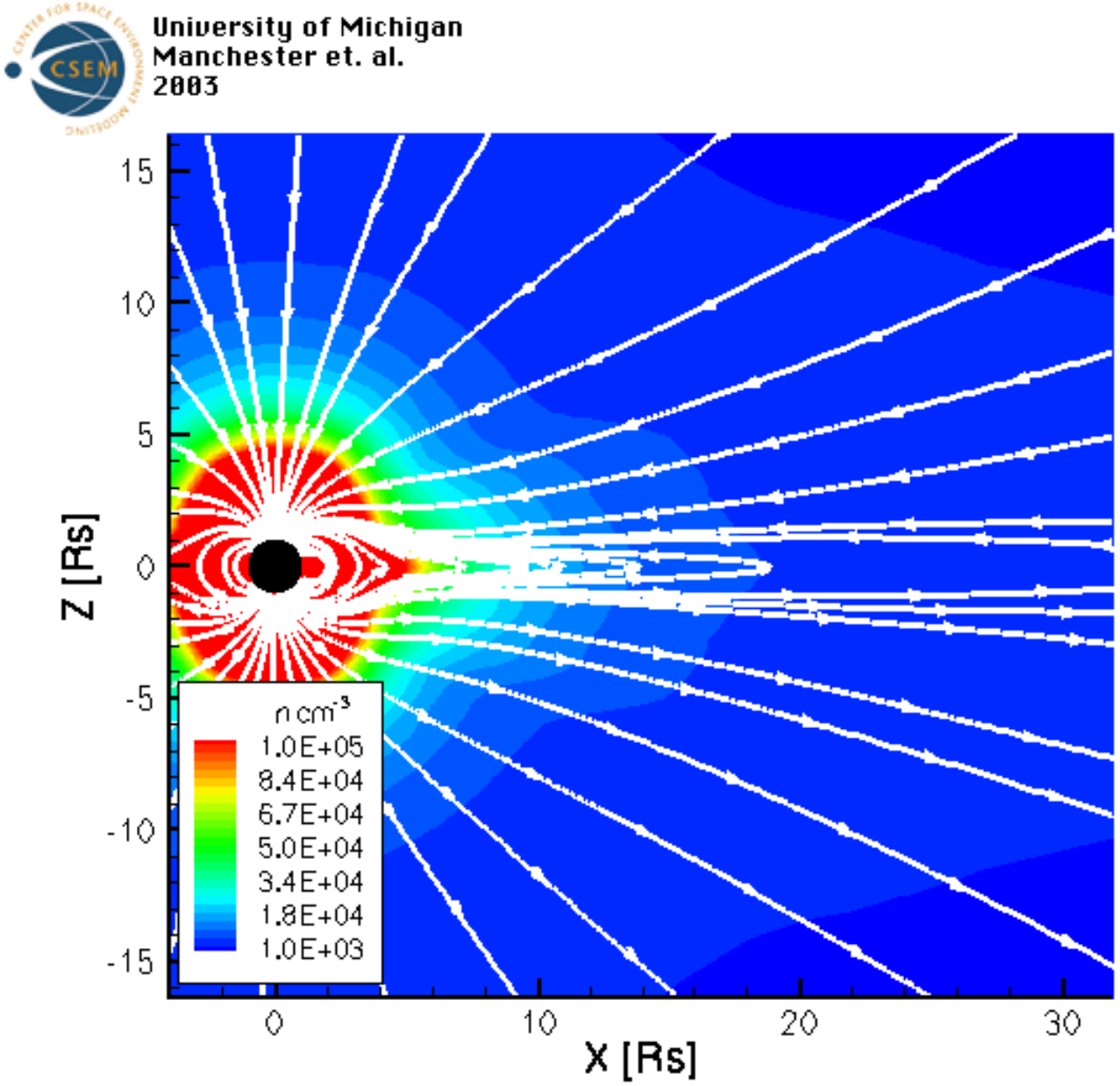

Vent solaire et Magnétosphère Terrestre

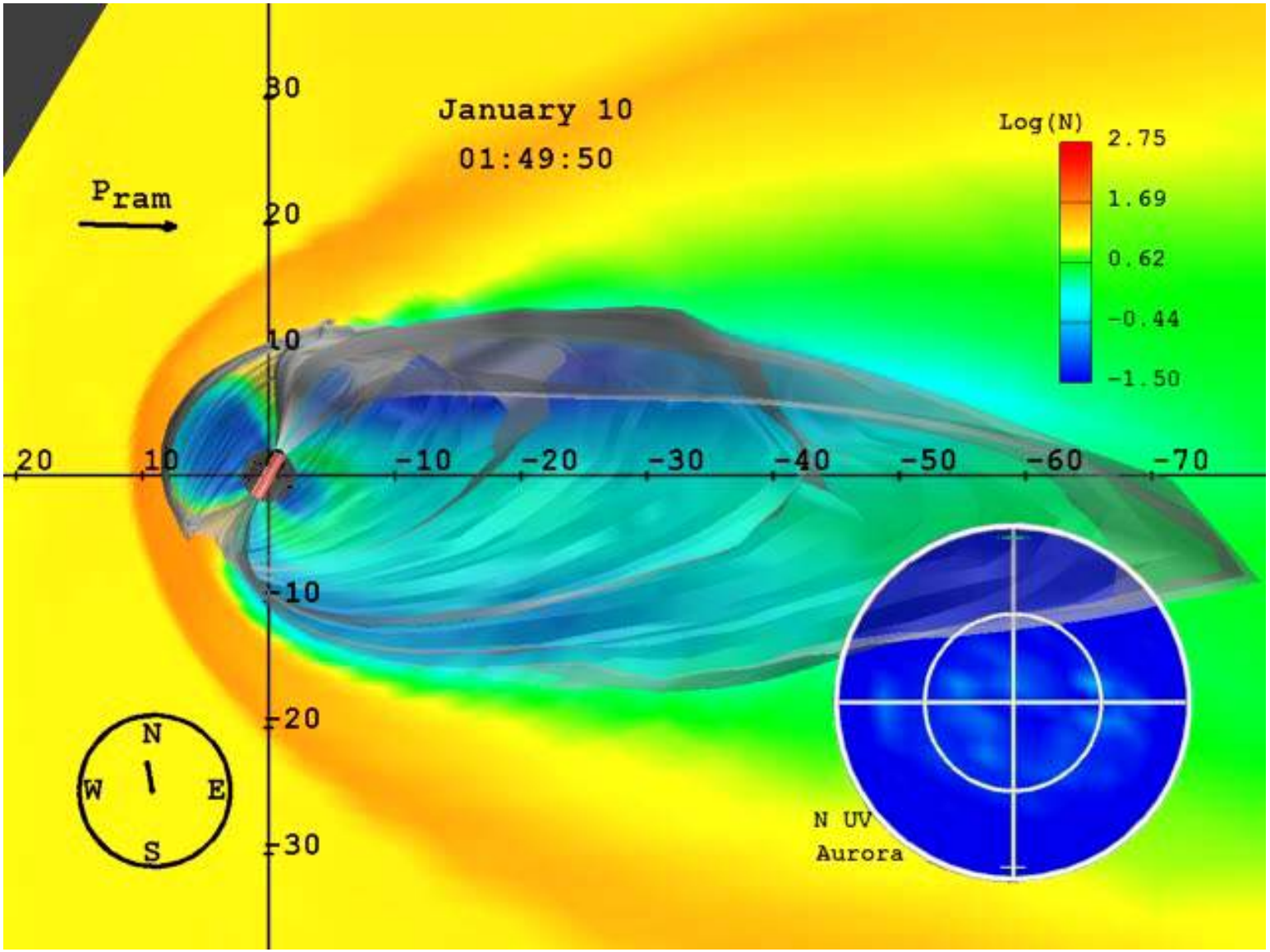

Nasa

Taille relative des Magnétosphères dans le Syst. Solaire

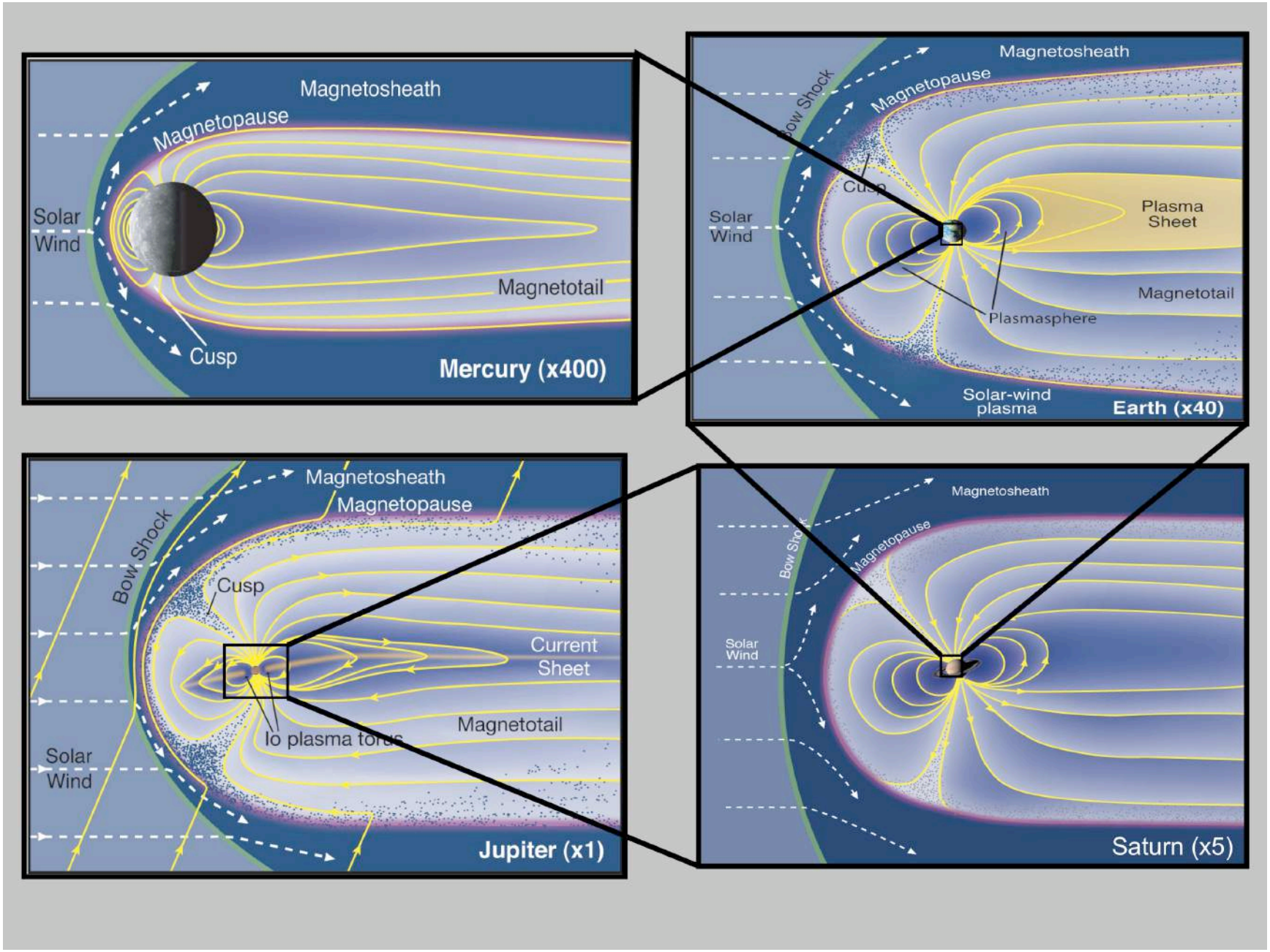

Planètes Gazeuses: Aurores Boréales

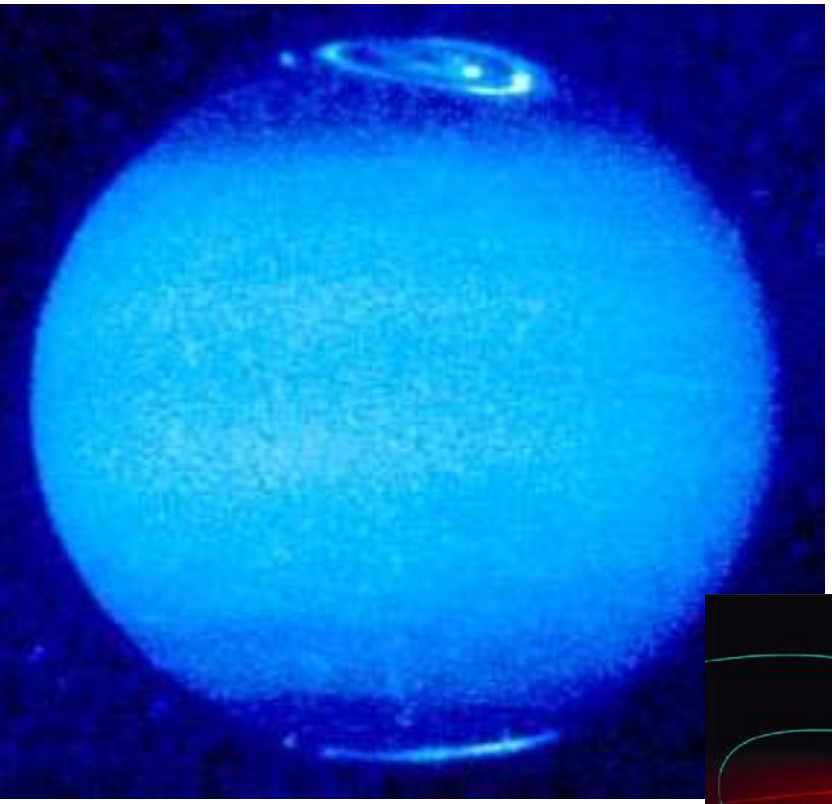

Jupiter, ~ 4 G

Dynamos actives, champ B fort

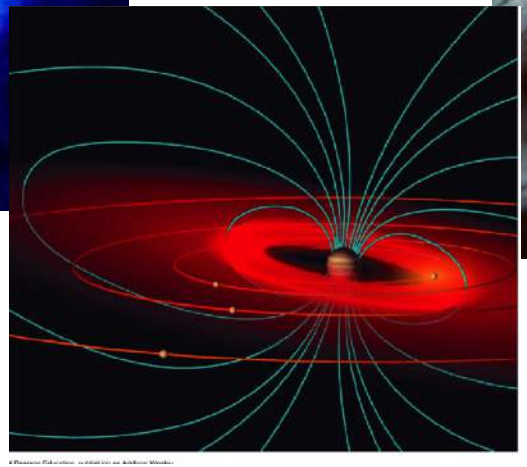

Saturne, ~0.4 G

Lunes joviennes:
Callisto & Europa: B induit
Io: 13 mG, induit/dynamo + plasma torus
Ganymède: dynamo 7.5 mG (vs Jup 1.2 mG @ 15 Rj)

Corona & Solar Wind

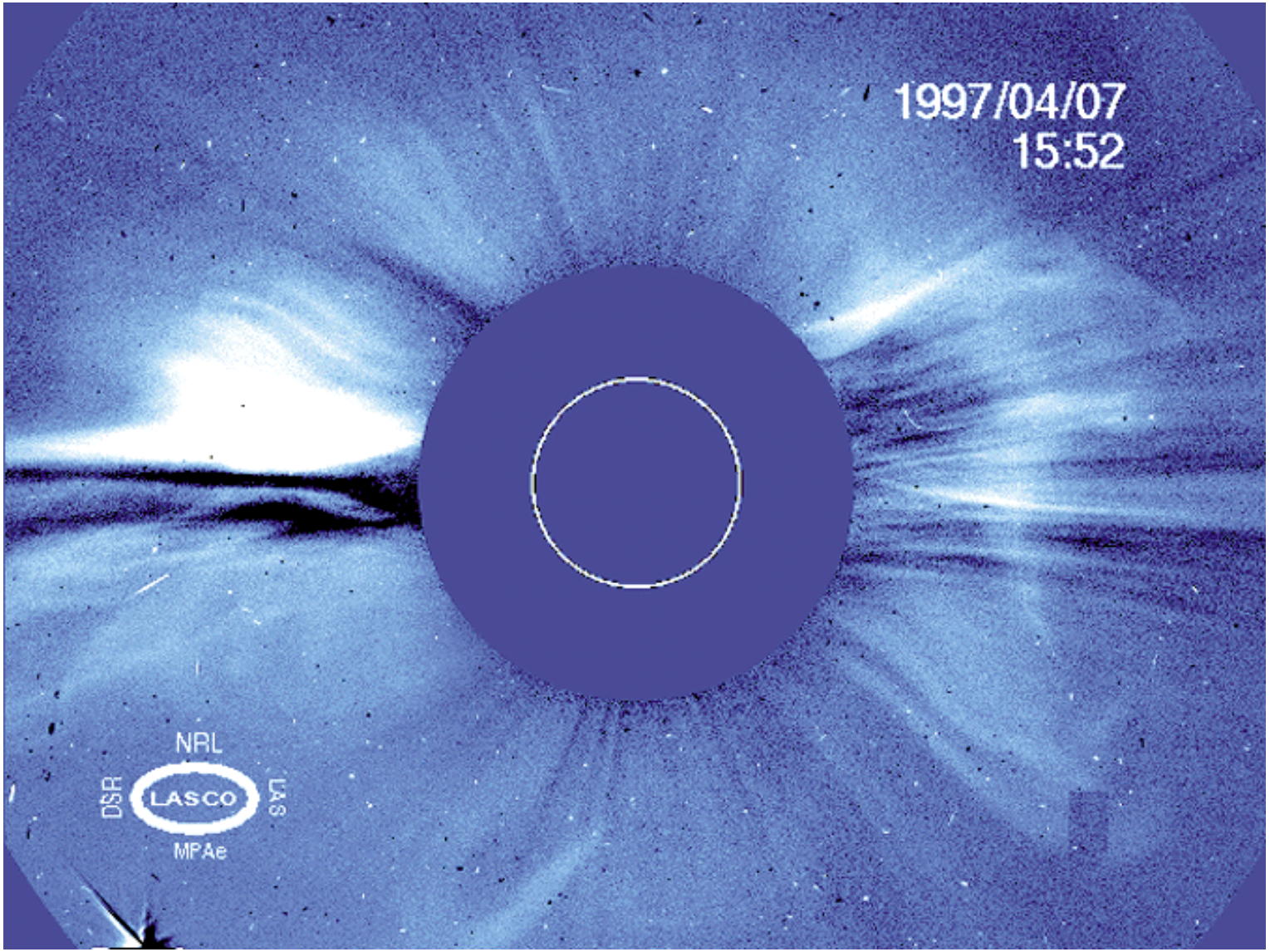

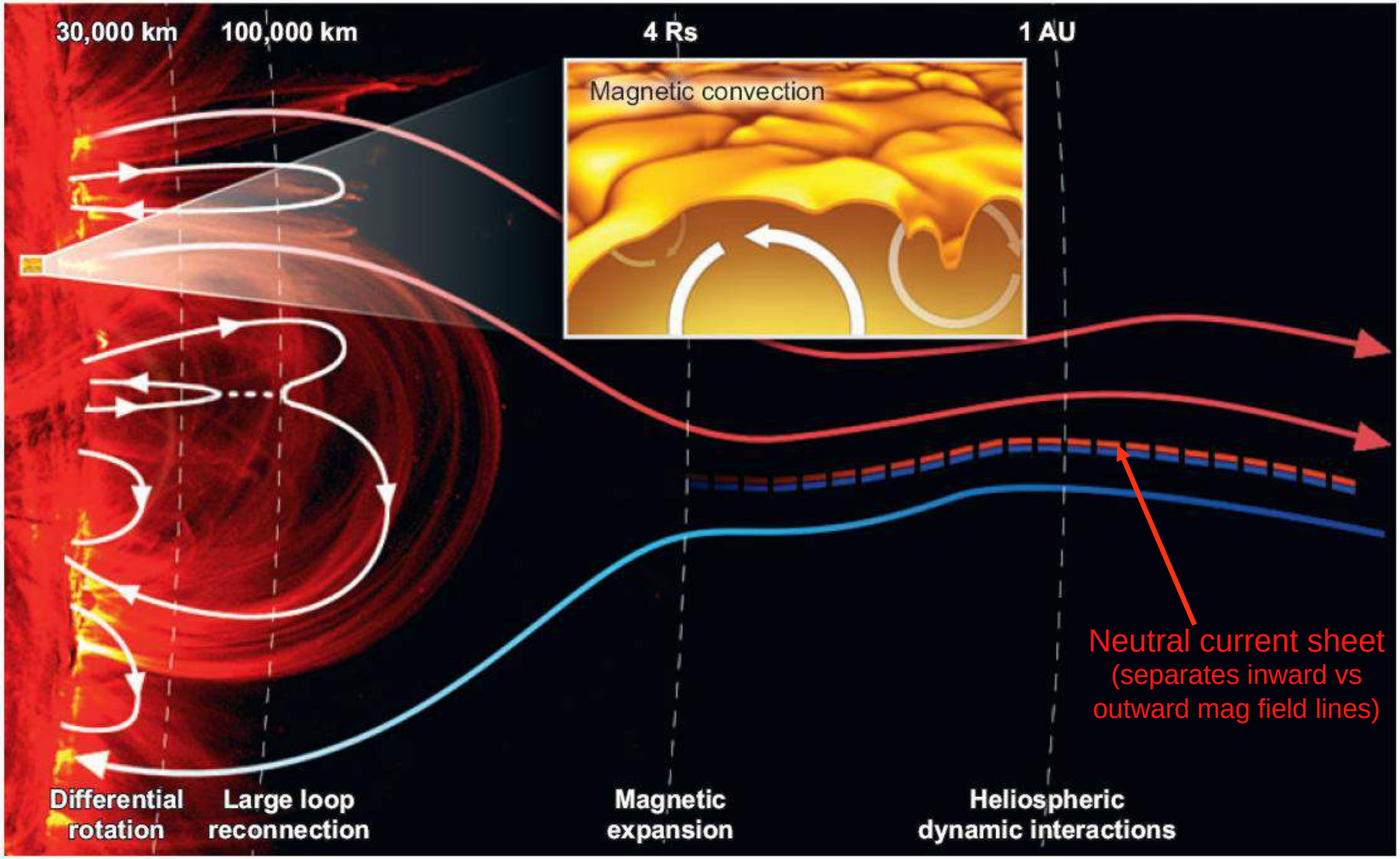

Figure 3

Schematic representation of the physical processes that shape the heliospheric magnetic field. The magnetic field emerges through the photosphere in small flux elements that interact with each other and with heliospheric field lines, leading to diffusive transport. Similarly, systematic flows, such as the flows caused by differential rotation, can also be projected into the heliosphere. Direct observations of these effects are difficult owing to the dynamic evolution of the heliospheric plasma caused by stream interactions and turbulent effects.

Table 1 Key average properties of the solar wind plasma near Earth[a]

Quantity	Definition	Source
$B_r = 2.5$ nT	Radial magnetic field	Wang & Neubauer 1990
$B_\varphi = 2.4$ nT	Toroidal magnetic field	Wang & Neubauer 1990
$B_\theta = 1.5$ nT	Latitudinal magnetic field	Wang & Neubauer 1990
$V = 600$ km/s	Solar wind speed	McComas et al. 1998
$\rho = 11 \cdot 10^{-21}$ kg/m^3	Solar wind mass density	Schwenn 1990
$T = 120{,}000$ K	Solar wind temperature	Schwenn 1990
Derived Quantity		
$V_A = 32$ km/s	Alfvén speed	
$C_S = 41$ km/s	Sound speed	
$\beta \sim 1$	Plasma beta	
$\lambda_{mfp} \sim 0.2$–0.5 AU	Mean free path of ion Coulomb collisions	Marsch 1990

[a]These quantities vary near Earth, and also have systematic variability as a function of distance from the Sun.

Parker's Solar Wind Model

Simple hydrostatic model (u=0) for an isothermal corona at T= 1 Million K leads to a pressure ratio between the solar surface (~100 mb, cf slide 3) and the pressure at « infinity » of 4 orders of magnitude, i.e p_inf / p_surf ~10^{-4} , whereas it should be at least 10^{-14} ! Since p_inf = p_ism (the pressure of the interstellar medium).

In 1955 E. Parker proposed that the Sun possesses a wind (solar wind of particles, mostly protons, electrons, alpha's), i.e a dynamical atmosphere with u=/=0 .

$$1/2\,u^2 - c_s^2 \ln u = 2c_s^2 \ln r + GM/r + C$$

5 solutions are found mathematically (cf. figures), only 3 are meaningful, type III, IV & V

Type V is the solar wind solution: A slow wind accelerating to supersonic speed. It leads to a very small p_inf compatible with p_ism

A is the sonic point, u=c_s

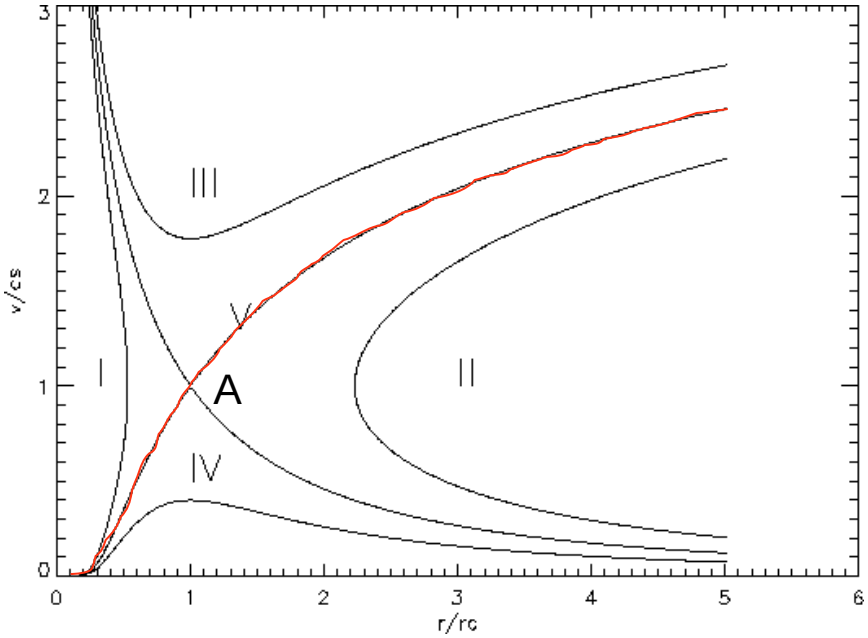

No fast wind is Observed near the Surface so III can be discarded.

IV remains subsonic (the solar breeze) but p_inf still too large Compared to p_ism

Check white board notes for more details

Vent solaire et Champ Coronal

Rapide là où les lignes de champ magnétiques sont ouvertes (troux coronaux)

Lent là où les lignes de champ magnétiques sont fermées (streamers)

Min

Max

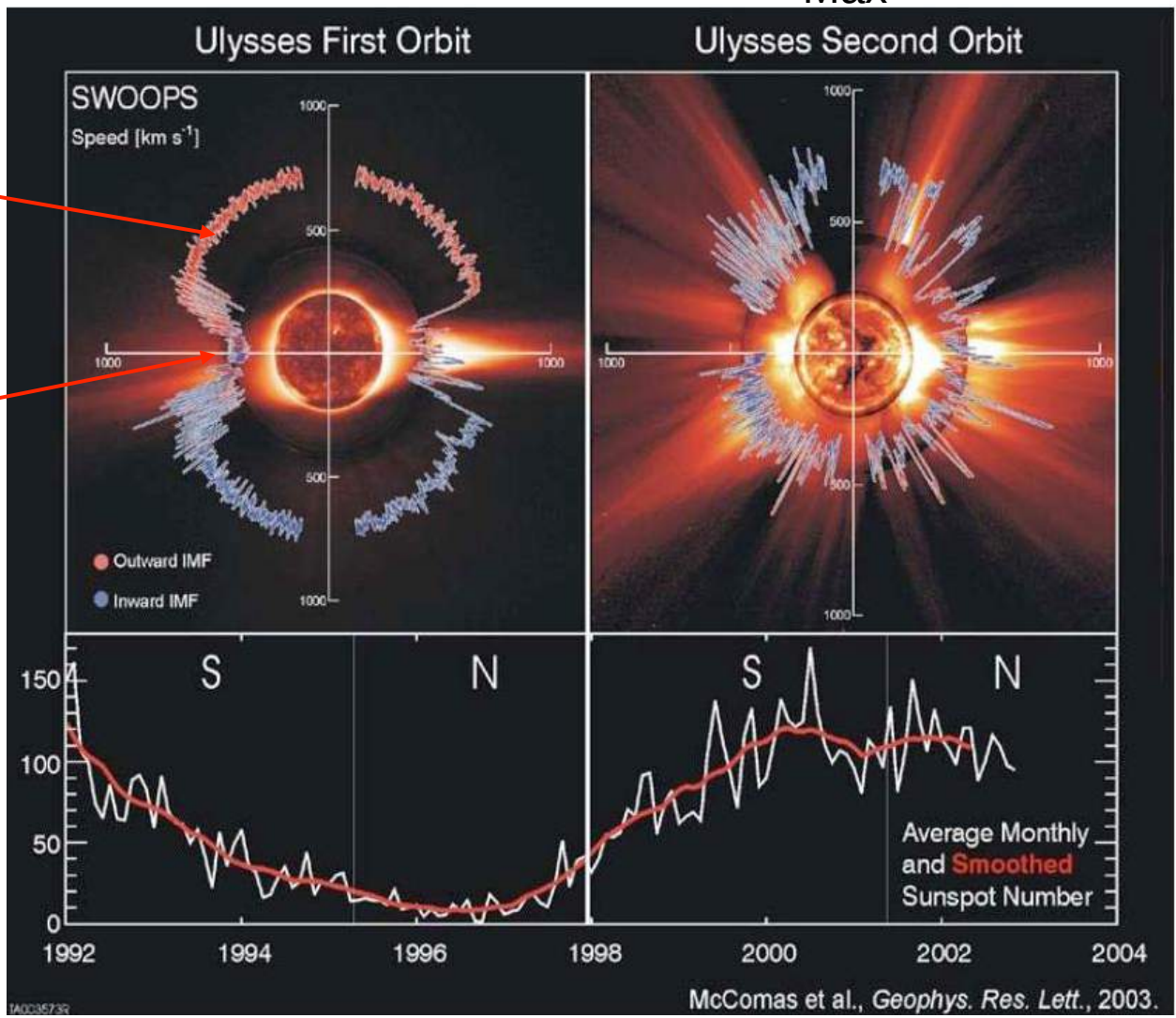

Il faut 2.5 à 4.5 jours au vent solaire pour atteindre la Terre.
Il est composé surtout d'hydrogène ionisé (proton + électrons), de 8% d'hélium et de traces

MHD Wind Simulations

Why are they necessary ?

- Magnetic fields > split monopole
- Rotation
- 3D, non-axisymmetry

Decreasing Alfvén surface !

Parametric study of the torque as a function of:

- Rotation
- Magnetic field strength
- Magnetic field topology

Coronal temperature and gamma held fixed.

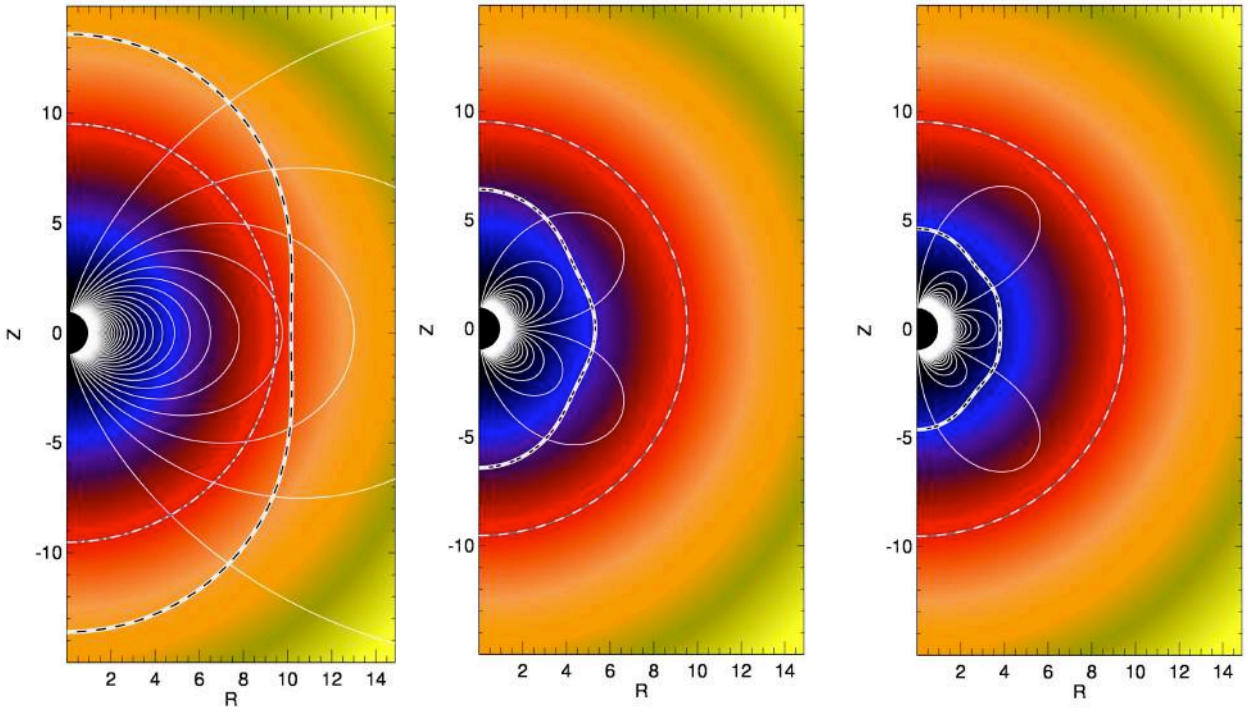

Dipole Quadrupole Octupole

60 cases with compressible MHD code PLUTO

Réville et al. 2015, ApJ 798:116

Modulation Cyclique du Vent Solaire

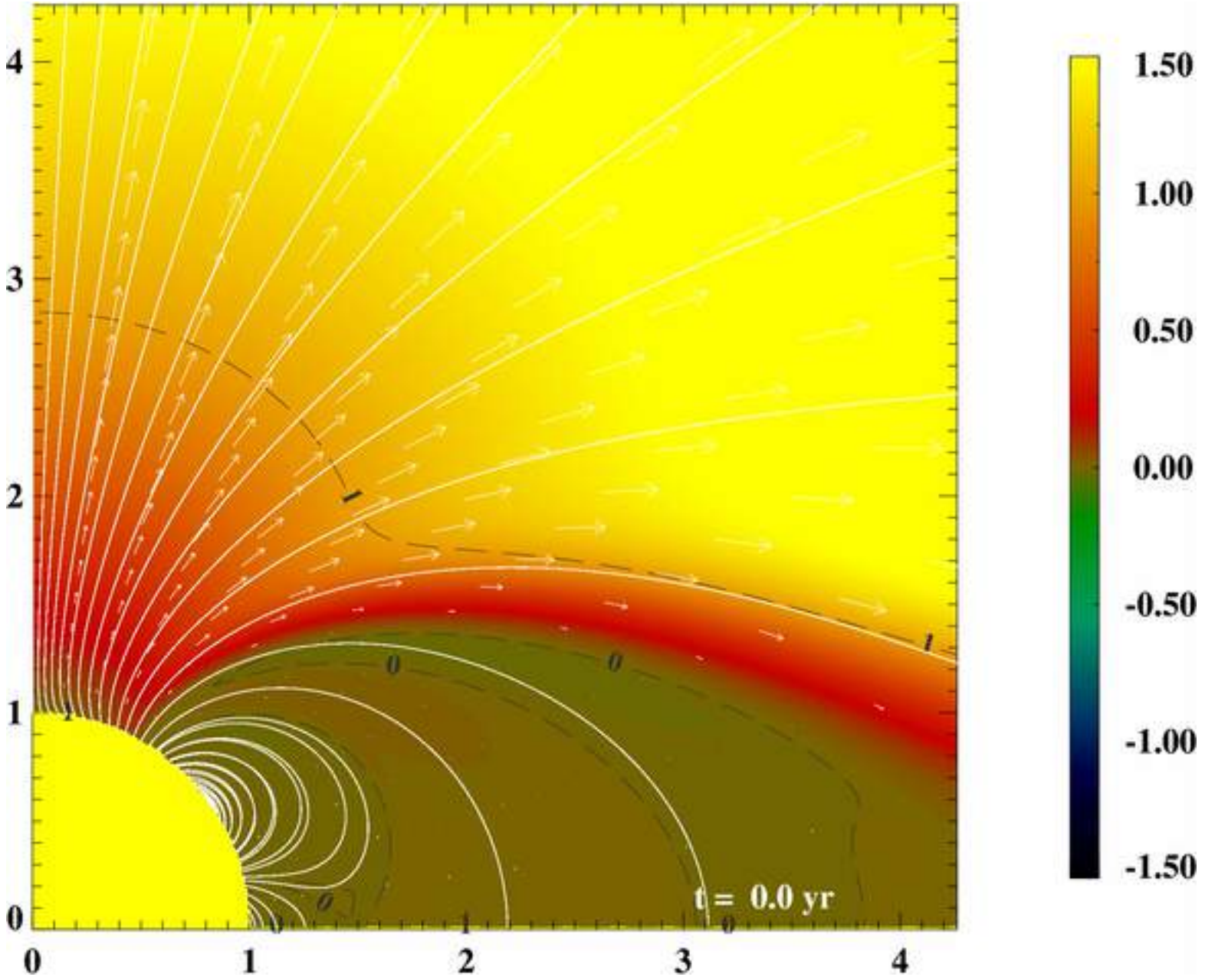

Pinto, Brun et al. 2011

Mass and Angular Momentum Loss by Solar Wind

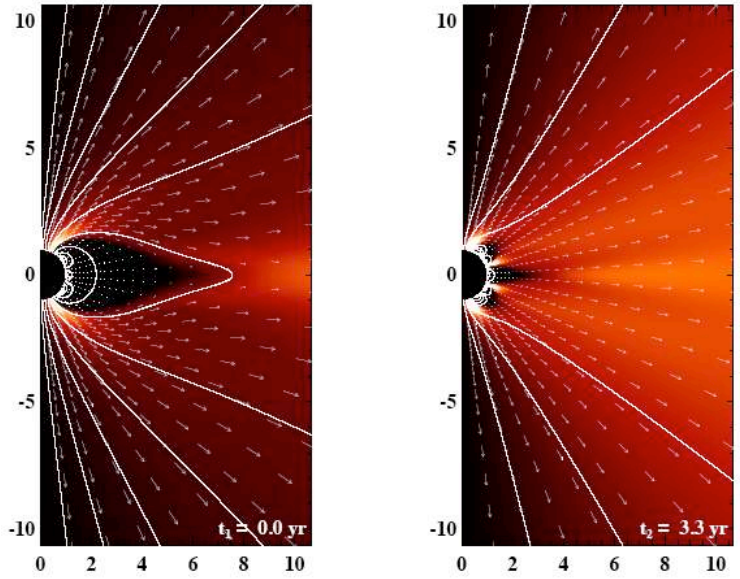

Figure 7. Mass flux $\rho V_r r^2 \sin\theta$ in the meridional plane at $t = 0$ yr (left) and at $t = 3.3$ yr, about the polarity inversion (right), that is, respectively, instants t_1 and t_2. The factor $r^2 \sin\theta$ is due to the spherical expansion of a surface element normal to the radial direction. Outflows which originate at lower latitude dominate the global mass loss rate.

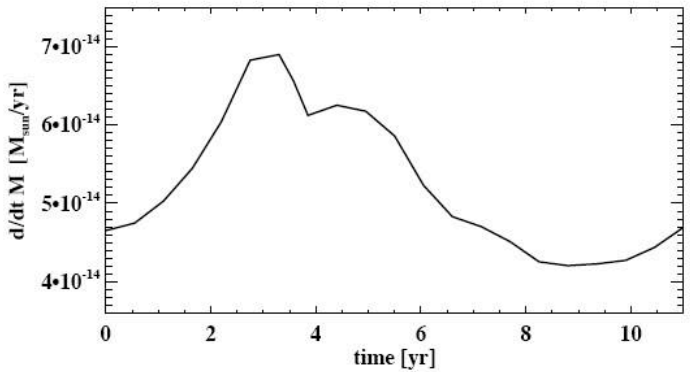

$$\dot{M} = 2\pi R_0^2 \int_0^\pi \rho V_r \sin\theta d\theta$$

The azimuthal magnetic field does not suddenly change from straight to spiralled. But quantitatively, it all works out *as if* there was a sharp transition. Following this picture, one can define an average Alfvén radius $\langle r_A \rangle$ — an "effective lever arm length". The specific angular momentum flux rate is then

$$l = \Omega_0 \langle r_A \rangle^2 \ . \tag{7}$$

The resulting torque applied on the sun is (Matt & Pudritz 2008)

$$\tau = -\dot{M}\Omega_0 \langle r_A \rangle^2 \ . \tag{8}$$

The angular momentum per unit volume J of a parcel of solar wind plasma rotating with azimuthal velocity v_ϕ is

$$J_w = \rho r \sin\theta v_\phi \ . \tag{9}$$

The angular momentum per unit volume crossing a surface element dA is then $\dot{J}_w = J_w v_r dA$. Integrating over a spherical surface of radius r_0 and assuming axisymmetry translates into

$$\dot{J}_w = 2\pi r_0^3 \int_0^\pi \rho v_r v_\phi \sin^2\theta d\theta \ . \tag{10}$$

We then define the magnetic spin-down time-scale as

$$\delta t_{sd} = \frac{J_\odot}{\dot{J}_w} \ , \tag{11}$$

where $J_\odot$ is the sun's angular momentum. We estimated

$$J_\odot = \frac{8\pi}{3}\Omega_0 \int_0^{R_\odot} \rho(r)\, r^4 dr \approx 1.84 \times 10^{48} \text{ g cm}^2 \text{ s}^{-1} \tag{12}$$

Mass and Angular Momentum Loss by Solar Wind

Alfven radius variation vs solar cycle.

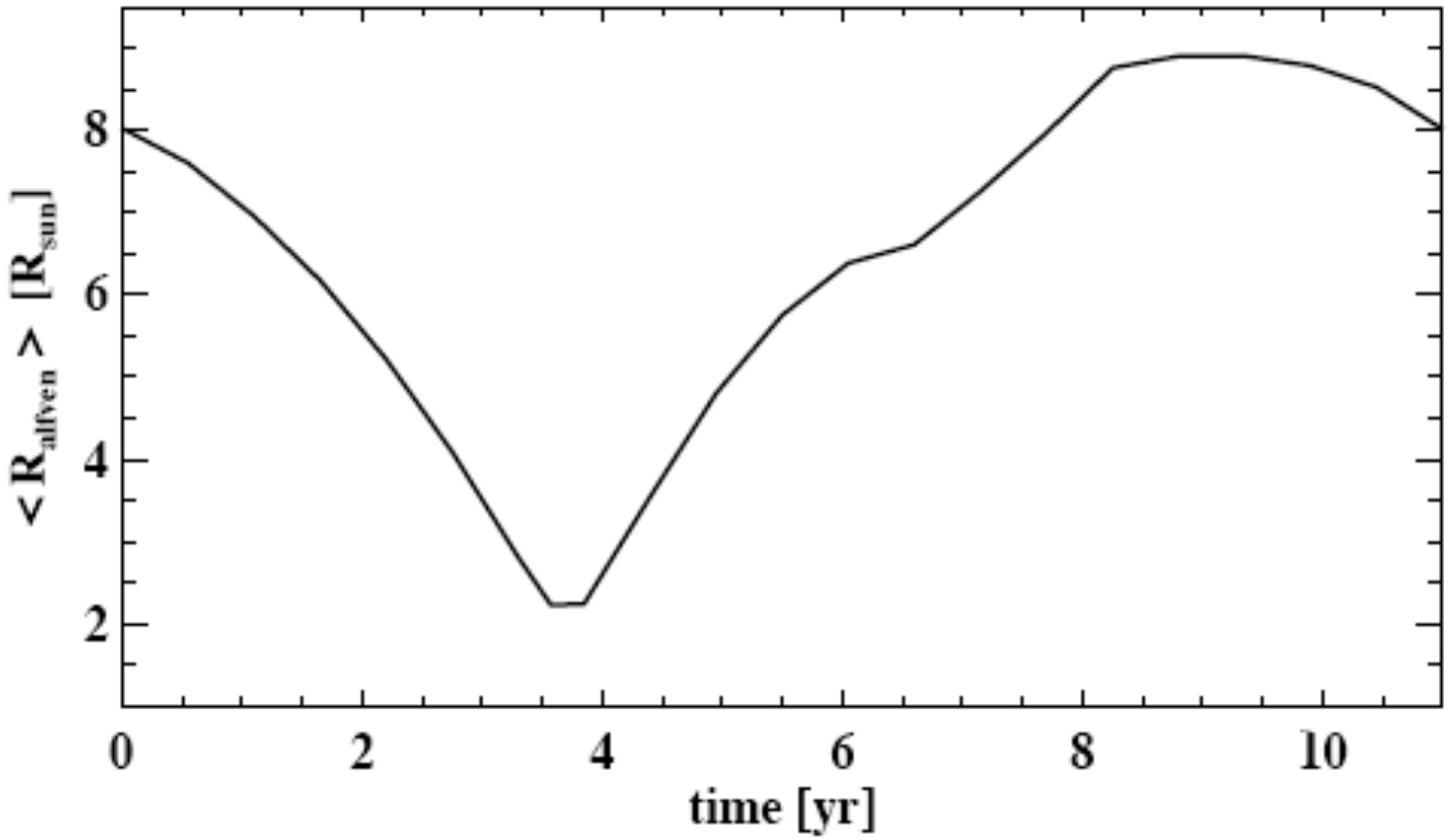

Pinto, Brun et al. 2011, ApJ

Magnetic field
in Corona and
Neutral current sheet

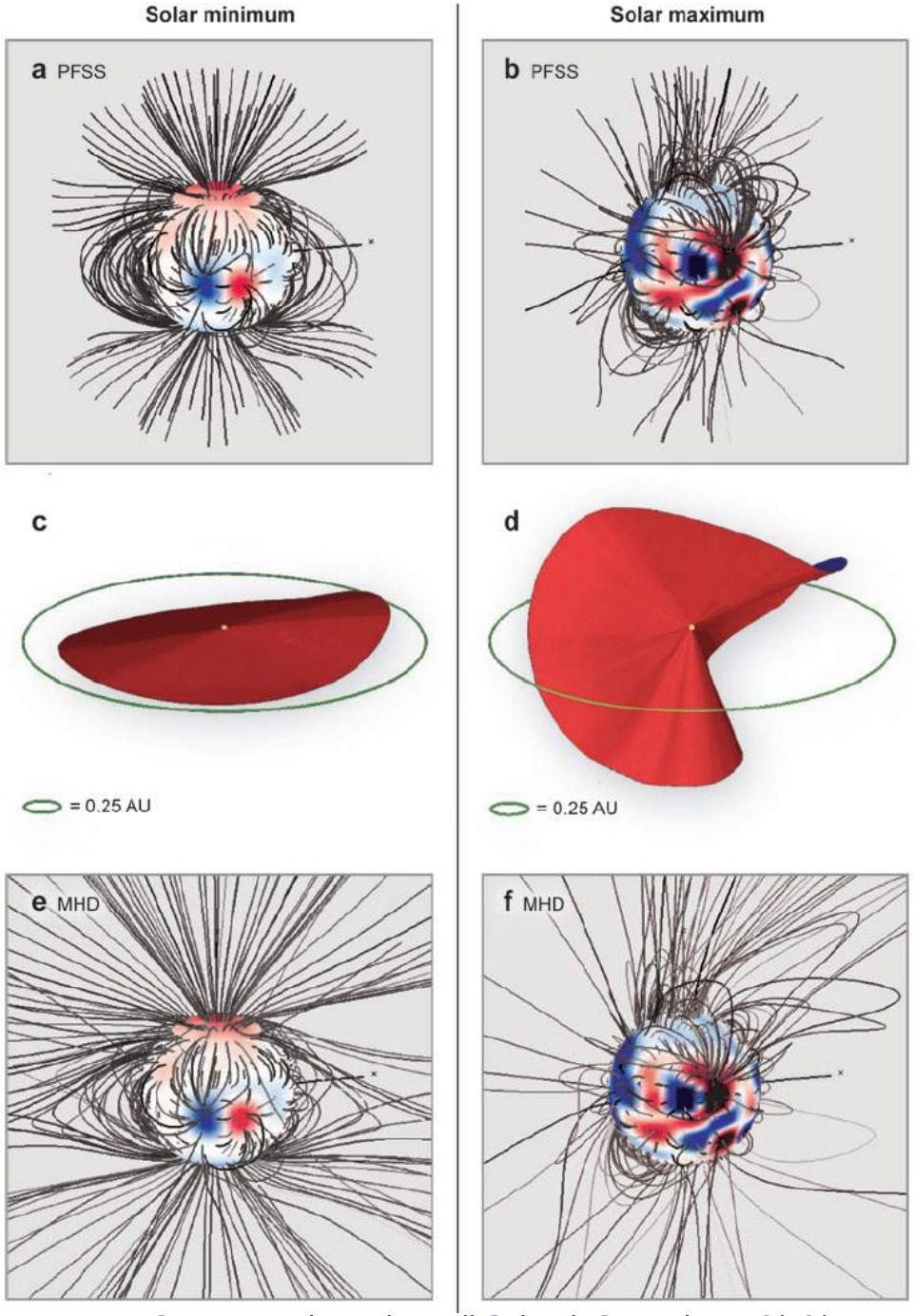

Couche de courant neutre du champ solaire interplanétaire

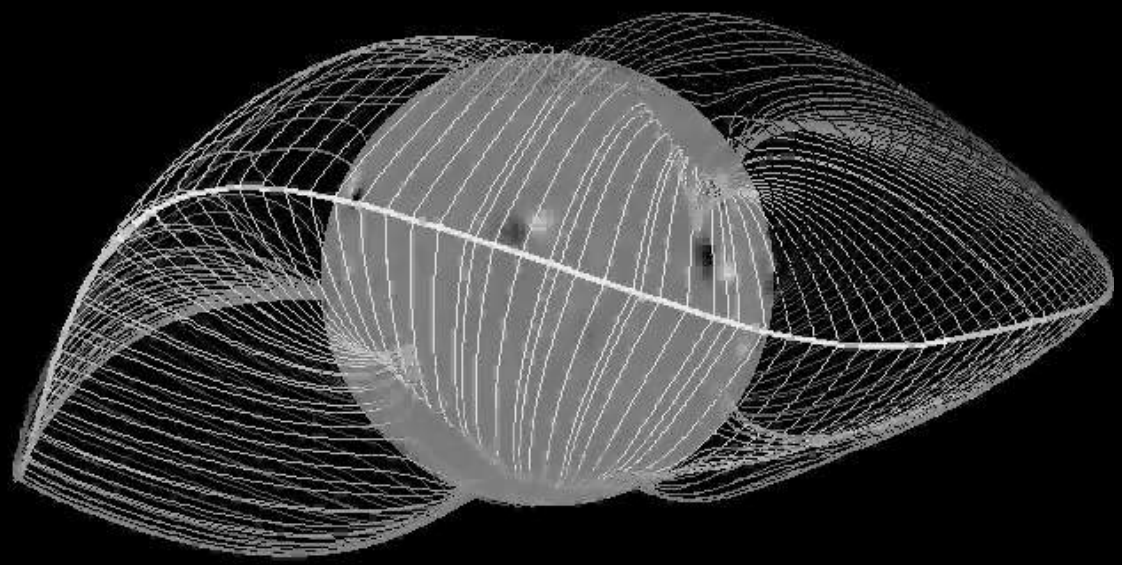

t = 0.0 y (27−day synodic reference frame) ϕ = 0.00

Mass and Angular Momentum Loss by Solar Wind

Spin down through magnetic braking (Schatzmann 1962)

Weber & Davis (1967)

Lever arm

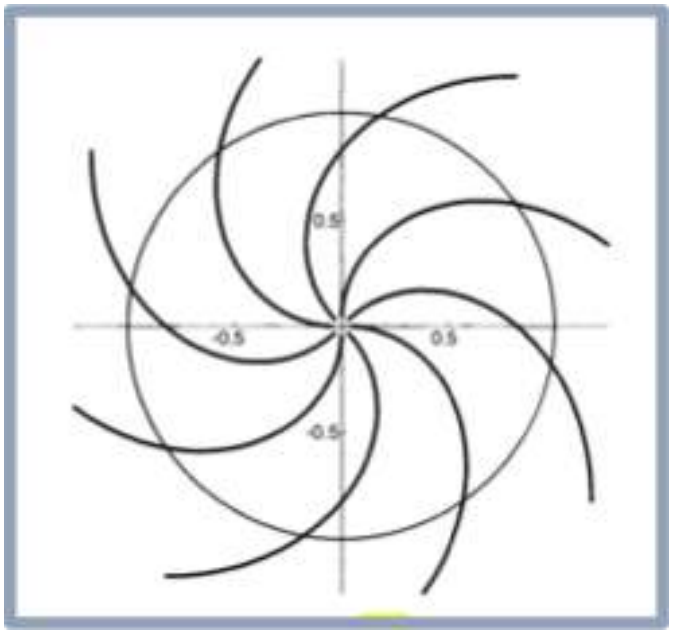

$$\frac{dJ}{dt} = \frac{dM}{dt} L = \frac{dM}{dt} r_A^2 \Omega$$

Angular momentum loss

The azimuthal magnetic field does not suddenly change from straight to spiralled. But quantitatively, it all works out *as if* there was a sharp transition. Following this picture, one can define an average Alfvén radius $\langle r_A \rangle$ — an "effective lever arm length". The specific angular momentum flux rate is then

$$l = \Omega_0 \langle r_A \rangle^2 \ . \qquad (7)$$

The resulting torque applied on the sun is (Matt & Pudritz 2008)

$$\tau = -\dot{M} \Omega_0 \langle r_A \rangle^2 \ . \qquad (8)$$

Héliosphère

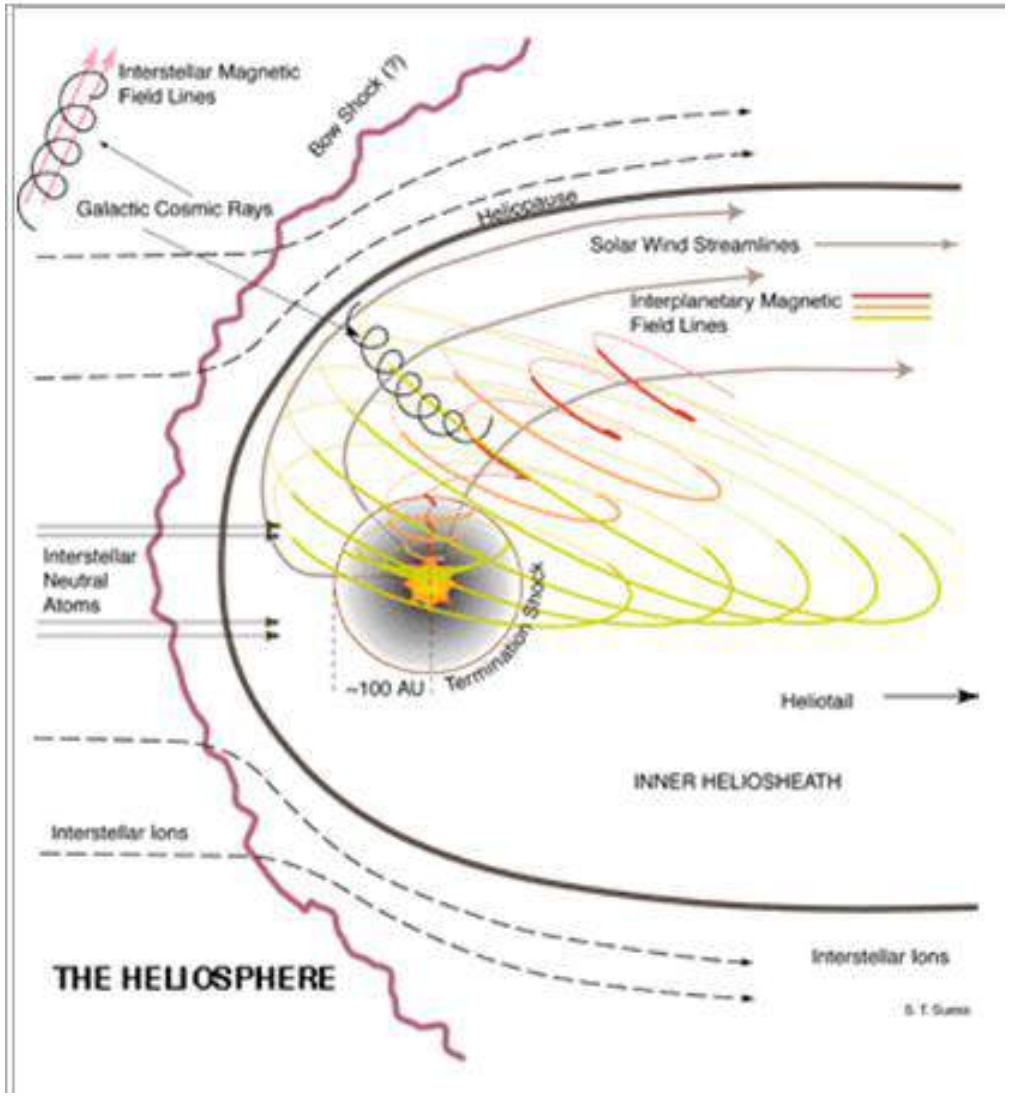

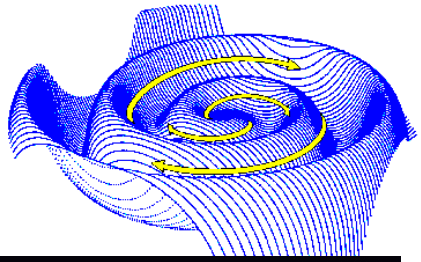

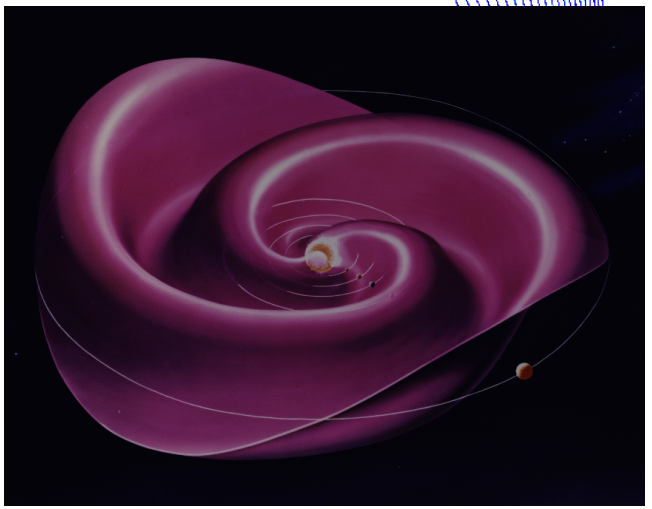

Spirale de Parker et Couche de Courant Neutre Héliosphérique

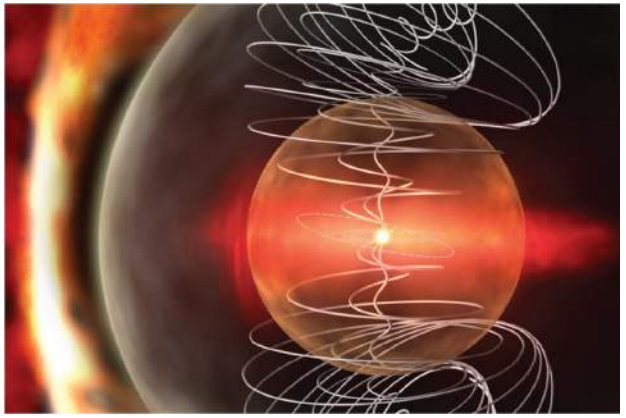

Figure 4

Solar motions projected into the heliosphere. (*a*) Parker field configuration, produced by a rigidly rotating Sun. There is no transport in latitude. (*b*) The Heliospheric field under the assumption of differential rotation into an asymmetric corona. Adapted from Zurbuchen, Schwadron & Fisk 1997. (*c*) The effect of random, diffusive motions in the heliosphere. Adapted from Jokipii & Kóta 1989.

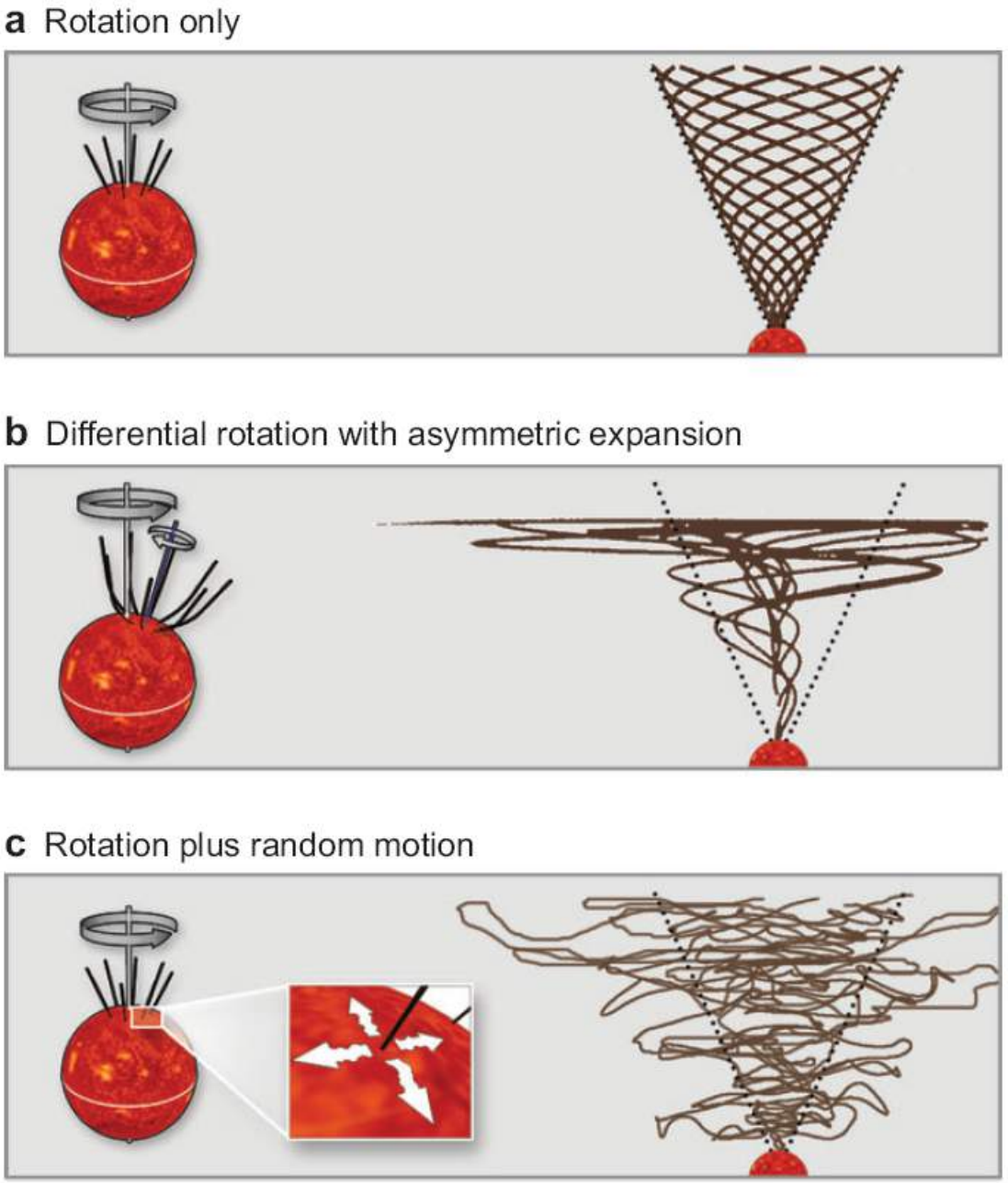

Parker's spiral + CME's

(from NOAA)

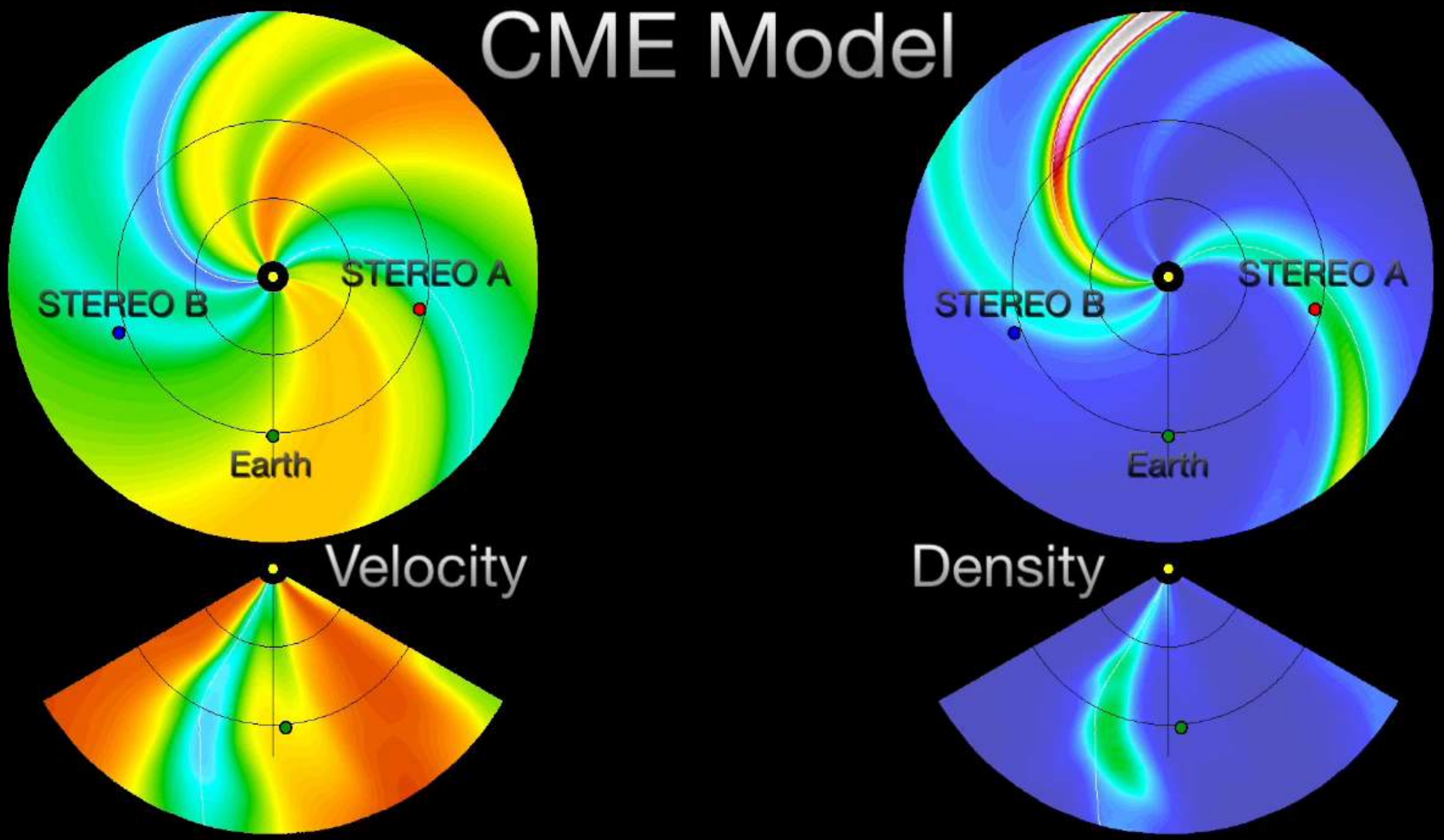

Héliosphère

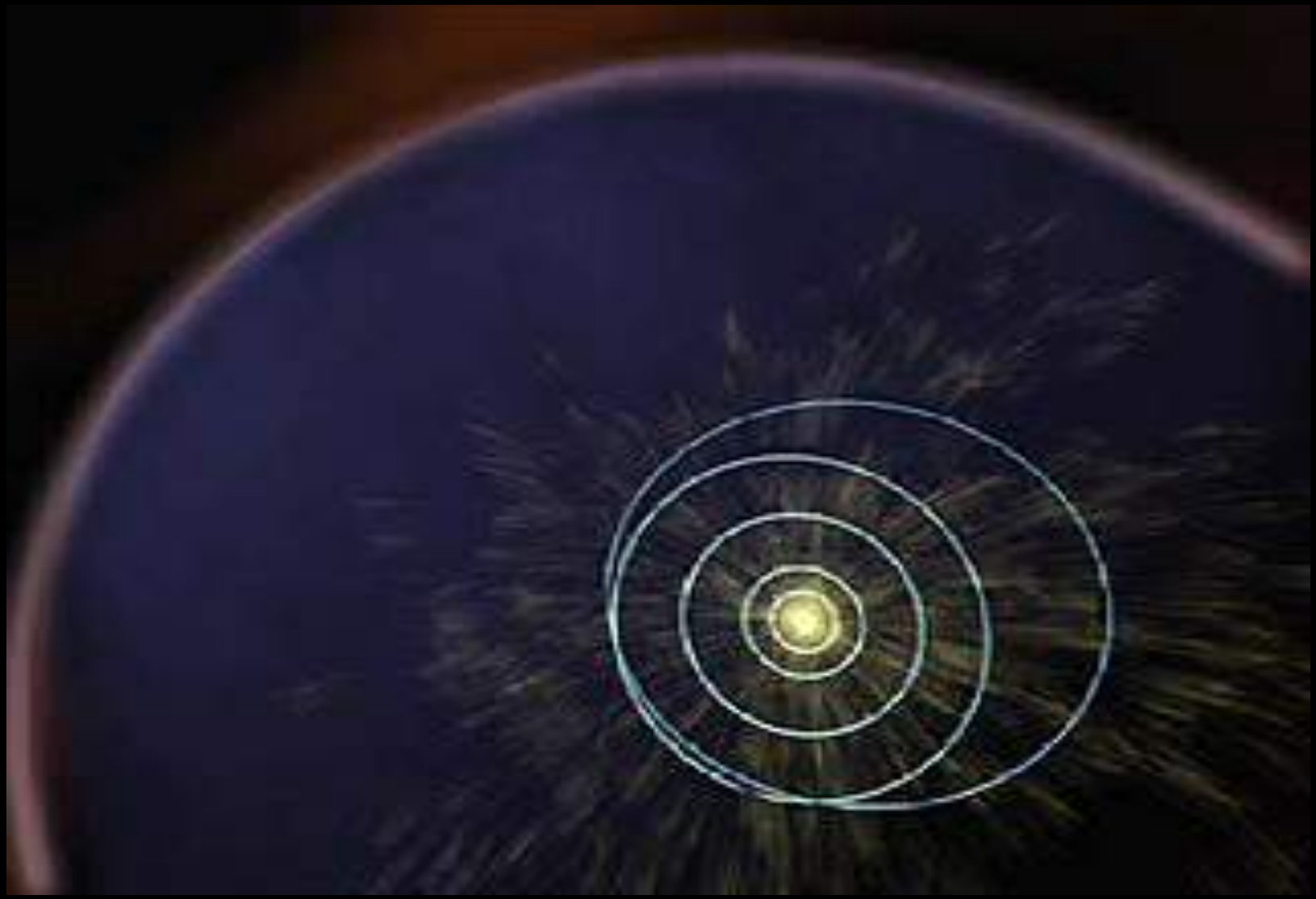

Nasa

Solar Motion in Local Interstellar Medium (ISM)

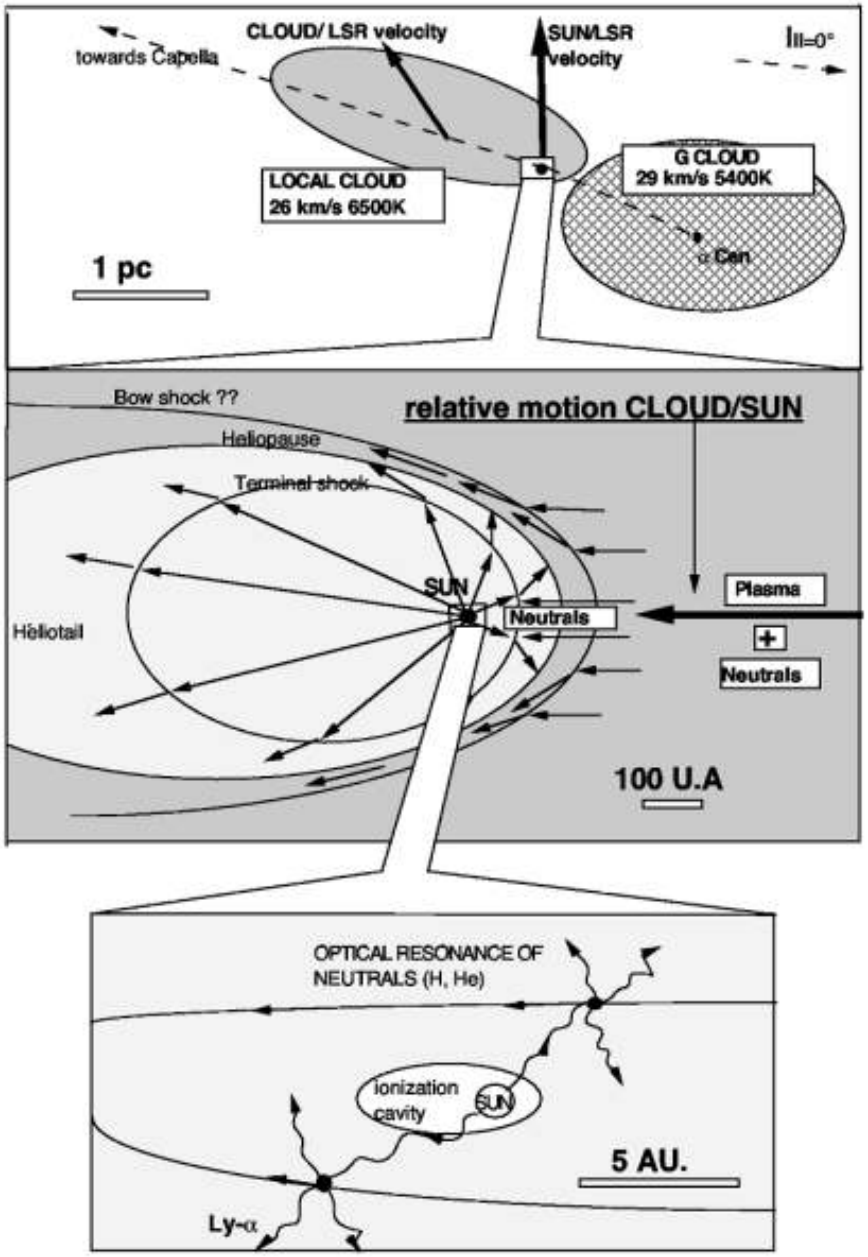

Relaxation of Magnetic Field inside Stars as they Evolve

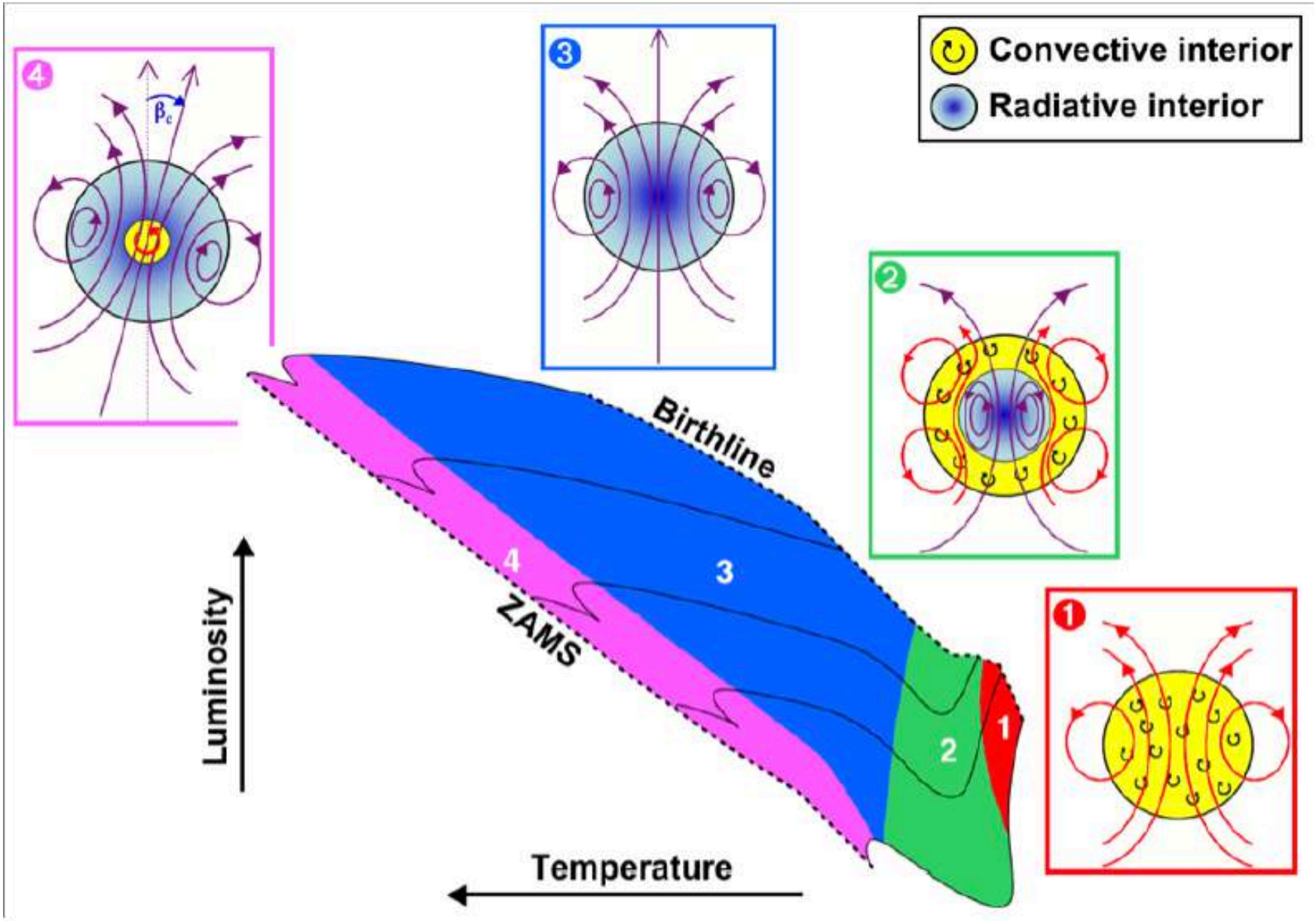

Alecian et al. 2013

Surface magnetic field and Zeeman Doppler Imaging

Spectropolarimeters:

Narval 375nm à 1050nm @TBL
& Espadons (370nm à 1000 nm) @CFHT

Zeeman Doppler Imaging consist in extracting Stokes parameters as a function of phase, on several wave-lengths to increase signal over noise ratio.

Works well on fast rotators.

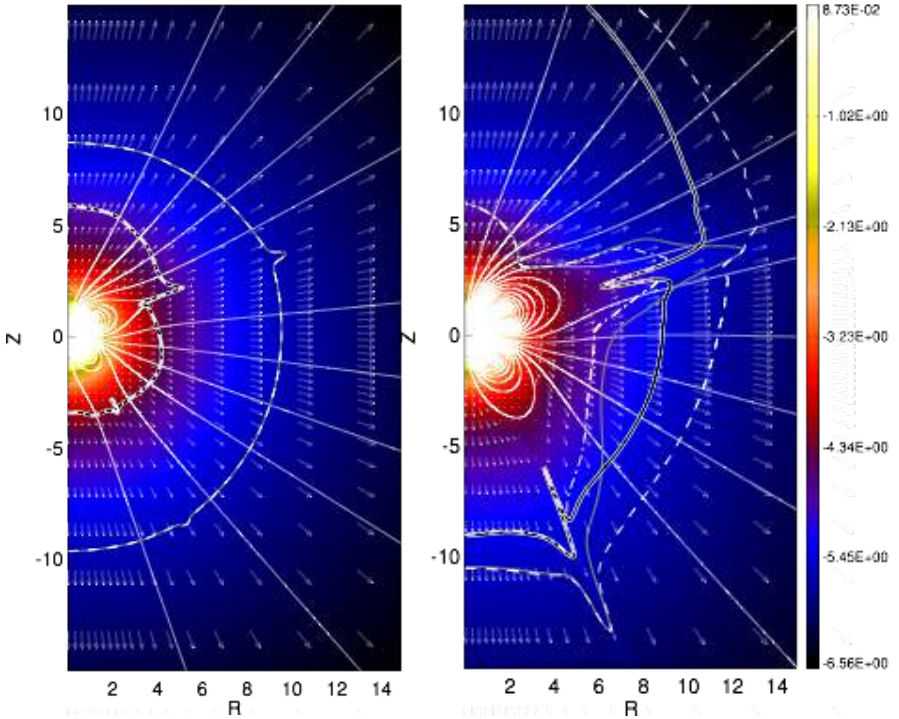

The Sun at maximum of cycle 22

Young K-Star TYC-0486-4943-1

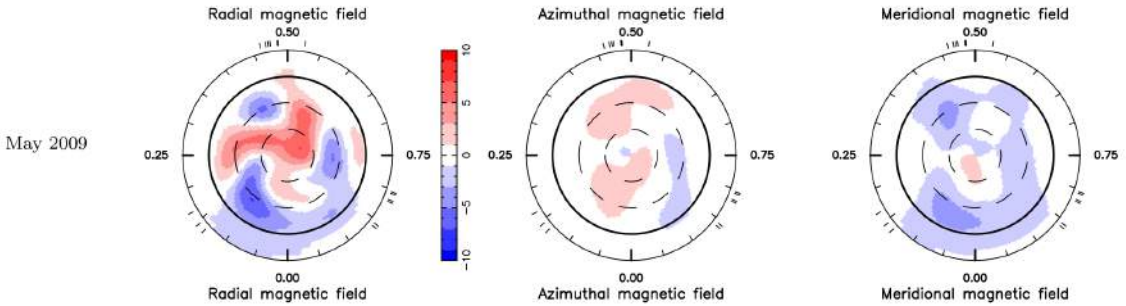

Tau Boo by Fares et al. 2013

Regression methods ->

List of spherical harmonics decomposition coefficients.

Magneto-Centrifugal Effect

Slow rotation

Fast rotation

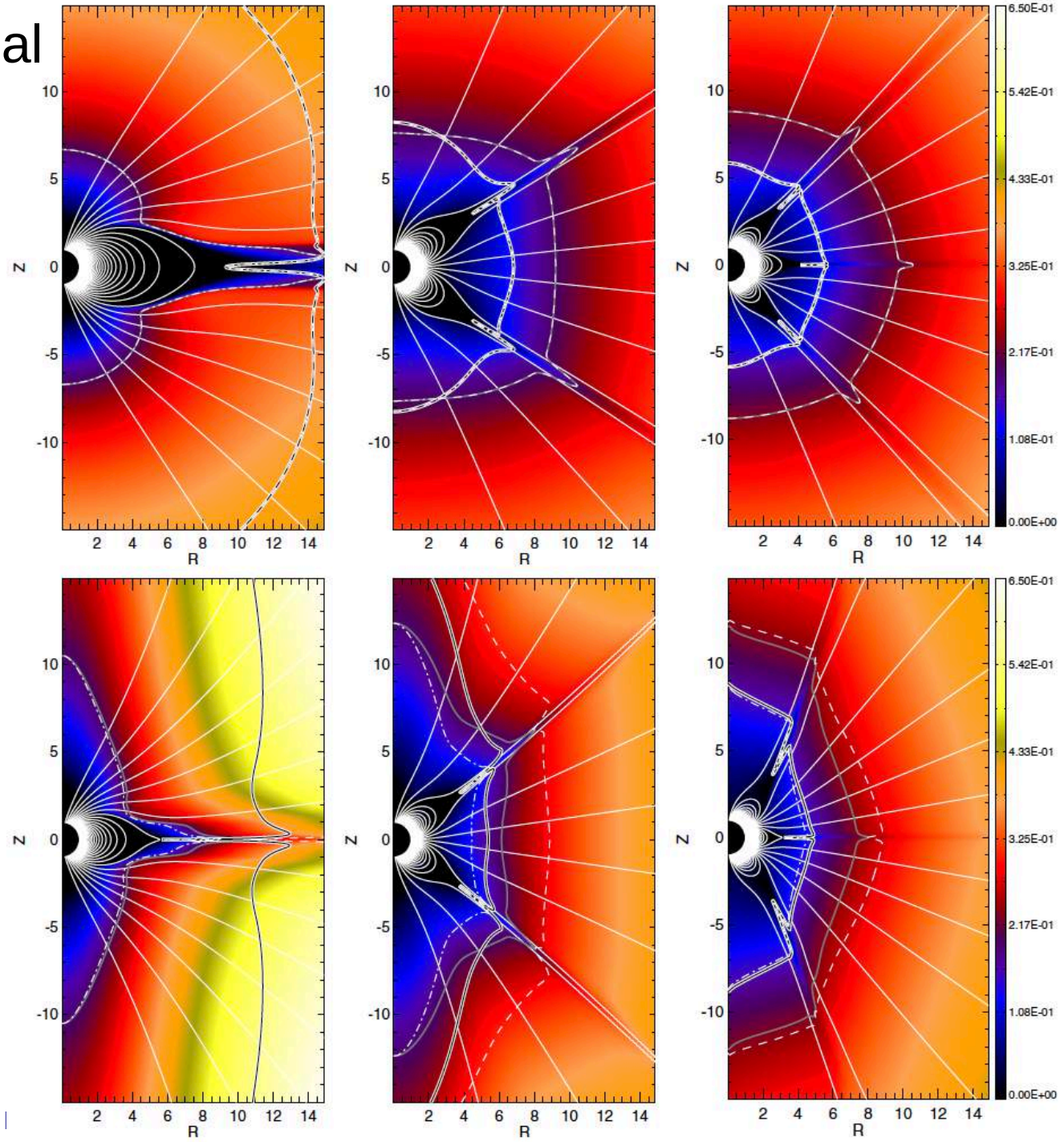

Reville et al. 2015a

MHD Wind Simulations and angular momentum loss law

The most general law as of today:

$$\frac{dJ}{dt} = \frac{dM}{dt}\Omega_* < r_A^2 >$$

open flux

$$\Phi_{open} = \int_S |\vec{B} \cdot d\vec{S}|$$

$$\frac{dJ}{dt} = \frac{dM}{dt}^{1-2m} \Omega_* R_*^{2-4m} K_1^2 \Phi_{open}^{4m} (1 + f^2 / K_2^2)^{-m} v_{esc}^{-2m}$$

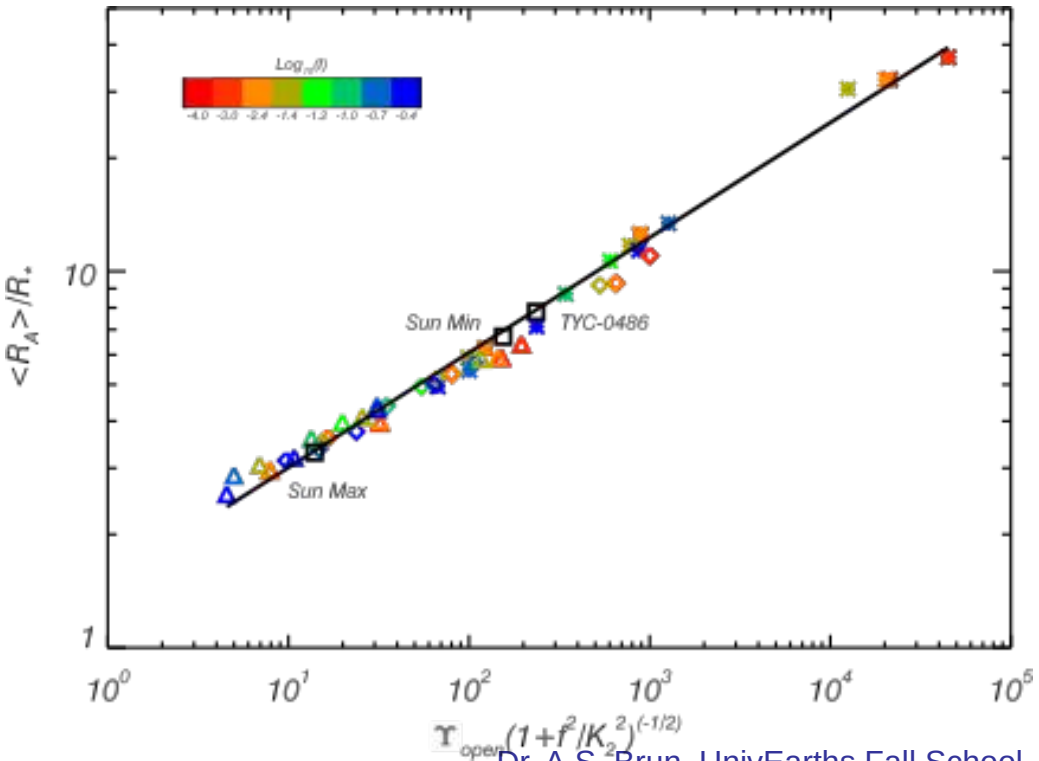

m=0.3
K1=1.4
K3=0.05

Réville et al. 2015, ApJ 798:116

3D Simulations of a aging K-Star

- BD-16351 27 Myr
- TYC-5164-567 120 Myr
- DX Leo 257 Myr
- AV 2177 584 Myr
- HD 190771 2.7 Gyr
- HD 146233 4.7 Gyr
- HD 3751 8 Gyr

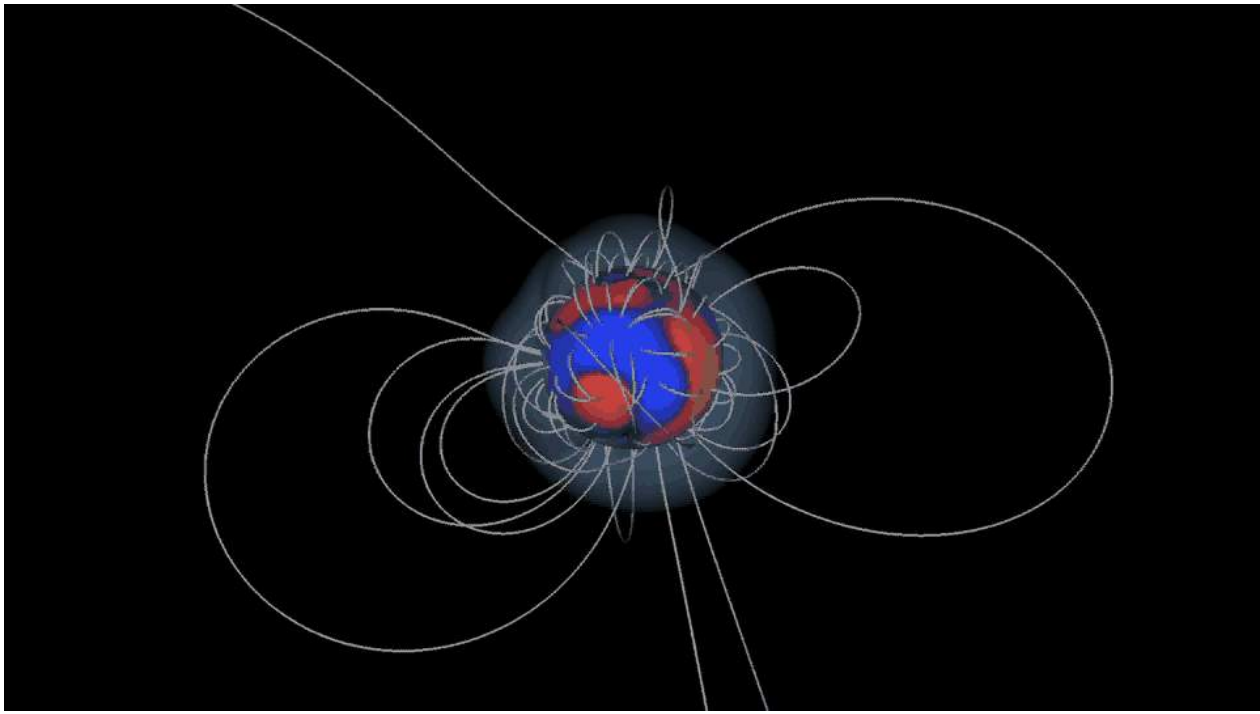

HD 190771

Reville et al. 2015

What about exoplanets ?

Exo-Planets Distribution near Host Star

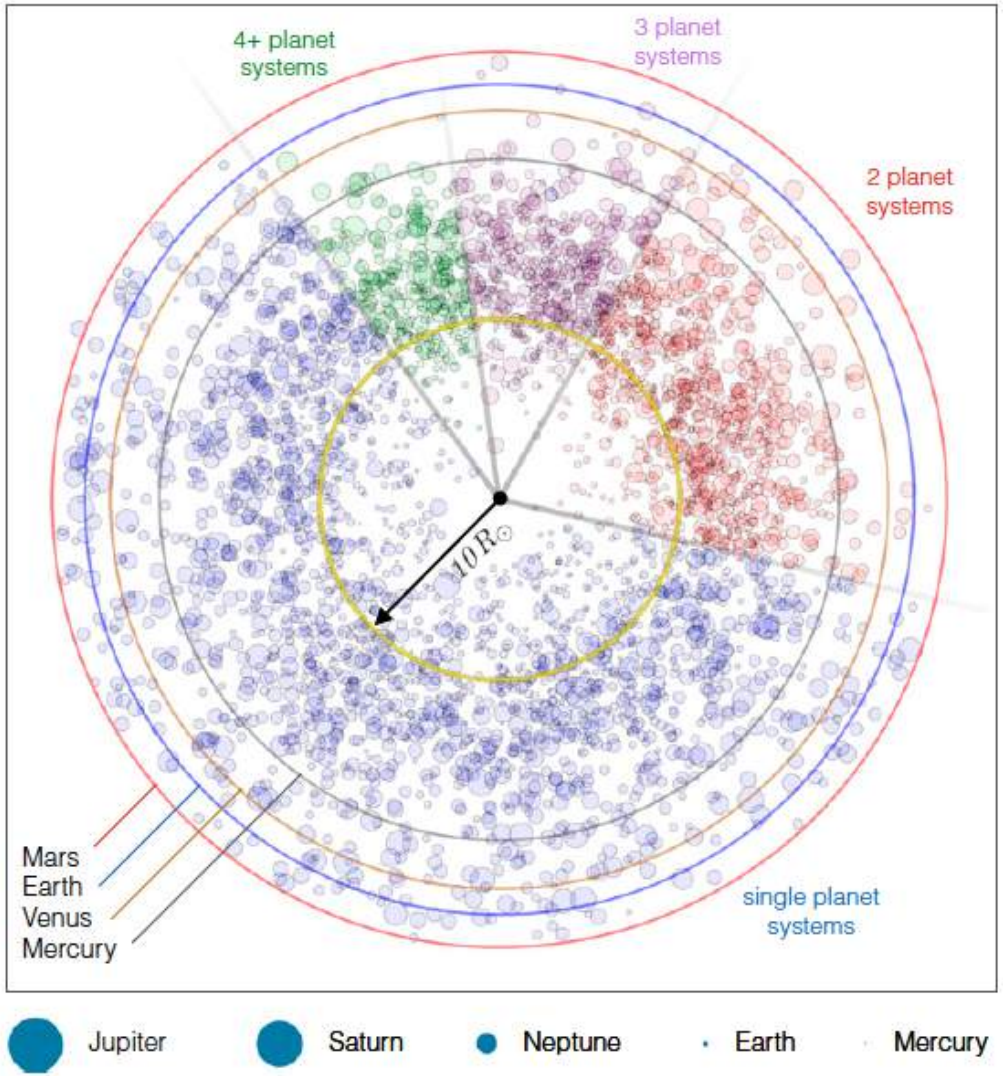

Alfven wings

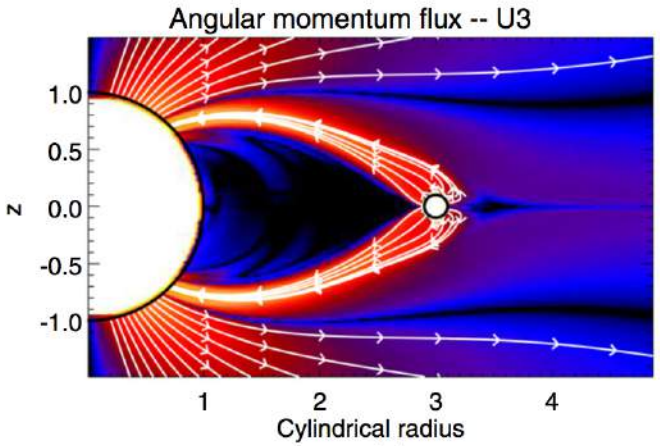

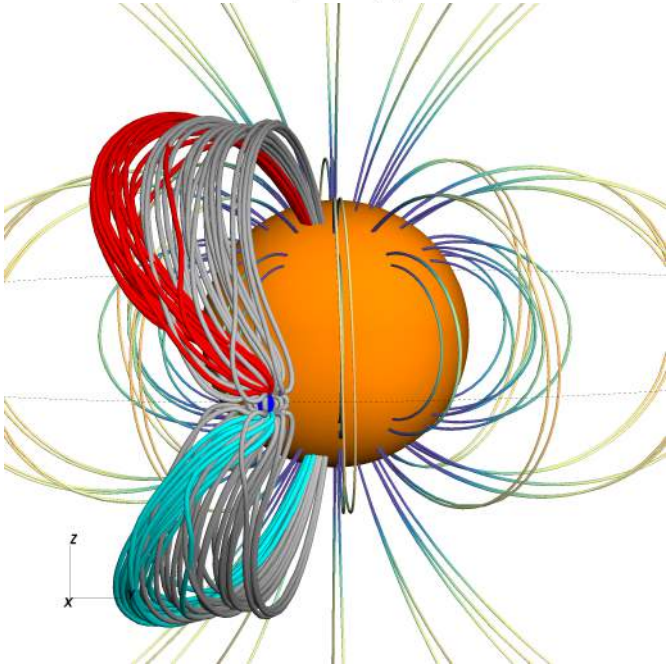

Strugarek, Brun, Matt, Réville, 2014, Apj 795

Strugarek et al. 2015, sub. Apj

What about close-in exoplanets ?

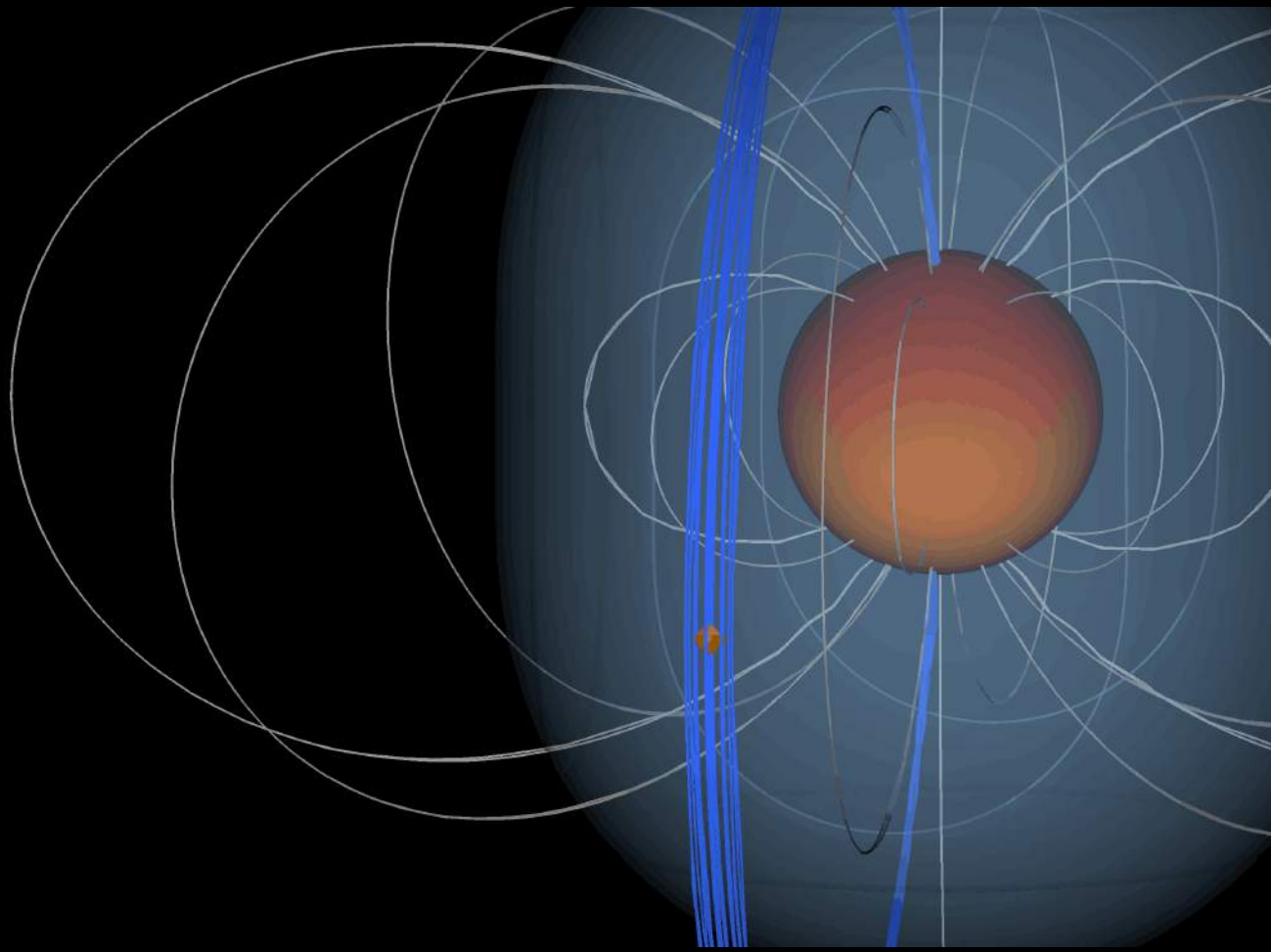

Wind interacts with exo-planets + direct magnetic connection: Alfven wings

Strugarek et al. 2014, 2015 ApJ

3-D MHD Flux Emergence Models

The current solar global dynamo paradigm relies on the so-called: interface dynamo

One crucial element of this model is the emergence at the solar surface of toroidal like structures, coming from the deep interior, i.e the tachocline

We present the first attempt to compute self-consistently 3-D MHD solar convective models of the evolution of such toroidal structures in spherical shells.

We wish to assess how such toroidal structures may pop up at the surface as active regions and how turbulent rotating convection may influence their rise

Work done with my PhD student L. Jouve (Jouve & Brun 2007, AN, 328, 1104)

Cartesian study (Fan, Abbett, Fischer, 2002, ApJ):

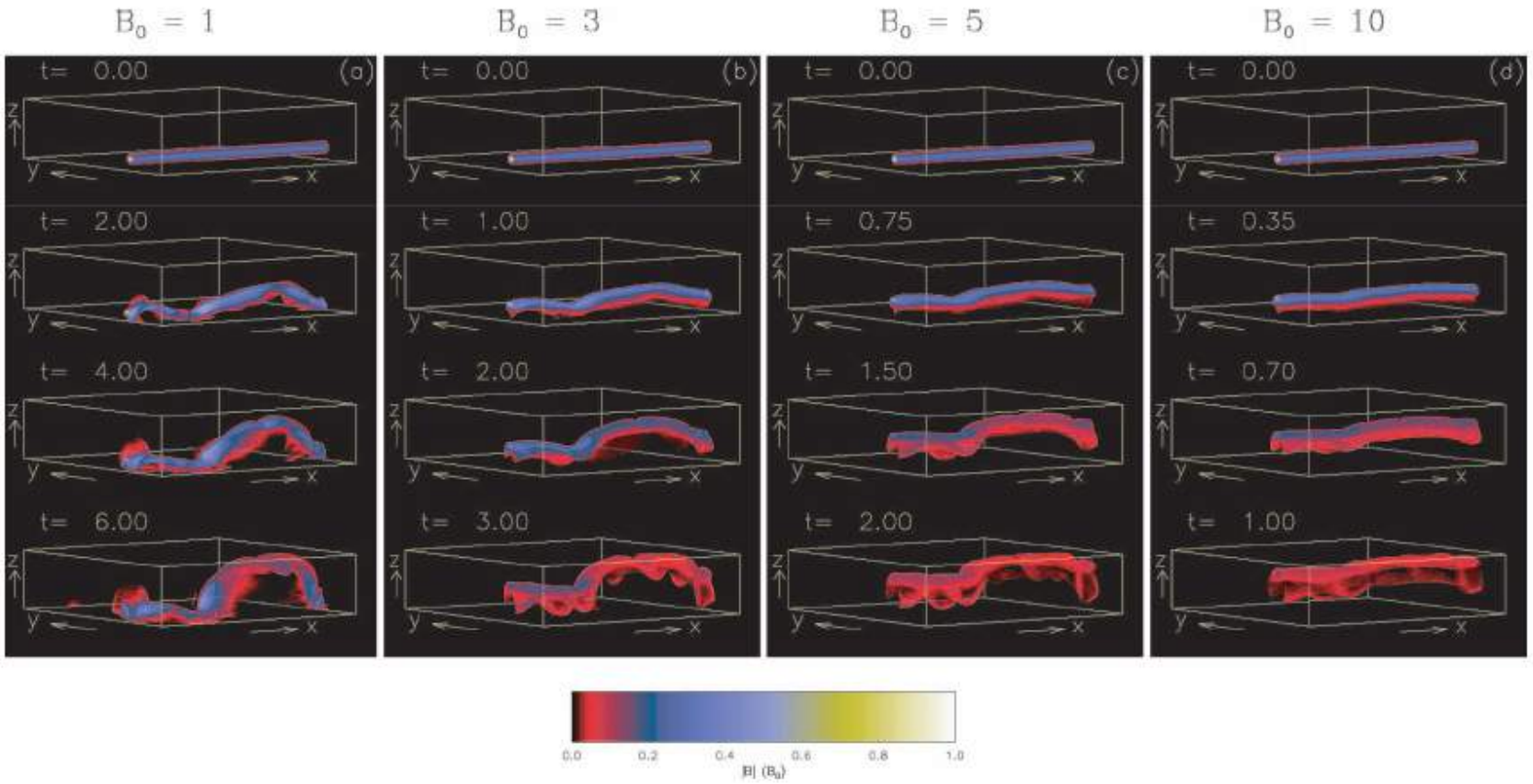

MHD Equations

$$\frac{\partial \rho}{\partial t} + \vec{\nabla}.(\rho \vec{v}) = 0$$

$$\frac{\partial \vec{v}}{\partial t} + (\vec{v}.\vec{\nabla})\vec{v} = -\frac{\vec{\nabla} p}{\rho} - \frac{\vec{\nabla}.\vec{\vec{D}}}{\rho} - g\hat{r} + 2\vec{v} \times \vec{\Omega} + \frac{1}{c}\vec{j} \times \vec{B}$$

$$\frac{\partial S}{\partial t} + \vec{v}.\vec{\nabla} S = \frac{1}{\rho \mathrm{T}} \vec{\nabla}.(\kappa \rho \mathrm{T} \vec{\nabla} S + \kappa_{\mathrm{r}} \rho \mathrm{c}_{\mathrm{p}} \vec{\nabla} T) + \frac{2\nu}{\mathrm{T}} [e_{ij} e_{ij} - \tfrac{1}{3} (\vec{\nabla}.\vec{v})^2] + Q_{ohm}$$

$$\frac{\partial \vec{B}}{\partial t} = \vec{\nabla} \times (\vec{v} \times \vec{B}) - \vec{\nabla} \times (\eta \vec{\nabla} \times \vec{B})$$

Case of a Stratified Compressible Fluid under the influence of Rotation and Magnetic field

3D MHD Code ASH (Anelastic Spherical Harmonics)
(Clune et al. 1999, Miesch et al. 2000, Brun et al. 2004)

A Realistic Model of the Solar Convection Zone

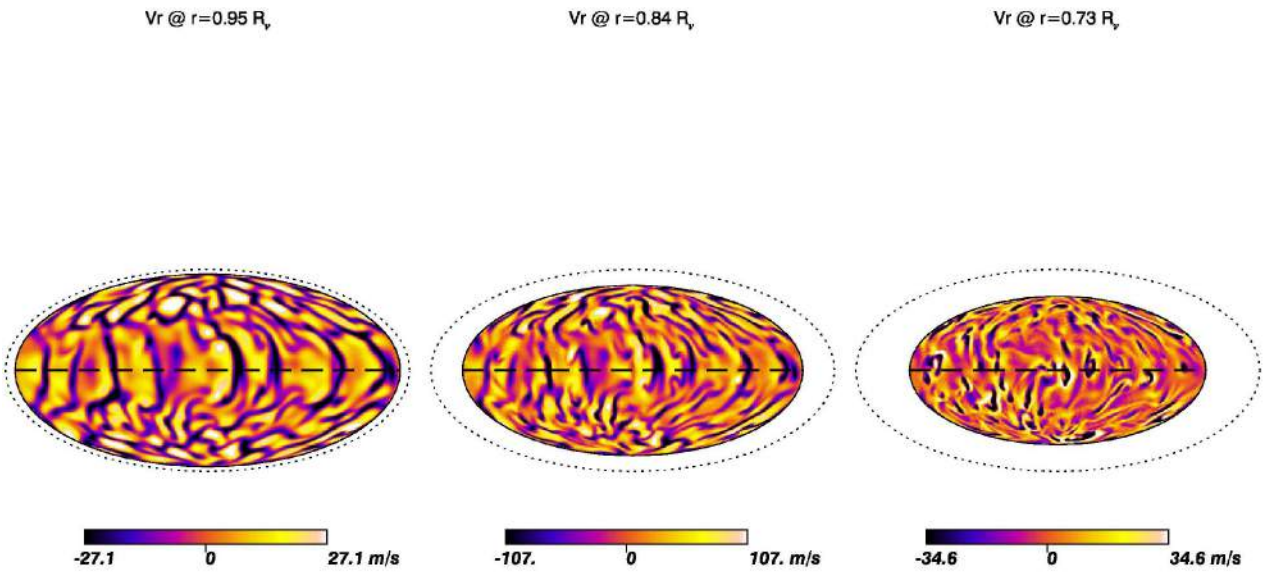

Meridional
Circulation ($\mathbf{V_p}=V_r\,\mathbf{e_r} + V_\theta\,\mathbf{e_\theta}$)

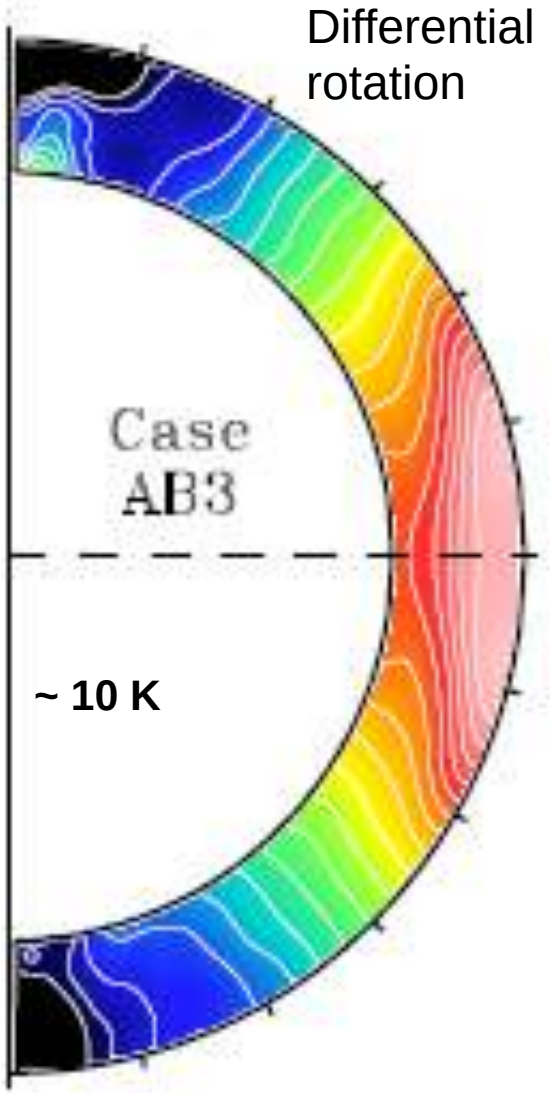

Miesch, Brun & Toomre 2006

$$S(r_{bot}, \theta) = a_2\, Y_2^0 + a_4\, Y_4^0$$

The Model

Knowing the expression of Yuhong Fan for Bphi and Aphi in an axisymmetric model :

$$\vec{B} = \vec{\nabla} \times [\frac{A_\varphi}{r \sin\theta} \vec{e}_\varphi] + B_\varphi \vec{e}_\varphi$$

$$A_\varphi = \frac{1}{2} q a^2 B_0 \exp[-(\omega^2 / a^2)]$$

$$B_\varphi = \frac{1}{r \sin\theta} a B_0 \exp[-(\omega^2 / a^2)]$$

with

$$\omega^2 = R_T{}^2 + r^2 - 2 r R_T \cos(\theta - \theta_T)$$

We get for our case these expressions for the stream functions:

$$\vec{B} = \vec{\nabla} \times \vec{\nabla} \times (C\vec{e}_r) + \vec{\nabla} \times (A\vec{e}_r)$$

$$A = r B_0 \exp[-(\frac{r - R_T}{a})^2][1 + th(\frac{\theta - \theta_T}{a / R_T})]$$

$$C = \frac{a^2}{2} q B_0 \exp[-(\frac{r - R_T}{a})^2][1 + th(\frac{\theta - \theta_T}{a / R_T})]$$

Initializing the Model

TWIST ET DEGRE D'ENROULEMENT DES LIGNES DE CHAMP

$$\vec{B} = B_r\vec{e}_r + B_\theta\vec{e}_\theta + B_\varphi\vec{e}_\varphi$$

$$\vec{B} = B_t\vec{e}_t + B_\varphi\vec{e}_\varphi \qquad \text{where} \qquad B_t\vec{e}_t = B_r\vec{e}_r + B_\theta\vec{e}_\theta$$

We can define the pitch angle or twist for us as the angle between the transverse field and the longitudinal field in the tube so that tan(ψ)=Bt/Bj. We have a value of the threshold of (a/Hp)^1/2.
In our case, we have (a/Hp)^1/2 ≈0.57 so we take tan(ψ)≈0.6 to be above the threshold.
We can have a relation between this twist and the winding degree of the field lines:

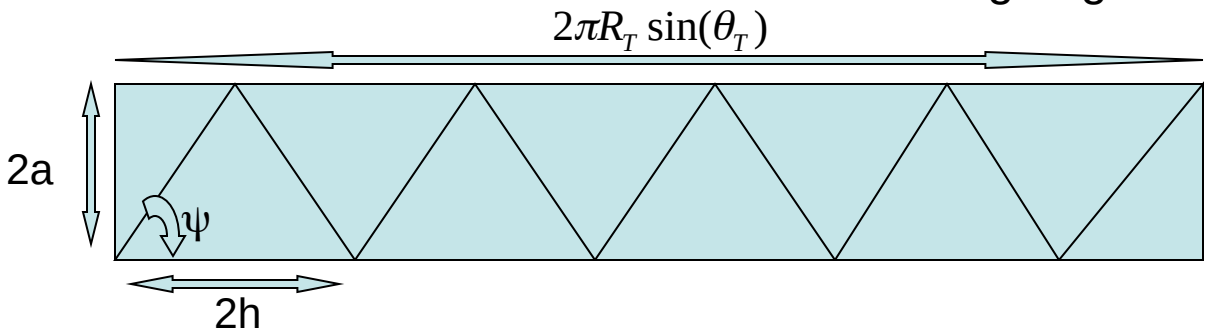

$$\tan(\psi) = \frac{2a}{h} \qquad n = \frac{\pi R_T \sin(\theta_T)}{h} = \frac{\pi R_T \tan(\psi)\sin(\theta_T)}{2a}$$

It gives a winding number of 17

Initializing the Model

We are trying to understand the influence of two significant parameters on the tube behaviour evolving in a self-consistantly developed convection: the initial tube twist and field strength.

To do so, we are studying 4 different cases:

- A twisted weak B case, a twisted strong B case
- An untwisted weak B case, an untwisted strong B case

Beq is approximately 3.5 10^4 G

For the twisted case, the twist is set to a value above the threshold quoted in Fan, Living Review Sol. Phys.,2004 which is (a/Hp)^(1/2).

Case	B_0/B_{eq}	Twist	a/H_p	$v_{rise}(m/s)$	$t_{rise}(days)$	$R_c = \frac{v_{conv}R}{\nu}$	$R_m = \frac{v_{rise}a}{\eta}$	P_r	P_m	$a^2/\eta(days)$
NoTwistFaiblePm1	4.3	0	0.36	>100	<10	150	20	0.25	1	46
NoTwistFortPm1	10.7	0	0.36	>300	<3.5	150	60	0.25	1	46
TwistFaiblePm1	4.3	0.6	0.36	100	10	150	20	0.25	1	46
TwistFortPm1	10.7	0.6	0.36	300	3.5	150	60	0.25	1	46

Results: influence of twist

Vorticity generation in the untwisted case due to the lack of magnetic tension.

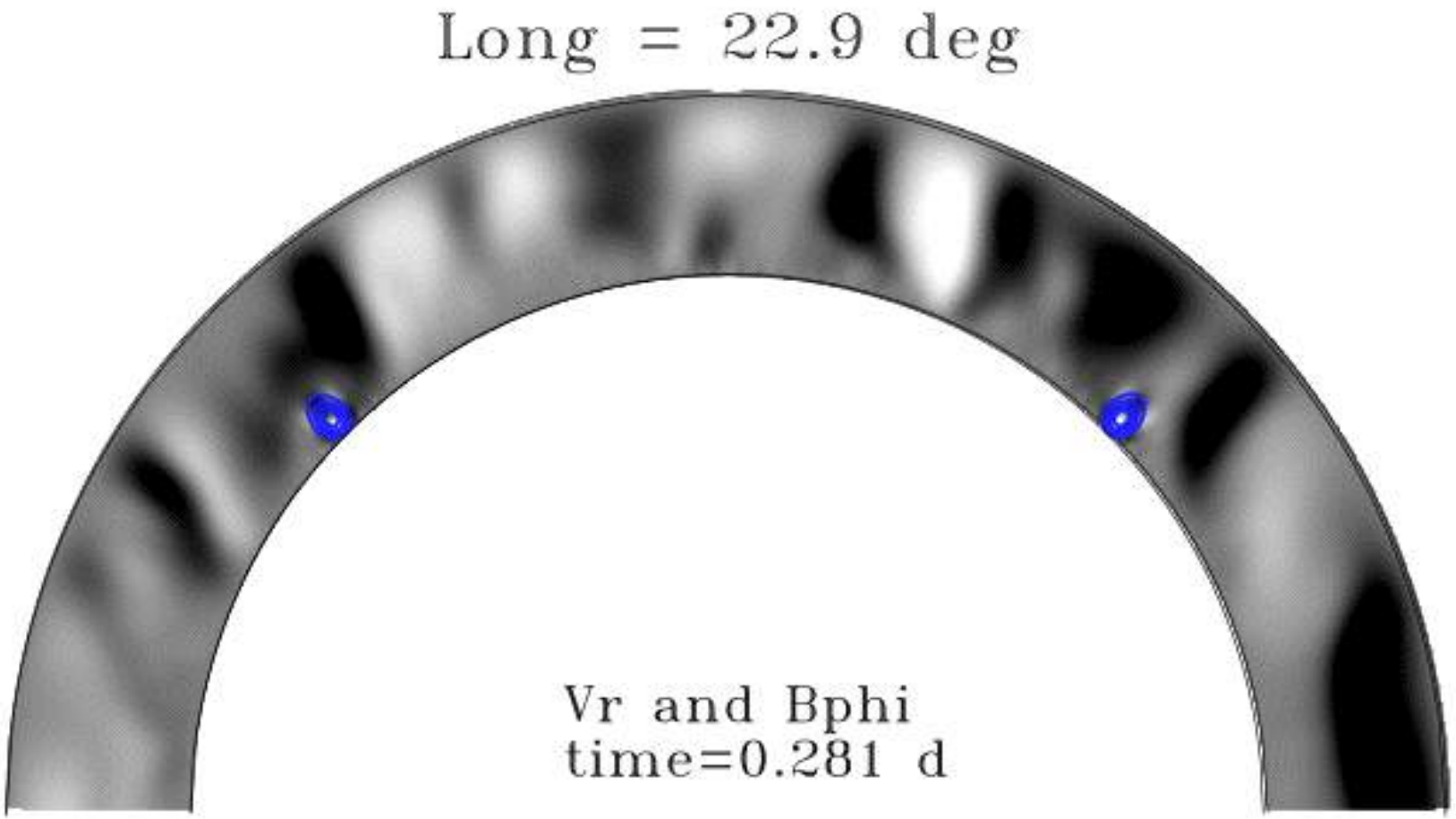

No twist *Twist*

Results: influence of twist

Vorticity generation in the untwisted case due to the lack of magnetic tension.

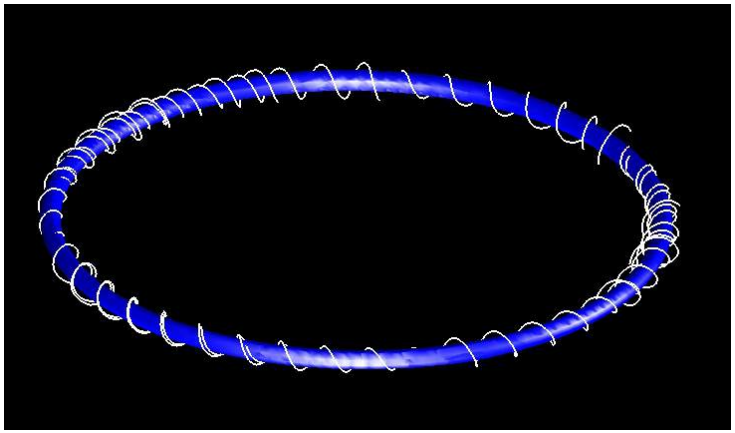

Twisted torus

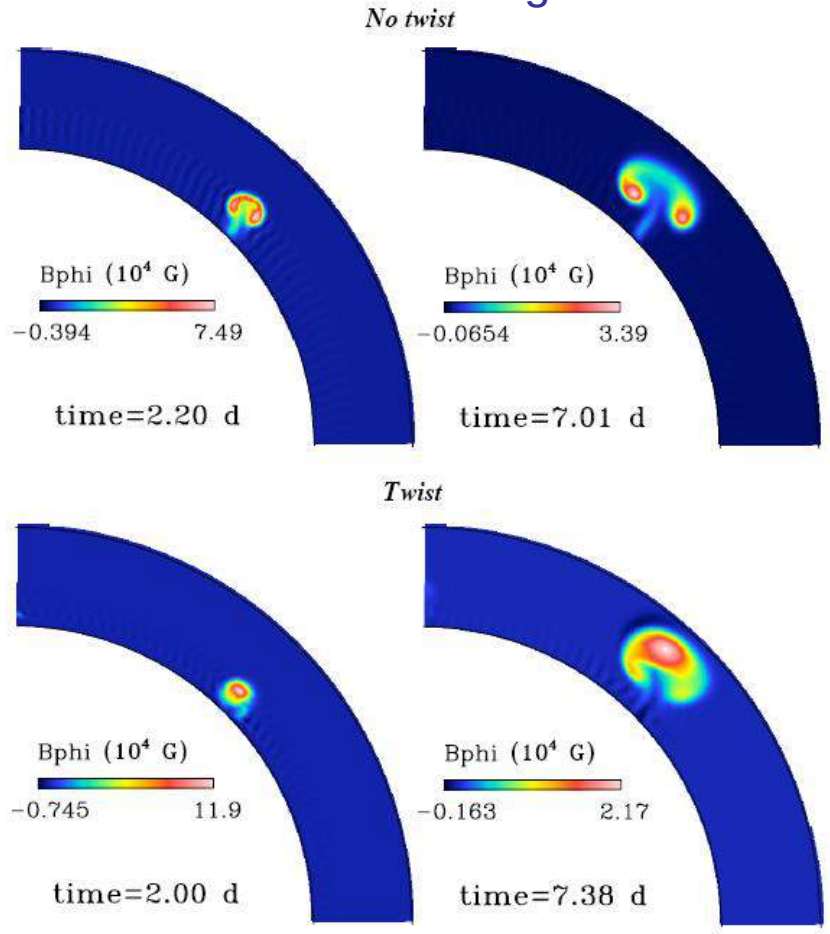

Fig. 1 (online colour at: www.an-journal.org) The four panels are snapshots of B_ϕ for the untwisted case (*two upper panels*) and the twisted case (*two lower panels*), cut at a specific longitude, shown in a northern quadrant of the sphere, after 2 days (*left panels*) and 7 days (*right panels*) of evolution.

Influence du twist

Création de vorticité (Emonet & Moreno-Insertis, 1998):

$$\rho \frac{D}{Dt}\left(\frac{\boldsymbol{\omega}_l}{\rho}\right) = \boldsymbol{\nabla}\left(\frac{\Delta\rho}{\rho}\right) \times \boldsymbol{g} + \frac{\boldsymbol{\nabla} \times \boldsymbol{F}_{\mathrm{Lt}}}{\rho} + \boldsymbol{\nabla}\left(\frac{1}{\rho}\right) \times \left[-\boldsymbol{\nabla}\left(\Delta p + \frac{B_l^2}{8\pi}\right) + \boldsymbol{F}_{\mathrm{Lt}} \right]$$

Source de vorticité

Puits de vorticité (terme de tension magnétique)

Terme négligeable

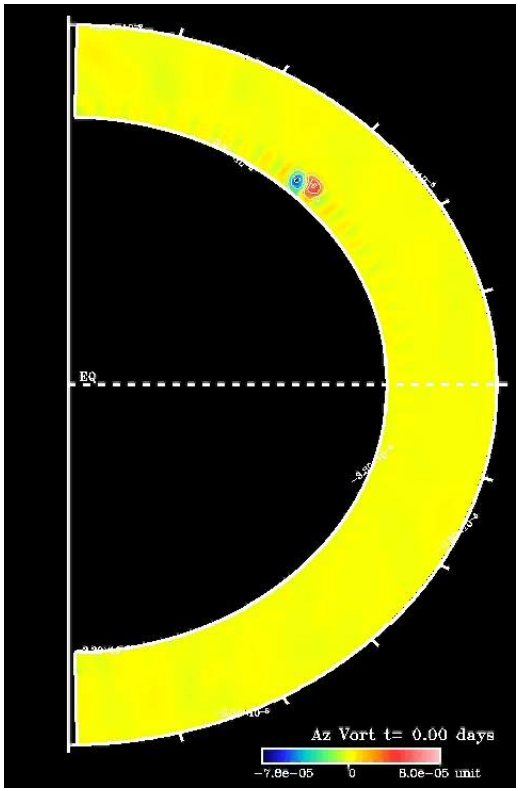

On doit avoir un twist suffisant pour contrer la création de vorticité due au couple gravitationel.

Si on écrit que le terme de source de vorticité est égal au terme de puits, on trouve un seuil pour le paramètre de twist au-dessus duquel le tube monte dans la ZC sans création de vortex:

$$\sin\psi = \frac{\sqrt{(B_r^2 + B_\theta^2)}}{B} \geq \sqrt{\frac{a}{H_p}} \times \sqrt{\left|\frac{\Delta\rho}{\rho}\right| \frac{\beta}{2}}$$

Results: Influence of the field strength

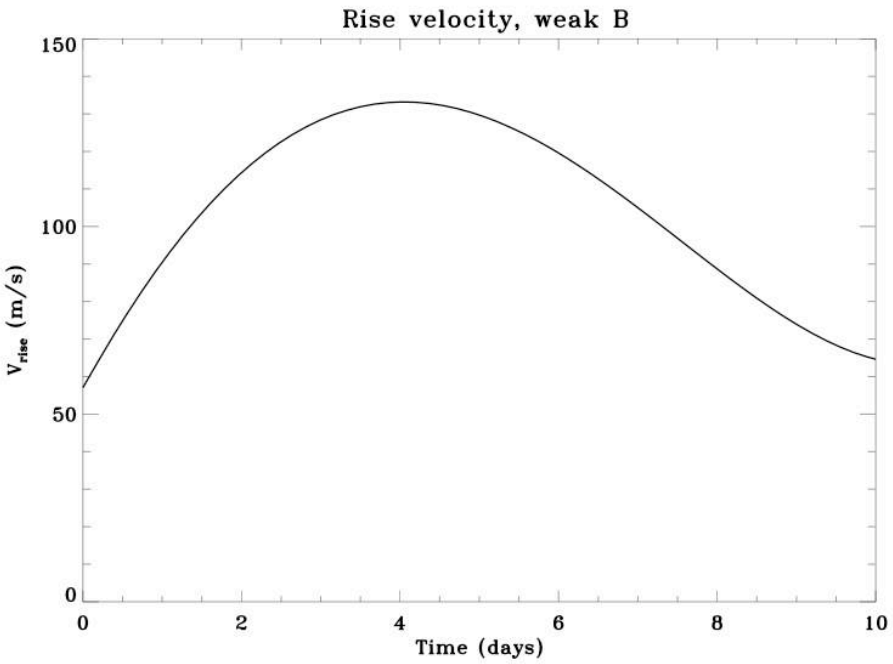

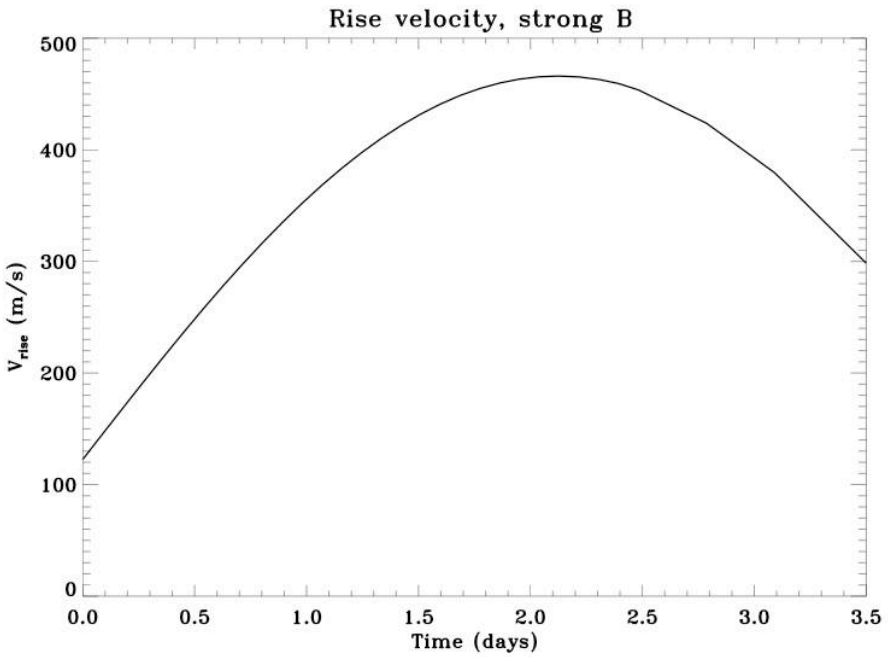

The tube acceleration in the first phase is due to the buoyancy force which is directly linked to the density deficit in the tube.

Thus we have in the acceleration phase:

$$acceleration \ \alpha \ \ \Delta\rho \ \ \alpha \ B_0^2$$

Convective cases

Influence of the initial magnetic intensity

Jouve & Brun, 2009, ApJ, 701. 1300

If B is weak, the evolution of the flux tube is much more influenced by convective motions.

Radial velocity and magnetic energy

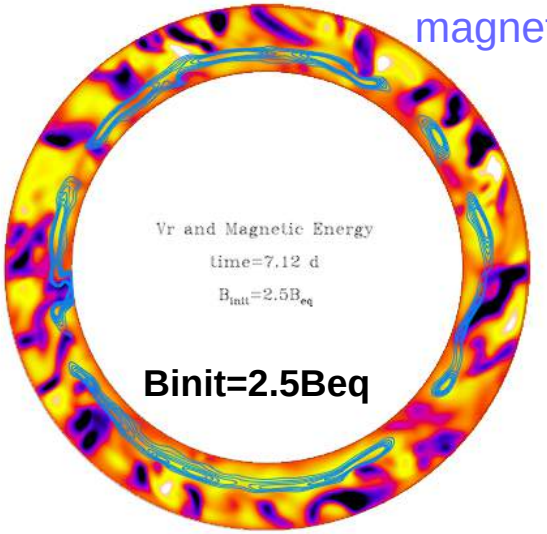

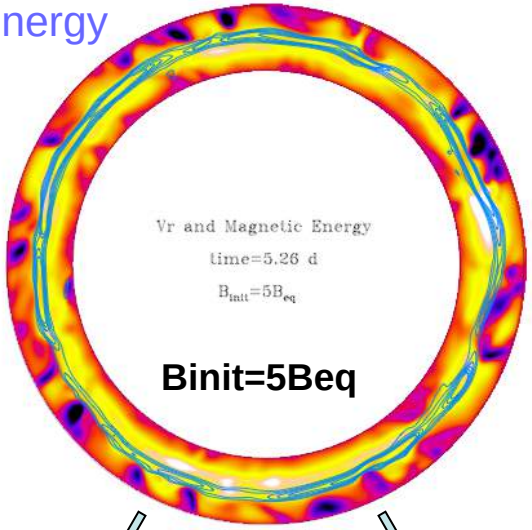

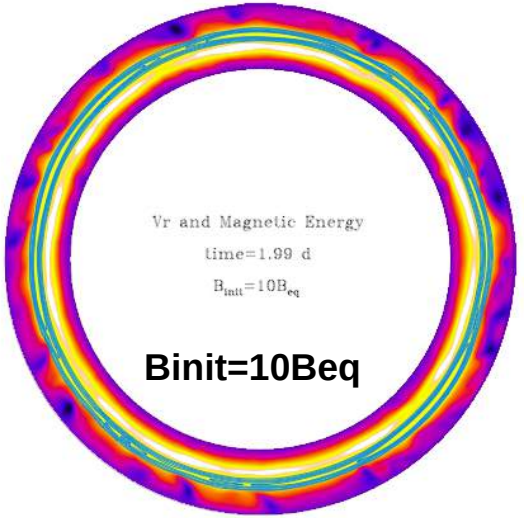

Radial velocity

R=0.87 R_S

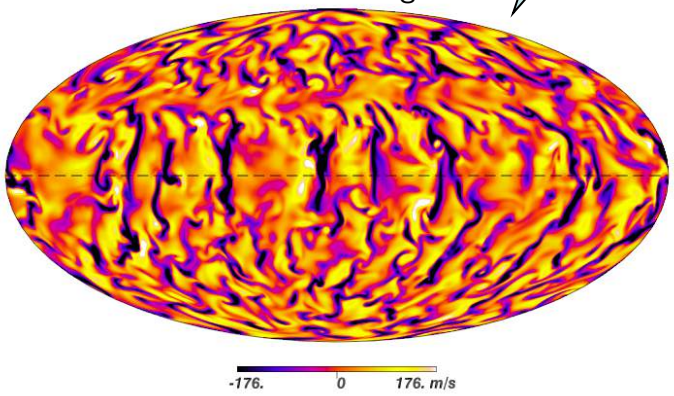

R=0.93 R_S

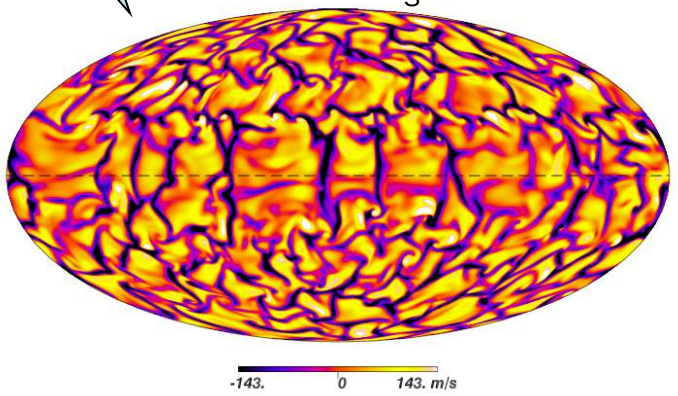

Meridional Circulation

More & more evidence for multi cellular MC

Mitra-Kaev & Thompson 2007

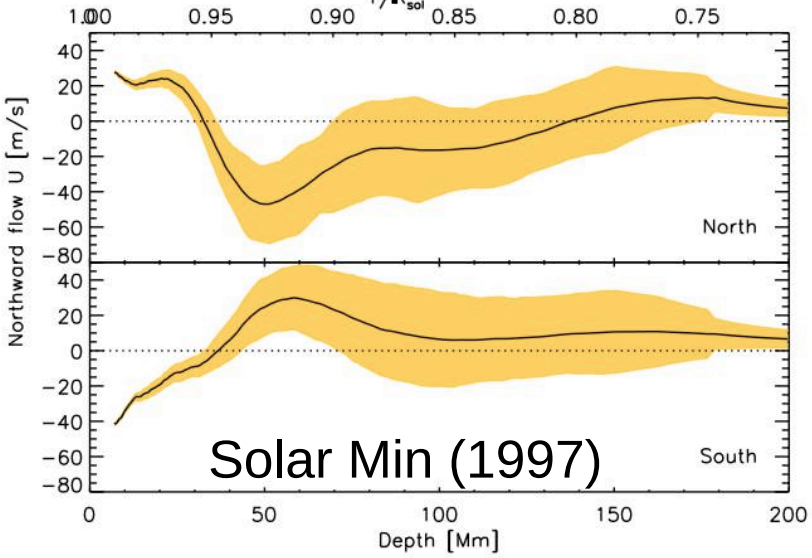

Influence of B (active region) on MC

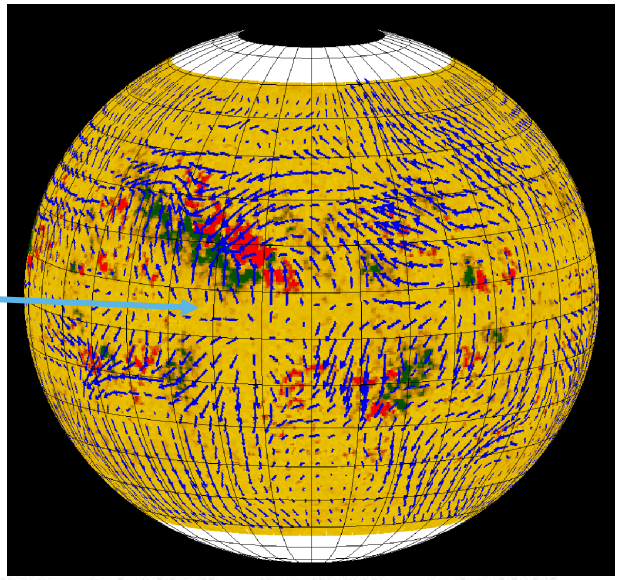

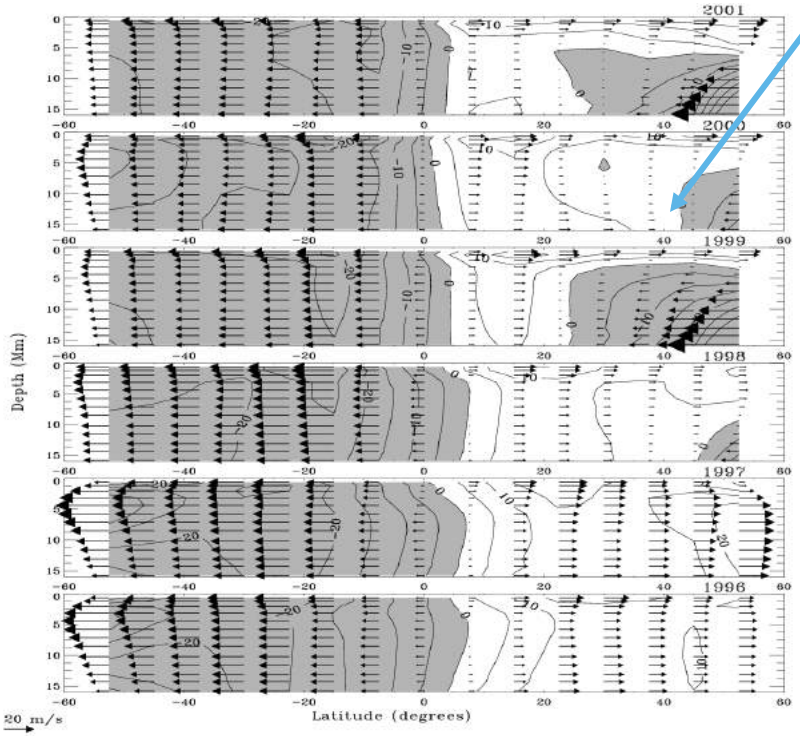

(Haber et al. 2002)

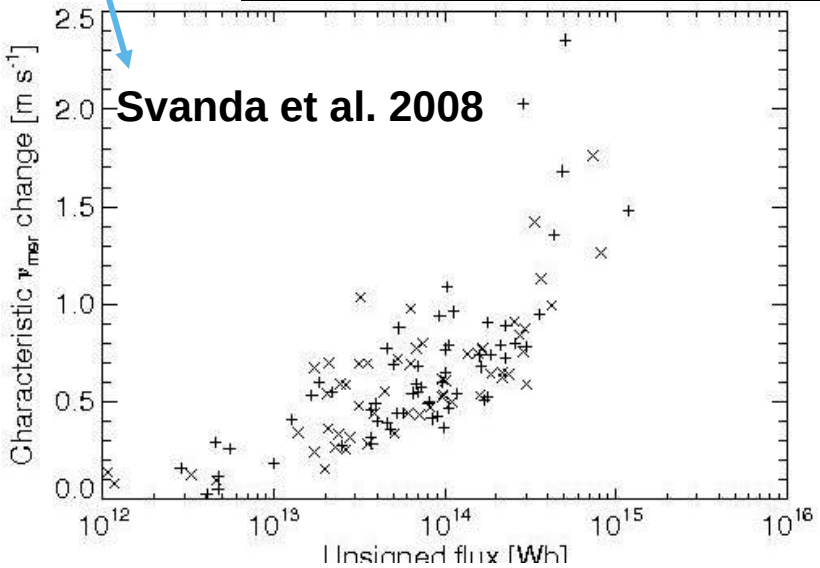

See also Hathaway et al. 1996, Gizon 2004, Zhao & Kosovichev 2004, etc…

Convective cases

Influence of meridional circulation

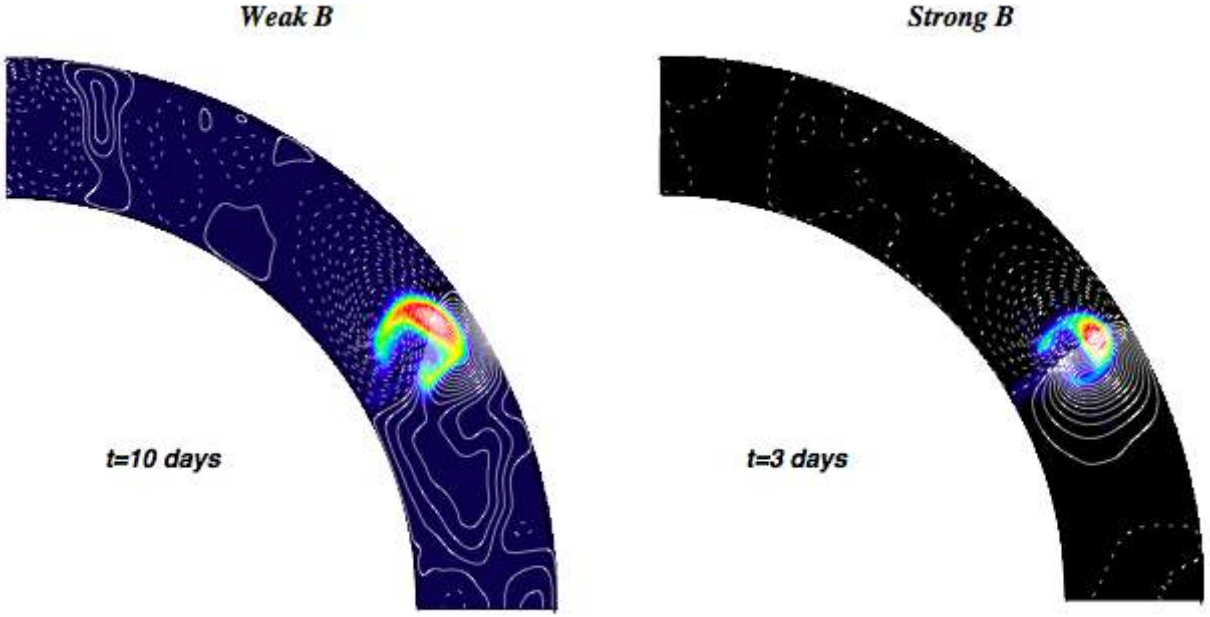

Strong B:
the MC produced by the Lorentz force dominates

Weak B:
the MC produced by the Lorentz force is of the same order as the background MC

Sub-surface weather:
Emerging regions modify the sub-surface flow field

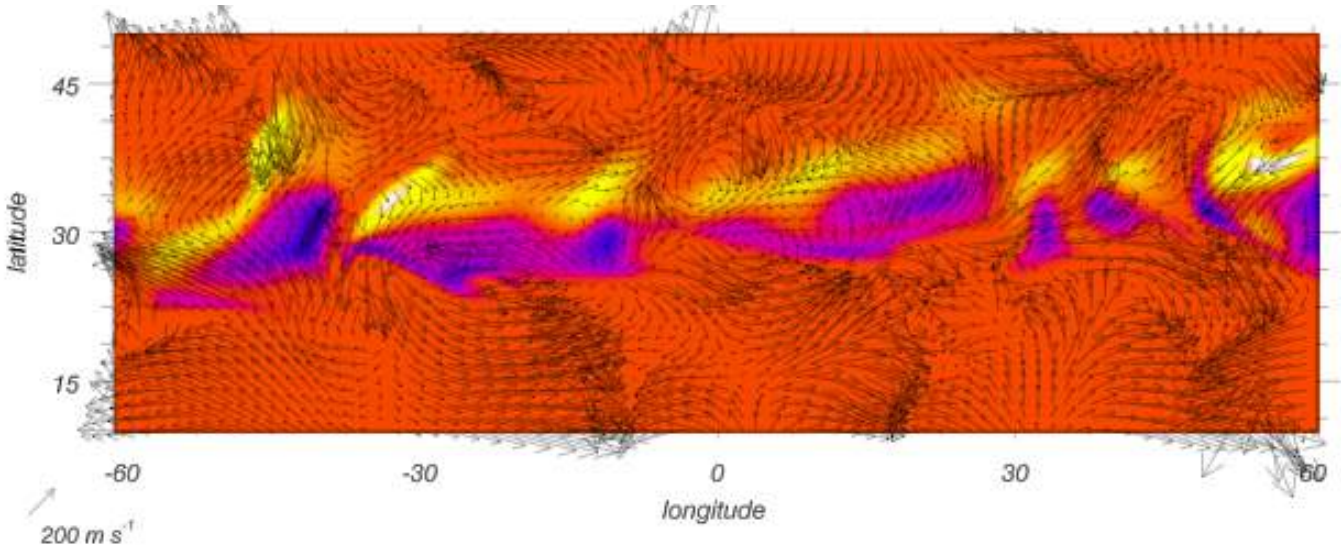

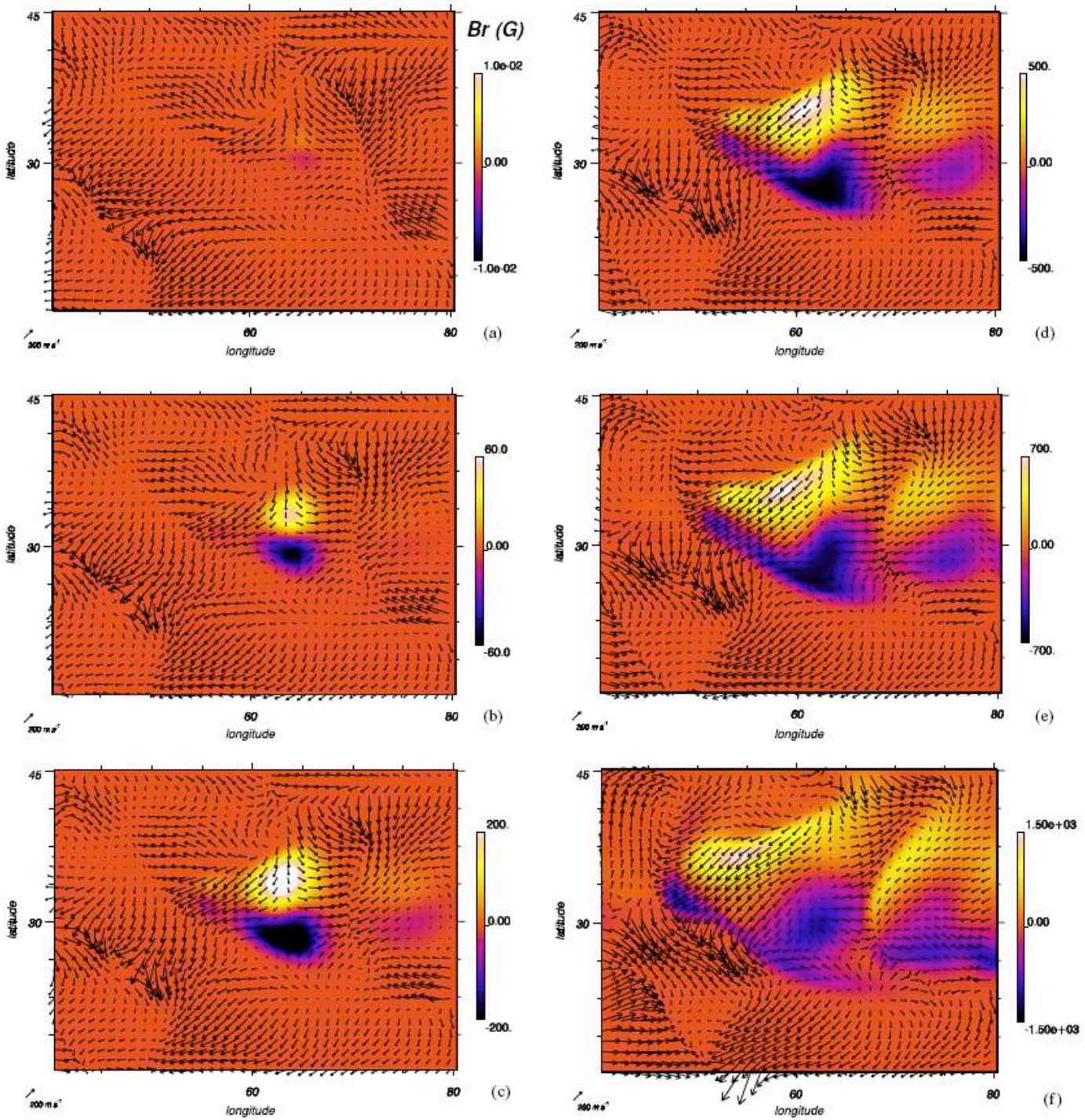
Br (G)
1.0e-02
0.00
-1.0e-02
45
30
latitude
60
80
longitude
(a)
500.
0.00
-500.
(d)
60.0
0.00
-60.0
(b)
700.
0.00
-700.
(e)
200.
0.00
-200.
(c)
1.50e+03
0.00
-1.50e+03
(f)

Flux emergence feed back on horizontal flow

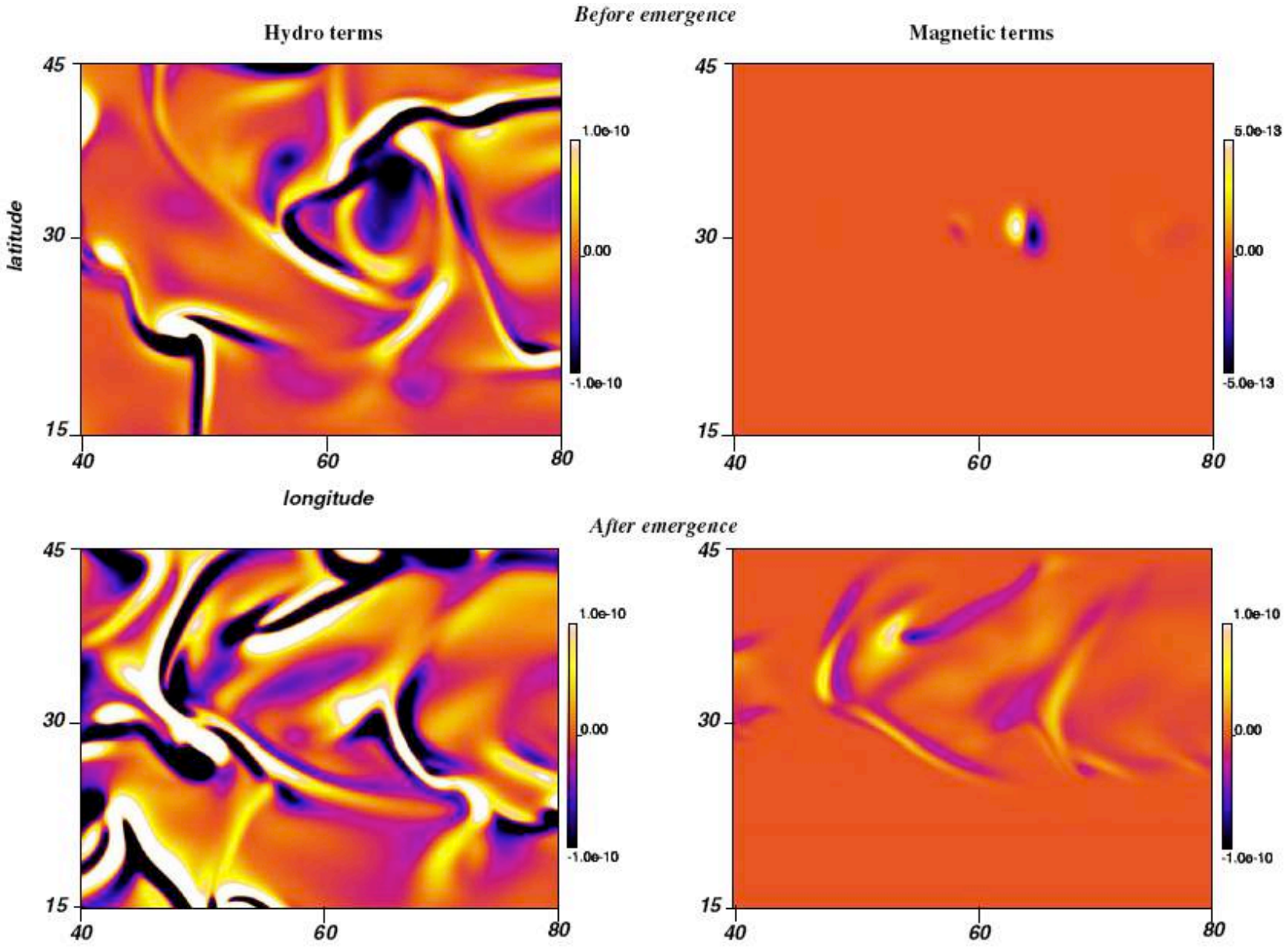

Structure of emerging regions

Potential field extrapolation in the corona:

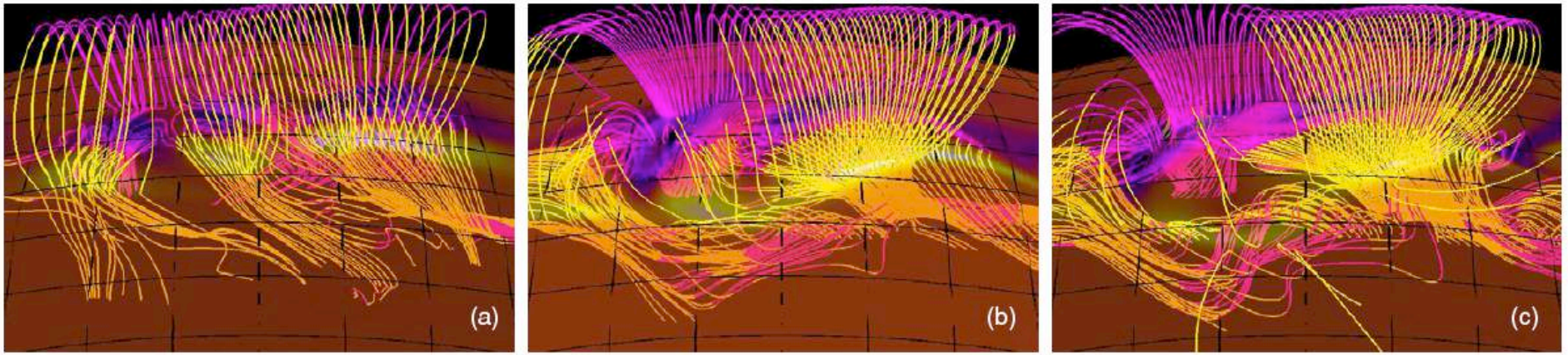

Initial orientation of field lines is linked to twist of structure, but subsequently evolves with dynamical action of convection flows. Partial emergence of tube structure (see Hood et al. 2009 for a specific study of that pb).

Summary of 3-D Simulations

• We need a sufficient twist to be able to keep a coherent rising fluxtube.

• We need a sufficient field strength to go from a convection dominated regime to a magnetic buoyancy dominated regime.

• But to get magnetic flux emerging at specific longitudes as active regions, we need to keep a reasonably low field strength otherwise the tube is rising as in a stratified layer and emerges at all longitudes without being affected by convection.

• Meridional flow seems to have a significant impact on the tube behaviour when the magnetic field intensity is sufficiently small.

• We do not see any clear effect of differential rotation and of the initial latitude of the tube but it still has to be worked on.

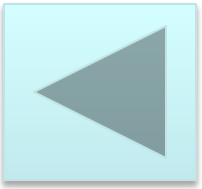

Back to obs